Titre: Title:	Amélioration de la conception de systèmes de pompes à chaleur géothermiques
Auteur: Author:	Laurent Gagné-Boisvert
Date:	2017
Type:	Mémoire ou thèse / Dissertation or Thesis
Référence: Citation:	Gagné-Boisvert, L. (2017). Amélioration de la conception de systèmes de pompes à chaleur géothermiques [Mémoire de maîtrise, École Polytechnique de Montréal]. PolyPublie. https://publications.polymtl.ca/2562/

URL de PolyPublie: PolyPublie URL:	https://publications.polymtl.ca/2562/
Directeurs de recherche: Advisors:	Michel Bernier
Programme: Program:	Génie mécanique

UNIVERSITÉ DE MONTRÉAL

AMÉLIORATION DE LA CONCEPTION DE SYSTÈMES DE POMPES À CHALEUR GÉOTHERMIQUES

LAURENT GAGNÉ-BOISVERT

DÉPARTEMENT DE GÉNIE MÉCANIQUE

ÉCOLE POLYTECHNIQUE DE MONTRÉAL

MÉMOIRE PRÉSENTÉ EN VUE DE L'OBTENTION

DU DIPLÔME DE MAÎTRISE ÈS SCIENCES APPLIQUÉES

(GÉNIE MÉCANIQUE)

MAI 2017

UNIVERSITÉ DE MONTRÉAL

ÉCOLE POLYTECHNIQUE DE MONTRÉAL

Ce mémoire intitulé :

AMÉLIORATION DE LA CONCEPTION DE SYSTÈMES DE POMPES À CHALEUR GÉOTHERMIQUES

présenté par : GAGNÉ-BOISVERT Laurent

en vue de l'obtention du diplôme de : Maîtrise ès sciences appliquées

a été dûment accepté par le jury d'examen constitué de :

M. KUMMERT Michaël, Doctorat, président

M. BERNIER Michel, Ph. D., membre et directeur de recherche

M. CIMMINO Massimo, Ph. D., membre

DÉDICACE

Il y a assez de tout dans le monde pour satisfaire aux besoins de l'homme, mais pas assez pour assouvir son avidité. -Mahatma Gandhi

REMERCIEMENTS

Je tiens tout d'abord à remercier Michel Bernier, mon directeur de recherche, pour les nombreux moments passés en sa compagnie. Excellent pédagogue et amoureux de la connaissance et de sa transmission, il m'a permis de découvrir le monde de la recherche ainsi que son importance pour le monde professionnel. Les conseils, la rigueur et la passion qu'il m'a transmis ont été essentiels à la réalisation de ce travail de recherche et me serviront à coup sûr pour la suite des choses.

Je remercie ensuite naturellement mes collègues devenus amis, notamment Bruno Marcotte, Corentin Lecomte, David Lessard, Pauline Brischoux et Samuel Letellier-Duchesne. Les conseils reçus et les bons moments partagés avec eux ont agrémenté mes recherches. Je souligne également l'appui financier de trois institutions dont la contribution a grandement servi ce travail : le CRSNG (Bourse d'études supérieures du Canada), ASHRAE (ASHRAE Graduate Student Grant-in-Aid) et Hydro-Québec (Bourse d'études supérieures Hydro-Québec).

Pour terminer, j'offre un merci bien spécial à ma famille, mes amis, ainsi qu'au nouveau membre de la famille qui verra bientôt le jour, pour votre support et votre motivation.

RÉSUMÉ

Les systèmes de pompes à chaleur géothermiques ont le potentiel de réduire la consommation énergétique des bâtiments ainsi que les émissions de gaz à effet de serre. Cependant, ces systèmes peuvent nécessiter un investissement initial plus important par rapport à des équipements de chauffage et de climatisation plus communs. Ils sont également complexes à concevoir et à simuler. Ce travail vise donc à améliorer la conception des systèmes géothermiques et à mieux comprendre leur fonctionnement afin de les dimensionner selon leur comportement réel et de prédire précisément leur consommation énergétique.

Les circulateurs sont d'abord étudiés. L'étude présente des corrélations permettant de prédire leur rendement en fonction de la puissance hydraulique à fournir. Il ressort de cette étude que les circulateurs récents ont des rendements environ deux fois plus élevés que les anciens circulateurs.

L'inclusion de la capacité thermique du fluide et du coulis a un impact notable sur le dimensionnement des puits géothermiques. En effet, les résultats de simulations utilisant un modèle de puits de type Thermal Resistance and Capacitance (TRC) indiquent que les longueurs de puits requises peuvent être sous-estimées jusqu'à 31% ou surestimées jusqu'à 24% par rapport à l'équation de dimensionnement de l'ASHRAE, qui néglige la capacité thermique des puits.

Les antigels utilisés dans les puits affectent également les performances d'un système géothermique. La puissance de pompage, l'échange thermique dans les puits, la transition laminaire-turbulent et la capacité d'une thermopompe sont fonction du type et de la concentration d'antigel utilisé. Des simulations utilisant différents types d'antigel ont démontré que le méthanol est l'antigel le moins pénalisant et qu'un faible débit de 0.027 L/s-kW (1.5 usgpm/tonne) est à favoriser par rapport au débit courant de 0.054 L/s-kW (3 usgpm/tonne). Les faibles débits engendrent un écoulement laminaire occasionnel dans les puits, ce qui entraîne une baisse du transfert de chaleur. Cependant, cette baisse est compensée par une puissance de pompage plus faible.

Finalement, un nouvel outil de simulation servant à évaluer la consommation énergétique des systèmes géothermiques à un ou deux tuyaux est proposé. Des études de cas ont démontré qu'un réseau à un tuyau nécessite jusqu'à 36% moins d'énergie de pompage qu'un réseau à deux tuyaux. Cependant, il consomme globalement jusqu'à 5% plus d'énergie à cause des températures d'entrée défavorables aux pompes à chaleur.

ABSTRACT

Geothermal heat pump systems have the potential to reduce building energy consumption and greenhouse gas emissions. However, these systems may require a larger initial investment compared to more common heating and cooling equipment. They are also complex to design and simulate. This work aims to improve the design of geothermal systems and to better understand their operation to size them according to their real behavior and to predict precisely their energy consumption.

Circulators are studied first. The study presents correlations allowing an estimation of their efficiency as a function of the hydraulic power. It was found that the efficiency of recent circulators is about twice as high as those found in older circulators.

Accounting for the fluid and grout thermal capacity has a significant impact on the sizing of geothermal boreholes. Simulation results using a Thermal Resistance and Capacitance (TRC) model indicate that the required borehole lengths may be underestimated by up to 31% or overestimated by up to 24% when compared to ASHRAE sizing equation, which neglects borehole thermal capacity.

The antifreeze used in boreholes also affects the performance of a geothermal system. Pumping power, borehole heat transfer, laminar-turbulent transition and heat pump capacity depend on the chosen antifreeze type and concentration. Simulations using different types of antifreeze show that methanol is the least penalizing antifreeze and that a low flow rate of 0.027 L/s-kW (1.5 usgpm/ton) should be favored over the common flow rate of 0.054 L/s-kW (3 usgpm/ton). Low flows cause occasional laminar flow in boreholes, decreasing heat transfer. However, this reduction is offset by a lower pumping power.

Finally, a new simulation tool for estimating the energy consumption of one- and two-pipe geothermal systems is proposed. Case studies have shown that a one-pipe network requires up to 36% less pumping energy than a two-pipe system. However, it presents an overall energy consumption up to 5% higher due to unfavorable heat pump inlet temperatures.

TABLE DES MATIÈRES

LISTE DES TABLEAUX

LISTE DES FIGURES

LISTE DES SIGLES ET ABRÉVIATIONS

Abréviations

a	Antigel
Avg	Average
BEP	Best Efficiency Point
BFTM	Borehole Fluid Thermal Mass
Circ	Circulateur
COP	Coefficient de Performance
corr	Corrigé
DST	Duct ground STorage
EA	Éthanol
ECM	Electronically Commutated Motor
EuP	European Association of Pump Manufacturers
GCHP	Ground-Coupled Heat Pump
GSHP	Ground-Source Heat Pump
HP	Heat Pump
MA	Méthanol
nom	Nominal
PG	Propylène Glycol
rev	Retour renversé
RMSE	Root-Mean-Square Error
s	Segment
TRC	Thermal Resistance Capacity
TRNSYS	Transient System simulation tool (logiciel)

VFD	Variable Frequency Drive
w	Water
WPD	Water Pressure Drop

Variables

C_1, C_2	Constantes d'une pompe à chaleur (-)
$C_{20\%}$	Facteur de correction de la norme EuroPump (-)
CAP	Capacité d'une pompe à chaleur (kW ou tonnes)
Cp	Capacité thermique (kJ/kg.K)
CR	Ratio de capacité (-)
CSF	Facteur de mise à l'échelle de la capacité (-)
C_v	Coefficient de débit (usgpm)
D	Diamètre du tuyau (m)
DF	Decrement Factor (-)
EEI	Energy Efficiency Index (-)
EIR	Energy Input Ratio (-)
f	Coefficient de friction (-) ou Fraction du débit du VFD (-)
$f_{capacity}$	Facteur de correction pour la capacité d'une pompe à chaleur (-)
f_{power}	Facteur de correction pour la puissance d'une pompe à chaleur (-)
f_{WPD}	Facteur de correction pour les pertes de charge (-)
F_{corr}	Facteur de correction pour l'équation de dimensionnement de l'ASHRAE (-)
F_{pump}	Facteur de correction de la pompe principale (-)
g	Accélération gravitationnelle (m/s^2)
h	Coefficient de convection ($W/m^2.K$)

H	Hauteur manométrique (m)
$Head_{max}$	Perte de charge maximale durant une année (kPa)
k	Conductivité thermique (W/m.K)
L	Longueur de puits géothermique ou de tuyaux (m)
LCC	Coût du cycle de vie ($)
$\dot{m}$	Débit principal (L/s)
$\dot{m}_i$	Débit dans la pompe à chaleur i (L/s)
$\dot{m}_{tot}$	Débit principal maximal (L/s)
$P_{élec}$	Puissance électrique d'une pompe (W)
P_{hydr}	Puissance hydraulique d'une pompe (W)
$P_{L,avg}$	Puissance électrique d'une pompe moyennée et pondérée (W)
PLF	Part-Load Factor (-)
PLR	Part-Load Ratio (-)
P_{ref}	Puissance électrique de référence pour la norme EuroPump (W)
PP	Paramètre de puissance (usgpm^3/in^5)
Q	Débit volumique d'un circulateur (L/s ou m^3/h)
Q_{Cap}	Capacité d'une pompe à chaleur (kW)
Q_{Loop}	Injection ou extraction de chaleur dans la boucle (kW)
q_h	Charge horaire au sol (W)
q_m	Charge mensuelle au sol (W)
q_y	Charge annuelle au sol (W)
r_b	Rayon d'un puits (m ou in)
R_b	Résistance thermique équivalente du puits (m.K/W)
R_{conv}	Résistance thermique de convection (m.K/W)

R_{grout}	Résistance thermique du coulis du puits (m.K/W)
R_{pipe}	Résistance thermique des tuyaux du puits (m.K/W)
R_t	Résistance thermique totale de l'échangeur côté source de la pompe à chaleur (m.K/W)
R_{6h}	Résistance thermique équivalente du sol durant 6 heures (m.K/W)
R_{1m}	Résistance thermique équivalente du sol durant 1 mois (m.K/W)
R_{10y}	Résistance thermique équivalente du sol durant 10 ans (m.K/W)
R^2	Coefficient de régression (-)
Re	Nombre de Reynolds (-)
SPF	Coefficient de performance saisonnier (-)
t	Temps (h)
T_g	Température du sol non perturbé (°C)
T_{inHP}	Température du fluide à l'entrée de la pompe à chaleur (°C)
T_{outHP}	Température du fluide à la sortie de la pompe à chaleur (°C)
V	Vitesse du fluide (m/s)
W_{HP}	Puissance consommée par une pompe à chaleur (W)
W_{Pump}	Puissance de pompage (W)
X	Position relative à l'axe des X (m)
Y	Position relative à l'axe des Y (m)

Symboles

α	Diffusivité thermique du sol (m^2/jour)
Δp	Perte de pression (kPa)
ΔT	Différence de température (°C)
ε	Rugosité du tuyau (m)

η	Rendement du fil à l'eau d'une pompe de circulation (%)
ρ	Masse volumique (kg/m^3)
μ	Viscosité dynamique (kg/m.s)
% m/m	Concentration massique (%)

CHAPITRE 1 INTRODUCTION

Le secteur des bâtiments est le plus grand consommateur d'énergie à l'échelle mondiale (AIE, 2013). Il représente ainsi 35% de l'énergie finale consommée (électricité, combustibles fossiles, bois, etc.) et engendre une part équivalente des émissions de dioxyde de carbone. Au Canada, les bâtiments consomment quant à eux 28% de l'énergie finale, soit 16% pour le secteur résidentiel et 12% pour le secteur commercial/institutionnel (NRCan-OEE, 2013). De plus, le chauffage, la climatisation et l'eau chaude domestique requièrent, respectivement, 82% et 59% de l'énergie consommée par les secteurs résidentiel et commercial canadiens. Réduire l'utilisation de l'énergie dans les bâtiments pourrait donc diminuer la consommation mondiale d'énergie. À plus petite échelle, au Québec, une part importante du chauffage des espaces et de l'eau chaude domestique utilise de l'électricité de sources hydroélectrique et éolienne. Une réduction de cette consommation d'électricité permettrait du coup d'augmenter l'exportation de cette énergie propre vers les provinces et états voisins où l'électricité provient de combustibles fossiles. Cela réduirait les émissions polluantes à l'échelle globale tout en constituant une opportunité d'affaire pour le Québec.

À ce titre, les systèmes de pompes à chaleur géothermiques ont le potentiel de réduire la consommation énergétique des bâtiments ainsi que les émissions polluantes qui y sont rattachées. Cependant, ces systèmes sont moins connus et peuvent nécessiter un investissement initial plus important par rapport à des équipements de chauffage et de climatisation conventionnels, ce qui réduit la propension à opter pour cette technologie. Il importe donc de comprendre et d'améliorer la conception et le fonctionnement des systèmes géothermiques afin que leur utilisation soit plus répandue.

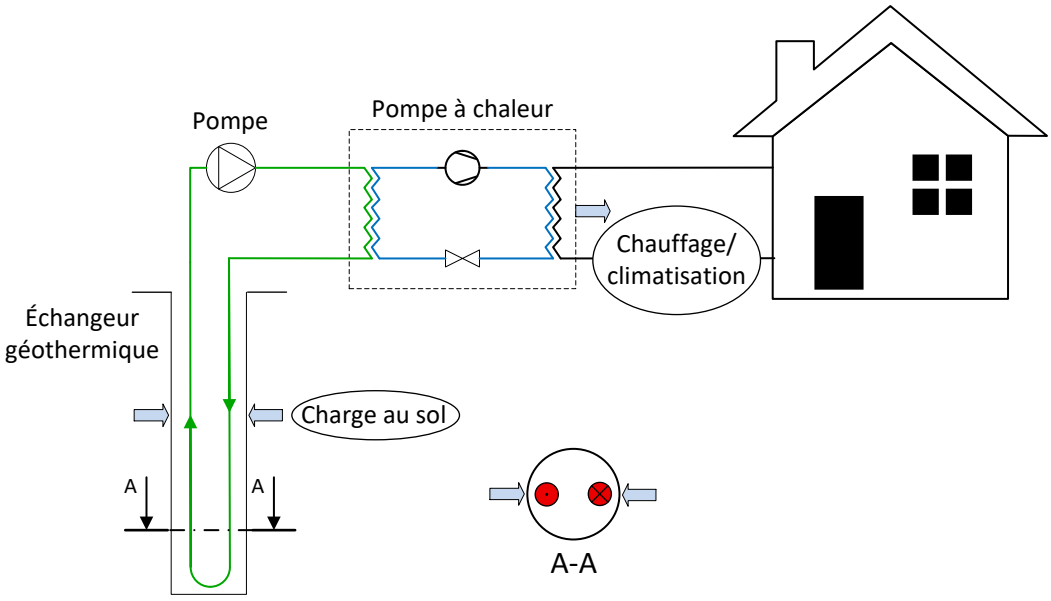

Figure 1.1 : Représentation schématique d'une installation de pompe à chaleur géothermique résidentielle, inspirée de Brischoux (2016)

1.1 Généralités

La Figure 1.1 montre une représentation schématique d'une pompe à chaleur résidentielle. Une pompe à chaleur sert à « pomper » de la chaleur d'un milieu à basse température vers un autre à température plus élevée. Le réfrigérant est d'abord évaporé dans l'évaporateur au moyen de chaleur extraite du milieu à basse température. Ensuite, le réfrigérant est comprimé, ce qui entraine une augmentation de sa température. Finalement, le réfrigérant à haute température rejette sa chaleur dans le condenseur. Dans le cas des pompes à chaleur géothermiques opérant en mode chauffage, le milieu à basse température est le sol et l'air de la maison constitue le milieu à haute température. En climatisation, le cycle est inversé et l'air de la maison est le milieu à basse température alors que le rejet à haute température se fait dans le sol.

Les coûts initiaux associés aux échangeurs géothermiques sont importants, surtout lorsque les puits sont verticaux. Leur dimensionnement est donc important afin de réduire les coûts et d'assurer un transfert thermique suffisant. Quelquefois, lorsque les besoins en chauffage sont importants, la température du sol au voisinage de l'échangeur géothermique baisse et il faut alors avoir recours à un mélange antigel-eau pour éviter le gel du fluide caloporteur. Différents mélanges sont alors disponibles, influençant le transfert de chaleur et la puissance de pompage selon la concentration

choisie. Finalement, pour les installations comportant plusieurs pompes à chaleur, plusieurs configurations de la tuyauterie acheminant le fluide aux unités et plusieurs stratégies de pompage sont possibles. Ces configurations, de même que la profondeur des puits, les pompes et le fluide caloporteur choisis, influencent la consommation d'énergie et les coûts de l'installation. L'amélioration de la conception d'un système de pompes à chaleur géothermique passe donc en partie par l'étude de ces éléments.

1.2 Objectifs du travail de recherche

Ce travail de recherche a pour but d'améliorer la conception des systèmes géothermiques et de développer des outils permettant de mieux comprendre le fonctionnement de ces systèmes. Les points abordés concernent l'effet de la capacité thermique du puits sur la profondeur requise, le choix du fluide caloporteur et la détermination de l'énergie de pompage pour les circuits internes à un ou deux tuyaux. Quatre objectifs spécifiques sont donc abordés dans autant de chapitres.

- Le premier objectif de cette étude vise à analyser le fonctionnement et le rendement des pompes de circulation utilisées dans les systèmes géothermiques. Ces pompes, appelées circulateurs, sont encore considérées comme ayant un faible rendement, ce qui n'encourage pas leur utilisation. Le rendement des circulateurs a augmenté au cours des dernières années et cette section vise à en rendre compte tout en permettant la prédiction.
- Le second objectif consiste à démontrer l'importance de considérer la capacité thermique des puits géothermiques lors de leur simulation et de leur dimensionnement. Ce mémoire aborde également l'erreur commise par l'équation de dimensionnement de l'ASHRAE, qui néglige la capacité thermique des puits.
- Le troisième objectif vise à améliorer la simulation de systèmes géothermiques utilisant des solutions d'antigel et d'en évaluer les effets sur les performances énergétiques.
- Le quatrième objectif consiste à confronter les réseaux de distribution géothermiques à un et deux tuyaux. Pour y parvenir, un outil permettant de les comparer au niveau énergétique a été développé dans l'environnement de simulation TRNSYS.

1.3 Organisation générale du mémoire

Ce mémoire par articles est composé de 9 chapitres. Le présent chapitre introduit diverses problématiques reliées à la conception de systèmes géothermiques, ce qui mène aux objectifs de ce travail de recherche. Le Chapitre 2 présente une revue de la littérature relative aux circulateurs, à la capacité thermique des puits, à l'utilisation d'antigels et aux réseaux de distribution. Le Chapitre 3 établit la démarche de ce travail ainsi que sa pertinence dans le contexte présenté au Chapitre 1.

Le corps de ce mémoire comprend ensuite quatre chapitres principaux qui visent tous l'amélioration de la conception des systèmes géothermiques. Le Chapitre 4 aborde le fonctionnement et le rendement des circulateurs, qui sont entre autres utilisés dans les systèmes étudiés aux chapitres suivants. Le Chapitre 5 est constitué du premier article, qui porte sur la capacité thermique des puits et qui a été présenté à la conférence annuelle de l'ASHRAE en 2016. Le Chapitre 6 présente le second article, qui aborde l'influence des antigels et qui a été présenté à la conférence de l'International Ground Source Heat Pump Association en mars 2017. Dans le Chapitre 7, le troisième article, soumis au journal Science and Technology for the Built Environment et portant sur les réseaux à un et deux tuyaux, est présenté. Par la suite, le Chapitre 8 constitue une discussion générale relative aux résultats obtenus et aux objectifs visés. Finalement, la dernière section conclut ce mémoire en établissant son importance, ses limites et certaines recommandations visant des travaux ultérieurs.

CHAPITRE 2 REVUE DE LA LITTÉRATURE

Ce chapitre a pour but de résumer les principaux travaux répertoriés dans la littérature et portant sur les circulateurs, la capacité thermique des puits, les antigels et les réseaux de distribution. Il est à noter que les trois articles présentés aux Chapitres 5, 6 et 7 comprennent également chacun une revue de la littérature.

2.1 Circulateurs

Les pompes sont des composantes essentielles des systèmes géothermiques. À ce titre, de récentes études ont démontré que les pompes consomment annuellement environ 10% de l'électricité mondiale (Grundfos, 2016). Des efforts, appuyés par de nouvelles règlementations (EuroPump, 2011), sont actuellement menés dans le but de réduire la consommation énergétique des pompes. De par leurs plus petites dimensions, les petites pompes, aussi appelées circulateurs, ont un rendement inférieur aux pompes de grandes dimensions. Cependant, des progrès sont actuellement observés et les circulateurs à haute efficacité consomment aujourd'hui jusqu'à 80% moins d'énergie que des circulateurs standards (Bidstrup, 2013).

2.1.1 Définition

Il existe plusieurs définitions d'un circulateur. En règle générale, un circulateur est une petite pompe couplée à un moteur électrique servant à faire circuler un fluide caloporteur ou de l'eau potable dans un bâtiment. Ce dernier sert généralement à fournir l'énergie nécessaire pour contrer les pertes de charge à travers un réseau de distribution en circuit fermé.

Les circulateurs sont classés différemment selon divers organismes :

- Pompe utilisée dans un système de chauffage ou une boucle secondaire de climatisation et développant une puissance hydraulique comprise entre 1 et 2500 W (EuroPump, 2011)
- Pompe avec moteur à rotor noyé d'une puissance électrique de moins de 1000 W (COSTIC, 2003)
- Pompe ayant une puissance électrique inférieure à 250 W (ASHRAE, 2003).

Dans cette étude, les circulateurs considérés sont de type « à rotor noyé ». Cela signifie que le moteur actionnant la pompe baigne dans le fluide pompé, ce qui le refroidit. Les pertes de chaleur du moteur chauffent donc directement le fluide. De plus, une puissance hydraulique maximale de

300 W est considérée. La puissance hydraulique, qui est le produit du débit et de la hauteur manométrique requise (ou, alternativement, de la puissance électrique et du rendement du circulateur), est abordée en détail dans la section « Méthodologie » du Chapitre 4. Une puissance de 300 W est choisie car elle englobe les cas typiques rencontrés pour ce genre d'applications. Par exemple, un circulateur fournissant 30 usgpm (6.8 m^3/h) à 50 pieds d'eau (15.2 m) a une puissance hydraulique de 283 W.

De plus, un circulateur peut être à multi-étage ou être équipé d'un entraînement à fréquence variable (Variable Frequency Drive ou VFD). Les circulateurs haute performance sont quant à eux munis d'un moteur ECM (electronically commutated motor). Ce dernier est un moteur synchrone à aimant permanent dont la vitesse de rotation peut varier afin d'atteindre le point de fonctionnement souhaité. Ces moteurs sont de plus en plus utilisés car ils sont très efficaces et versatiles (Grundfos, 2016).

Finalement, au niveau de l'entretien, les circulateurs à rotor noyé ne requièrent aucune intervention car le fluide pompé sert de lubrifiant (Grundfos, 2016). De plus, ces circulateurs n'ont aucun joint, couplage ou assemblage de roulement, ce qui réduit les risques de problèmes et les coûts d'entretien.

2.1.2 Rendement

Une étude du Comité Scientifique et Technique des Industries Climatiques (COSTIC, 2003) a établi deux corrélations entre le rendement nominal de 77 circulateurs provenant de quatre grands manufacturiers et leur puissance électrique, $P_{élec}$, ou hydraulique, P_{hydr}, (Équations 2.1 et 2.2). L'étude du COSTIC révèle que les circulateurs présentent des rendements très variés, et ce, même au sein d'une même famille d'appareils. La corrélation proposée par le COSTIC (Figure 2.1) prédit un rendement de 25% pour un circulateur ayant une puissance hydraulique de 50 W ou électrique de 200 W. Cette même étude est présentée à nouveau en 2010 dans un guide du COSTIC sur les circulateurs (COSTIC, 2010) sans que des améliorations de rendement ne soient mentionnées.

$$\eta_{nom} = 0.0211 {P_{élec}}^{0.467} \tag{2.1}$$

$$\eta_{nom} = 0.0646 {P_{hydr}}^{0.344} \tag{2.2}$$

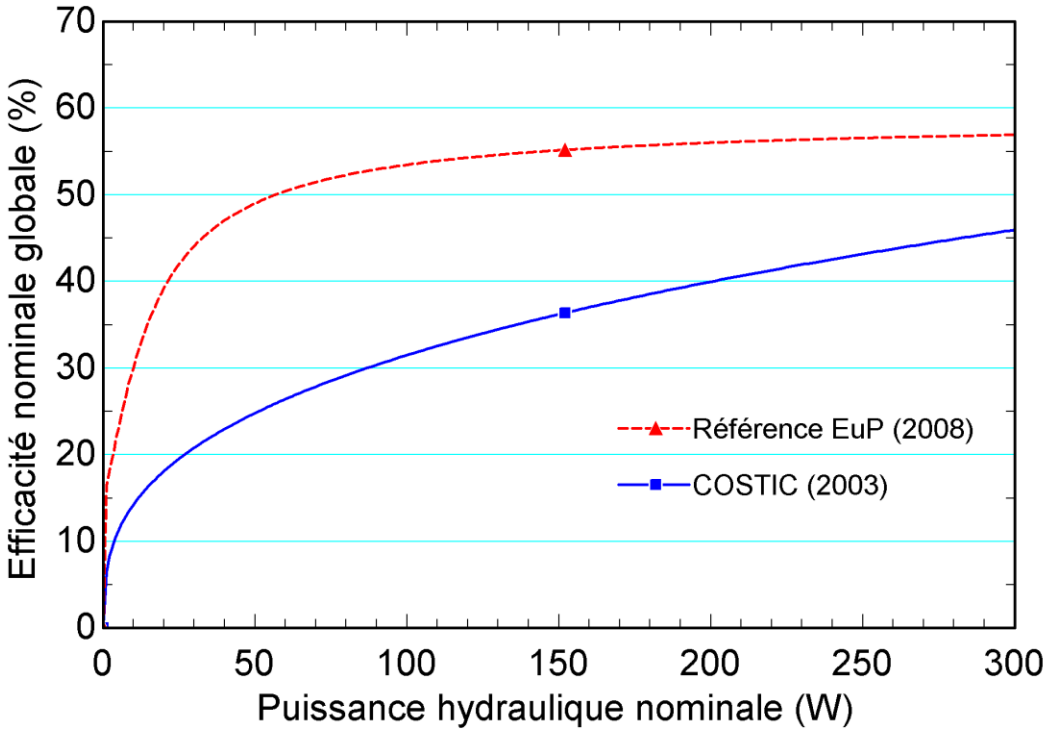

Figure 2.1: Rendement nominal de circulateurs présenté par le COSTIC et EuroPump

Un rapport de l'ASHRAE (2003) présente des résultats expérimentaux sur le rendement de certains circulateurs utilisés dans les systèmes géothermiques. L'étude conclut que les circulateurs (puissance électrique < 250 W) possèdent une efficacité globale de 20 à 28%. Il est mentionné que l'efficacité est encore moindre pour les plus petits circulateurs. Le rapport recommande d'éviter le recours aux circulateurs lorsque les pertes de charge du système dépassent 25 pieds d'eau (75 kPa). Cependant, l'utilisation d'un système géothermique décentralisé muni d'un circulateur sur chaque boucle est recommandée pour des bâtiments occupés moins de 60 heures par semaine. Les auteurs mentionnent aussi que si l'efficacité des circulateurs est améliorée et que les pertes de charge d'un système sont minimisées, l'énergie de pompage peut représenter moins de 5% de l'énergie totale requise par un système géothermique.

Kavanaugh et Rafferty (2015) mentionnent que les circulateurs ne devraient pas être utilisés si leur rendement est inférieur à 30% et si les pertes de charge du système dépassent 30 pieds d'eau (90 kPa).

Une étude allemande (Ludwig et Roth, 2008) a évalué le rendement de circulateurs à haut rendement disponibles en Europe. Cette étude a mené à l'Équation 2.3, qui estime la puissance électrique requise par un circulateur en fonction de sa puissance hydraulique. L'équation peut aussi servir à calculer le rendement de référence des circulateurs en divisant P_{hydr} par $P_{élec}$. Ce rendement est présenté sur la Figure 2.1.

$$P_{élec} = P_{ref} = 1.7P_{hydr} + 17(1 - e^{-0.3P_{hydr}}) \quad pour\ 1\ W \leq P_{hydr} \leq 2500\ W \tag{2.3}$$

En 2009, la European Association of Pump Manufacturers (EuroPump ou EuP) a établi la norme européenne en matière de circulateurs (2011). La norme EuP, la plus contraignante à ce jour, se base sur l'Équation 2.3 pour déterminer la puissance électrique de référence d'un circulateur, P_{ref}. Elle nécessite ensuite d'évaluer $P_{L,avg}$, une puissance électrique moyennée et pondérée basée sur l'utilisation annuelle du circulateur. $P_{L,avg}$ est obtenue en multipliant la puissance électrique du circulateur fonctionnant à différentes charges (100%, 75%, 50% et 25%) par une fraction normalisée du temps passé à fonctionner à chaque charge. Ces fractions, établies par EuroPump, sont présentées dans l'Équation 2.4 alors que les puissances sont obtenues à l'aide de tests expérimentaux.

$$P_{L,avg} = 0.06P_{L,100\%} + 0.15P_{L,75\%} + 0.35P_{L,50\%} + 0.44P_{L,25\%} \tag{2.4}$$

Le rapport des puissances moyennée et de référence est multiplié par un facteur de correction, $C_{20\%}$, afin d'obtenir le Energy Efficiency Index du circulateur, EEI (Éq. 2.5). La norme EuP utilise donc cet index pour régir l'efficacité des circulateurs, un faible EEI témoignant d'une pompe plus efficace.

$$EEI = \frac{P_{L,avg}}{P_{ref}} C_{20\%}\,, \qquad où\ C_{20\%} = 0.49 \tag{2.5}$$

Depuis le 1er août 2015, les circulateurs vendus en Europe doivent avoir un $EEI \leq 0.23$, alors que la limite était de 0.27 en 2013. Les circulateurs servant de référence et ayant mené à l'Équation 2.3 possédaient des EEI entre 0.17 et 0.27 (Bidstrup, 2016). Actuellement, les circulateurs haute performance atteignent des EEI inférieurs à 0.20. De plus, le facteur $C_{20\%}$, qui est fixé par la

règlementation, sert à calibrer l'index. Il a été choisi lors de la création de la norme afin que seulement 20% des circulateurs aient un $EEI \leq 0.20$.

Il est pertinent de noter que cette norme est légèrement moins contraignante pour les circulateurs intégrés aux installations géothermiques ou solaires. Ces derniers doivent fournir une plus grande pression pour de faibles débits, ce qui implique une faible vitesse spécifique. Il est donc plus difficile d'atteindre un aussi haut rendement pour ces applications. La norme permet donc un EEI plus élevé pour ces cas. Les normes européennes ont également été résumées par Bidstrup (2012).

Finalement, les États-Unis ont mis sur pied en 2016 un comité de recherche du Département de l'énergie des États-Unis (DOE) visant à établir une norme concernant l'efficacité des circulateurs. Une norme américaine, qui serait alignée avec la norme européenne, est prévue pour l'année 2017 (DOE, 2016). Cette norme inclurait des rendements minimaux pour les circulateurs ainsi qu'une procédure pour les tester.

2.2 Capacité thermique des puits géothermiques

La capacité thermique d'un matériau représente l'énergie devant être injectée (extraite) dans une certaine masse ou volume de matériau afin d'en augmenter (réduire) la température. Si le sol ou le puits a une plus grande capacité thermique, plus d'énergie pourra en être extraite pour chaque degré d'élévation de température, améliorant les performances du système et réduisant la longueur de puits requise. La capacité thermique du sol est déjà considérée dans les calculs de dimensionnement et la simulation de puits géothermiques. Cependant, la capacité thermique du puits est plus rarement prise en compte.

Le premier à aborder la capacité thermique des puits est, semble-t-il, Hellström (1991). Il a constaté que la capacité thermique du fluide caloporteur d'un puits engendre des effets transitoires importants durant 2 à 3 heures pour des puits typiques. Une part importante de la charge est alors absorbée par le fluide au lieu d'être transférée dans le sol. Cette période dure plus longtemps si les puits ont une petite diffusivité thermique ou un grand rayon.

Cependant, de manière générale, la capacité thermique d'un puits n'est pas considérée. Un puits est plutôt assimilé à une résistance thermique équivalente constante dans le temps, R_b, tel que présenté par Kavanaugh et Rafferty (1997). Ils mentionnent dans leur guide de conception de systèmes géothermiques que la capacité thermique du coulis, des tuyaux et du fluide est négligeable

par rapport à celle du sol entourant les puits. Les formes originale et alternative de l'équation de dimensionnement de l'ASHRAE (Éq. 2.6) (ASHRAE, 2015), qui sont utilisées dans la pratique, se basent notamment sur cette hypothèse voulant que le transfert de chaleur se produisant dans les puits se fasse en régime permanent. De plus, le modèle le plus utilisé pour simuler des puits géothermiques, le modèle DST (Duct ground STorage) développé par Hellström et al. (1996), considère une résistance thermique constante entre le fluide et la paroi du puits.

$$L = \frac{q_h R_b + q_y R_{10y} + q_m R_{1m} + q_h R_{6h}}{\frac{T_{inHP} + T_{outHP}}{2} - T_g} \tag{2.6}$$

Young (2004) a développé un modèle dynamique de puits géothermique considérant la capacité thermique du coulis et du fluide. Le modèle BFTM (Borehole Fluid Thermal Mass) a ensuite été comparé à un modèle classique en régime permanent, les deux servant à simuler le comportement d'un puits géothermique. Les résultats ont montré une différence atteignant 1.3 °C (2.3 °F) pour la température de sortie du puits lors de courtes pointes de fonctionnement. Il a néanmoins conclu que la consommation énergétique annuelle d'un système géothermique est bien prédite par un modèle en régime permanent. Un autre modèle considérant la capacité thermique du fluide (Xu et Spitler, 2006) a démontré que le comportement d'un puits était ainsi mieux reproduit et que cette capacité amortissait les pics de température du fluide.

Salim-Shirazi et Bernier (2013) ont ensuite développé un modèle dynamique remplaçant un puits à deux tuyaux par un cylindre considérant la capacité thermique du fluide et du coulis. En se basant sur des simulations utilisant leur modèle, ils ont conclu que la température sortant du puits est toujours plus élevée en mode chauffage lorsque la capacité thermique est prise en compte. Sur une base annuelle, ils ont noté que le fait de négliger la capacité thermique sous-estime le COP des thermopompes de 4.5% en moyenne, ce qui est dû à des températures moins favorables. Dans les deux cas, ils mentionnent que la différence est plus notable lorsque le fonctionnement du système est intermittent.

Ma et al. (2015) ont proposé de modifier le calcul des résistances dans l'équation de dimensionnement de l'ASHRAE. Ils ont utilisé un modèle quasi-3D qui considère la capacité thermique afin de les calculer. Cette technique a conduit à des longueurs de puits requises plus courtes, une observation plus marquée lorsque la pointe de charge dure moins de trois heures.

Finalement, un modèle TRC (Thermal Resistance and Capacity) apparaît comme une des meilleures techniques pour simuler des puits géothermiques puisqu'il tient compte de la capacité thermique du fluide et du coulis. Cette méthode a notamment été proposée par Bauer et al. (2010). Le modèle qui sera utilisé dans ce mémoire est celui de Godefroy et Bernier (2014). Il a été implémenté dans l'environnement TRNSYS et validé expérimentalement. Des simulations l'utilisant ont démontré que la consommation énergétique d'une pompe à chaleur peut être surestimée de 3% lorsque la capacité thermique est négligée. De plus, cette étude a confirmé que la capacité thermique du fluide a plus d'influence que celle du coulis.

2.3 Solutions d'antigel

Le fonctionnement d'un système géothermique en climat nordique nécessite l'ajout d'un antigel à l'eau servant de fluide caloporteur afin d'éviter le gel et le bris des équipements. Cependant, les antigels affectent le comportement et les performances de l'installation géothermique. Ainsi, la puissance de pompage, le transfert de chaleur dans les puits et la capacité des pompes à chaleur sont affectés.

Dans les installations géothermiques, des solutions de méthanol, de propylène glycol et d'éthanol sont communément utilisées. Chaque solution présente des avantages et des inconvénients. En 1997, une étude de l'ASHRAE a conclu que le propylène glycol est l'antigel à privilégier de par sa faible toxicité. Cependant, Bernier et al. (2005) ont conclu qu'il est également l'antigel le plus pénalisant au niveau énergétique. De plus, il est important de considérer les inhibiteurs, parfois toxiques, devant être ajoutés aux diverses solutions.

L'utilisation d'antigel affecte la perte de charge d'un système, et donc son énergie de pompage. Cette dernière est parfois négligée par rapport à la consommation énergétique totale d'une installation géothermique. En réalité, le pompage peut constituer jusqu'à 45% de la consommation totale, et ce, même pour des systèmes récents (Liu et al., 2015). Le recours à une solution d'antigel n'aide en rien cette situation puisque la viscosité résultante est généralement plus grande. À ce titre, Kavanaugh et Kavanaugh (2012) ont suggéré une puissance de pompage maximale de 2.1 $kW_{électrique}$/100 $kW_{thermique}$. La consommation énergétique du pompage peut donc être limitée en suivant cette recommandation.

Spitler et Jin (2003) ont étudié les effets d'une solution d'antigel sur le coefficient d'échange dans l'échangeur côté source d'une pompe à chaleur. Ils ont développé un facteur de correction (Decrement Factor) ajustant le coefficient d'échange, calculé pour l'eau. Une autre étude a conclu qu'une solution de propylène glycol augmente la consommation énergétique d'un système de 6 à 7% par rapport au méthanol et à l'éthanol mais que le coût du cycle de vie est peu influencé par l'antigel utilisé (Khan et Spitler, 2004).

Au niveau des puits, l'utilisation d'antigel augmente la viscosité du fluide caloporteur, ce qui augmente la possibilité d'avoir un écoulement laminaire entraînant une réduction du coefficient d'échange à l'intérieur des puits. Spitler et Ghelin (2015) ont mis en doute la recommandation de l'industrie voulant que le débit dans un puits doit être turbulent en tout temps et que les pertes de charge doivent être maintenues entre 1 et 3 pi_{H_2O}/100 pi de tuyau (10 à 29 kPa/100 m). Ils ont ainsi confirmé les affirmations de Kavanaugh (2011) selon qui un grand débit assurant un écoulement turbulent dans les puits peut nécessiter une puissance de pompage excessive en échange de peu de gains thermiques et économiques. Un débit plus faible engendrant un écoulement laminaire occasionnel est souvent préférable selon eux. Ils ont aussi confirmé la recommandation de Mescher (ASHRAE, 2011) à l'effet que la perte de charge dans les puits devrait être inférieure à 25 pi (75 kPa) pour une perte de charge totale de 50 pi (150 kPa) dans l'ensemble du circuit.

2.4 Réseaux de distribution à un tuyau

Dans un système géothermique centralisé, c'est-à-dire pour lequel un champ de puits alimente l'ensemble des pompes à chaleur d'un bâtiment, il est possible de distribuer le fluide caloporteur provenant des puits selon différentes stratégies. Les configurations à retour direct et à retour renversé, qui sont dites à deux tuyaux, sont communément utilisées. De plus, la configuration à un tuyau, moins fréquemment utilisée, constitue une autre option présentant plusieurs avantages (Boldt et Keen, 2015). Stethem (1994) a remis en lumière les systèmes à un tuyau, ces derniers ayant été communs vers 1950 puis délaissés (Stethem, 1995). Il a actualisé les avantages d'un réseau à un tuyau en réitérant les besoins réduits de tuyauterie et de valves par rapport aux systèmes à deux tuyaux. Il a également mentionné que les systèmes de pompes à chaleur à un tuyau peuvent s'avérer particulièrement efficaces dans des écoles ou des bâtiments ayant de nombreux étages.

Kavanaugh et McInerny (2001) ont ensuite étudié l'influence de la stratégie de pompage sur la consommation d'énergie des pompes. Suite à cette étude, Kavanaugh et al. (2003) ont conclu qu'un système décentralisé est plus efficace pour un bâtiment occupé moins de 60 heures par semaine. Selon leurs travaux, un système centralisé utilisant une pompe à vitesse variable est néanmoins un excellent candidat et demeure le plus efficace pour des bâtiments occupés plus de 60 heures par semaine.

Intégrant la dimension économique, Bernier et al. (2005) ont comparé le coût du cycle de vie de systèmes géothermiques centralisés et décentralisés. Selon leurs conclusions, les coûts reliés au pompage sont plus bas pour un système centralisé. Cependant, un système décentralisé coûte moins cher globalement, principalement à cause de la tuyauterie supplémentaire nécessaire dans un système centralisé.

Souhaitant améliorer les systèmes centralisés, Cunniff et Zerba (2006) ont conclu que les réseaux à un tuyau utilisant des circulateurs permettent d'acheminer le fluide où il est requis au lieu de le forcer à travers de nombreuses valves coûteuses et énergivores. Selon eux, de tels réseaux nécessitent moins de matériaux, d'énergie, et de coûts d'installation.

Mescher (2009) a vanté les avantages des systèmes de pompes à chaleur géothermiques à un tuyau. Il a mentionné qu'ils sont plus efficaces et moins coûteux, tout en étant plus simples à concevoir, installer et équilibrer. Il a conclu que l'installation des tuyaux pouvait coûter de 0.50 à 1.50 $ de moins par pied carré (1.60 à 4.90 $/m^2). Selon lui, un réseau à un tuyau est presque aussi efficace qu'un système décentralisé, d'autant plus qu'il profite de la diversité des charges pouvant réduire la longueur de puits requise.

À plus grande échelle, l'étude de systèmes géothermiques à un tuyau a démontré qu'ils ont obtenu les cotes Energy Star les plus élevées avec les systèmes décentralisés (Kavanaugh, 2011). Cette étude démontre aussi qu'un système à un tuyau est efficace lorsqu'il est ajouté lors de travaux de rénovations, ce qui a également été mentionné par Mescher (2009).

CHAPITRE 3 DÉMARCHE ET PERTINENCE DU TRAVAIL DE RECHERCHE

Ce projet permet de répondre à certaines questions que se posent les concepteurs de systèmes géothermiques et de remettre en question certaines pratiques de l'industrie.

3.1 Problématique et cohérence avec les objectifs

Les concepteurs évitent parfois d'intégrer des circulateurs à leurs systèmes puisqu'ils les considèrent comme des équipements peu efficaces. Cela biaise potentiellement leur analyse lorsqu'ils considèrent des systèmes décentralisés ou à un tuyau. Le Chapitre 4 étudie donc le rendement de circulateurs disponibles sur le marché. Il vise à dresser un portrait de leur efficacité afin de remettre les pendules à l'heure.

Ensuite, le dimensionnement des puits constitue une des étapes influençant le plus le coût d'une installation géothermique. Cependant, les méthodes de dimensionnement et de simulation actuelles ne considèrent pas la capacité thermique des puits. Cela peut donc surestimer la longueur de puits requise prescrite par le concepteur, ce qui rend l'option géothermique moins rentable. Le Chapitre 5 a du coup comme objectif de rendre compte des erreurs de dimensionnement occasionnées lorsque la capacité thermique des puits n'est pas considérée et d'évaluer l'erreur engendrée lorsque l'équation de dimensionnement de l'ASHRAE (Éq. 2.6) est utilisée.

De plus, le recours à une solution d'antigel comme fluide caloporteur peut avoir une grande influence sur les performances énergétiques d'un système. Cependant, les concepteurs en tiennent compte en se basant sur quelques facteurs de correction fournis par les manufacturiers. Le Chapitre 6 développe donc des techniques pour considérer l'influence de l'antigel sur les différentes composantes d'un système, ce qui améliore la précision des simulations. Une règle non écrite recommande aussi d'opérer en régime turbulent pour maximiser le transfert de chaleur dans les puits. Certaines études contredisent cette recommandation et ce chapitre vient corroborer leur conclusion.

Plusieurs études font également la promotion des réseaux de distribution interne munis d'un seul tuyau. Ces derniers sont moins communs mais présentent de nombreux avantages par rapport aux réseaux à deux tuyaux. Ils nécessitent notamment moins de matériaux. Leur performance

énergétique est cependant difficile à évaluer considérant la variation de température à l'entrée des différentes pompes à chaleur. À ce titre, il n'existe pas d'outil de simulation servant à conseiller les concepteurs à savoir quel réseau favoriser pour une situation en particulier. Le Chapitre 7 vise donc à développer un tel outil qui permet de comparer les performances énergétiques de différentes stratégies de distribution du fluide caloporteur.

3.2 Organisation du travail de recherche

Les différents chapitres principaux sont inter-reliés selon la logique suivante. Des circulateurs sont simulés dans les Chapitres 5, 6 et 7. Il apparaît donc pertinent de se pencher sur leur fonctionnement (Chapitre 4) avant de les simuler. Le Chapitre 5 démontre que la capacité thermique influence le comportement d'un puits géothermique simulé, ainsi que la consommation énergétique des pompes à chaleur. En conséquence, il est important d'étudier la question avant de simuler des puits dans les Chapitres 6 et 7. L'étude portant sur les fluides caloporteurs (Chapitre 6) vise à estimer le plus précisément possible la consommation énergétique d'un système. Le rendement du circulateur utilisé et la capacité thermique du puits influencent notamment ce résultat. Il est donc pertinent d'en tenir compte. L'étude des réseaux à un tuyau (Chapitre 7) est quant à elle intimement reliée au rendement des circulateurs (Chapitre 4) et aux calculs de pompage abordés au Chapitre 6. L'outil développé est également utilisé conjointement avec un modèle de puits considérant la capacité thermique (Chapitre 5). Ces quatre chapitres sont donc présentés dans un ordre logique et visent le même objectif global, soit l'amélioration de la conception des systèmes de pompes à chaleur géothermiques.

CHAPITRE 4 FONCTIONNEMENT ET RENDEMENT DES CIRCULATEURS

Les systèmes de mécanique du bâtiment utilisent des pompes afin d'acheminer des fluides entre les unités de production et d'utilisation d'énergie. Les petites installations ainsi que les grands systèmes décentralisés de distribution à un tuyau (one-pipe) ont recours à des circulateurs, qui sont simplement de petites pompes. Les systèmes à un tuyau utilisent un circulateur afin d'alimenter chaque unité (pompe à chaleur, ventilo-convecteur, etc.) en extrayant du fluide d'une boucle centrale puis en l'y réinjectant par la suite (voir Chapitre 7).

4.1 Modes de fonctionnement

Le fonctionnement d'un système est généralement représenté sur un graphique donnant la hauteur manométrique totale développée par la pompe (en mètre de fluide) en fonction du débit volumique. Lorsque le fluide est connu, il est possible de représenter le fonctionnement en remplaçant la hauteur manométrique totale par la pression différentielle tel que montré à la Figure 4.1.

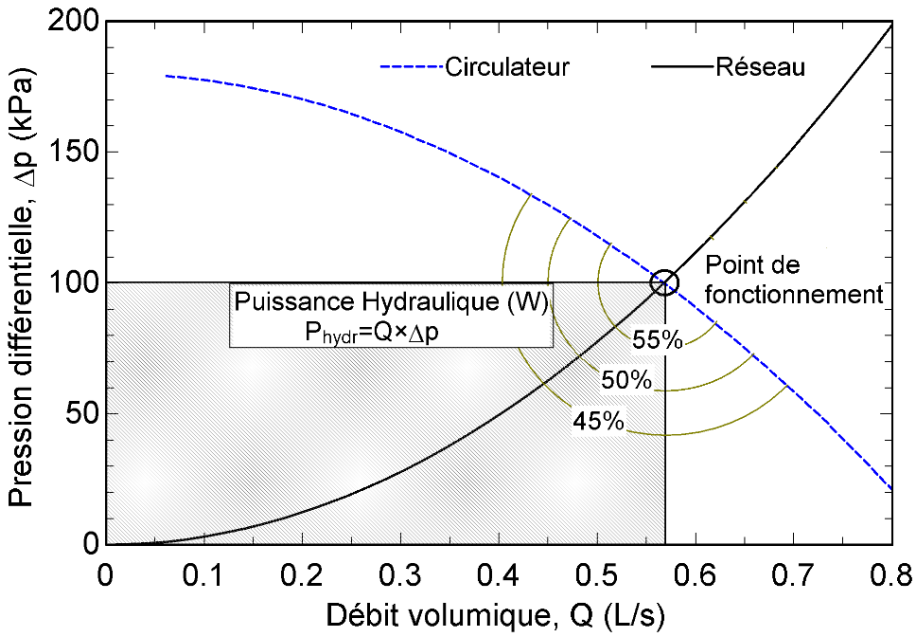

Figure 4.1 : Courbes typiques d'un réseau hydraulique et d'une pompe avec courbes d'iso-rendement

L'intersection entre la courbe du réseau hydraulique et la courbe caractéristique du circulateur constitue le point de fonctionnement du système. Le circulateur fonctionne en son point de meilleur rendement lorsque le point de fonctionnement se situe au centre des courbes d'iso-rendement. Le produit de la pression différentielle par le débit constitue la puissance hydraulique que fournit la pompe en ce point de fonctionnement.

Ensuite, lorsque la pression ou le débit requis par le système change, le fonctionnement du circulateur est modifié. À ce titre, les circulateurs opèrent selon quatre modes de fonctionnement différents dépendamment de leur construction et de leur application (COSTIC, 2010).

1. Vitesse fixe et pression différentielle variable
2. Vitesse variable avec maintien d'une pression différentielle constante
3. Vitesse variable avec maintien d'une pression différentielle proportionnelle au débit
4. Vitesse variable modulant le débit dans un réseau fixe

Les circulateurs à vitesse fixe subiront ces changements alors que ceux à vitesse variable s'y adapteront afin de réduire leur consommation électrique tout en maintenant un rendement acceptable. Cette adaptation se fait à l'aide d'un variateur de fréquence (VFD), qui modifie la vitesse de rotation de la pompe.

4.1.1 Vitesse fixe et pression différentielle variable

Ce mode de fonctionnement est le plus simple, mais aussi le moins versatile. Lorsque la hauteur manométrique d'un système varie, le fonctionnement de son circulateur à vitesse fixe change en se déplaçant le long de sa courbe caractéristique. Par exemple, si un robinet de réglage se ferme partiellement, la hauteur manométrique augmente. Cela engendre un nouveau point de fonctionnement sur la courbe caractéristique du système.

4.1.2 Vitesse variable avec maintien d'une pression différentielle constante

Ce mode de fonctionnement est utile lorsqu'un circulateur alimente plusieurs unités en parallèle. Si une unité n'est pas utilisée à un certain moment, une valve se ferme afin de ne pas l'alimenter inutilement. Le circulateur doit donc fournir un débit plus faible afin d'alimenter moins d'unités. Néanmoins, la pression requise par le réseau ne change pas car les branches parallèles ont la même perte de charge. Le circulateur peut donc réduire sa vitesse de rotation afin de réduire son débit

tout en maintenant une pression identique. Le point de fonctionnement du système se déplace alors horizontalement sur la Figure 4.1. Une puissance hydraulique plus faible est requise, réduisant la consommation d'énergie du circulateur.

4.1.3 Vitesse variable avec maintien d'une pression différentielle proportionnelle au débit

Ce mode de fonctionnement, semblable au précédent, est caractéristique d'un réseau plus complexe dans lequel, par exemple, plusieurs unités sont placées en série et en parallèle. Durant l'opération, ces derniers sont mis en marche ou arrêtés à l'aide de valves. La courbe caractéristique du système est ainsi modifiée et le circulateur adapte sa vitesse afin de fournir le débit requis. Un débit plus faible dans le réseau n'affecte pas la perte de charge des unités alimentées en parallèle mais réduit celle des unités en série et des tuyaux principaux. Une nouvelle pression différentielle est donc observée proportionnellement au débit.

4.1.4 Vitesse variable modulant le débit dans un réseau fixe

Si le réseau est constitué d'une ou de plusieurs unités qui peuvent fonctionner à capacité variable, le circulateur peut réduire sa vitesse, et donc son débit, afin de s'adapter aux besoins de l'unité. La hauteur manométrique de l'installation est du coup réduite puisque moins de débit y circule. L'intersection de la courbe du circulateur à vitesse réduite avec la courbe initiale du réseau résume le nouveau point de fonctionnement. Il est à noter que le débit fourni par un circulateur à vitesse variable ne peut descendre sous une limite basse sans quoi l'équilibrage du système sera perturbé.

4.2 Objectifs de l'étude de ce chapitre

L'étude présentée dans ce chapitre poursuit trois objectifs :

- Analyser le rendement des circulateurs actuellement sur le marché;
- Développer un outil permettant de prédire le rendement nominal d'un circulateur selon l'application;
- Étudier la variation du rendement d'un circulateur fournissant un débit inférieur ou supérieur à son débit nominal.

Le premier objectif est essentiel afin de donner l'heure juste aux concepteurs. Les concepteurs se basent sur d'anciennes études (ASHRAE RP1217, COSTIC) afin d'estimer le rendement des circulateurs, ce qui ne favorise pas leur utilisation. Kavanaugh et Rafferty (2015) présentent un guide pour classer la puissance électrique des pompes installées en fonction de la capacité d'un système géothermique (Tableau 4.1). Le recours à des circulateurs moins efficaces réduit cette cote, qui est souvent utilisée dans l'industrie. Cette situation peut être illustrée par un cas simple. Si le pompage d'un système de 10 kW (3 tons) consomme 260 W électrique, une cote de D lui est accordée. Si le rendement de la pompe est doublé, sa consommation baisse à 130 W, ce qui lui confère une cote de A et favorise son utilisation. Cette étude vise donc à rendre compte des progrès réalisés par les manufacturiers de circulateurs au cours des dernières années.

Tableau 4.1 : Guide pour la puissance de pompage des systèmes de pompes à chaleur géothermiques (Kavanaugh et Rafferty, 2015)

Puissance de pompage installée ($W_{pompe,hydr}/kW_{thermique}$)	**Puissance consommée par le pompage ($W_{pompe,élec}/kW_{thermique}$)**	**Cote (-)**
≤ 10.5	≤ 13	A
≤ 16	≤ 19	B
≤ 21	≤ 25	C
≤ 32	≤ 36	D
> 32	> 36	F

Le deuxième objectif du présent chapitre vise à permettre aux concepteurs d'estimer le rendement d'un circulateur en fonction de la perte de charge et du débit requis par une application quelconque. Considérant que l'énergie de pompage d'une installation géothermique peut représenter de 15 à 48% de sa consommation d'énergie totale (Liu et al., 2015), il est primordial de connaître le rendement des circulateurs afin d'estimer la consommation d'énergie d'une installation. La prédiction du rendement est aussi utile lors de la simulation énergétique d'une installation.

Le troisième objectif est également pertinent car il est rare que le point de fonctionnement d'un circulateur corresponde exactement au point de rendement maximal (aussi appelé « best efficiency point ») tel que montré à la Figure 4.1. Il est donc utile de pouvoir estimer la baisse de rendement occasionnée par l'utilisation d'un circulateur à un point autre que celui correspondant au rendement maximal.

4.3 Méthodologie

Dans le cadre de cette étude, une méthodologie semblable à celle du COSTIC (2003) a été suivie. Le rendement du fil à l'eau « nominal » de 86 circulateurs est obtenu à leur point de meilleur rendement. La puissance hydraulique nominale est également calculée pour chacun d'entre eux. Les données sont extraites de catalogues de manufacturiers (Grundfos, 2016) (Salmson, 2016). Il est à noter que ces données sont basées sur de l'eau à 60 °F (15.5 °C). Les résultats sont néanmoins valides pour des fluides ayant une viscosité semblable (Grundfos, 2016). Ensuite, le rendement de chaque circulateur en fonction de sa puissance hydraulique est placé sur un graphique et une régression entre ces deux variables est obtenue. Les détails de cette méthodologie sont donnés aux paragraphes suivants.

Le point de départ est la détermination de la hauteur manométrique nominale et du débit nominal correspondant au point de fonctionnement pour lequel le rendement est le plus élevé. Pour les circulateurs considérés dans cette étude, ces valeurs se retrouvent dans l'utilitaire de sélection de pompes des manufacturiers. La puissance hydraulique nominale est alors obtenue à l'aide de l'Équation 4.1 (en W).

$$P_{hydr} = \frac{HQ\rho g}{3600} \tag{4.1}$$

où H est en m, Q en m^3/h, ρ en kg/m^3 et g en m/s^2. L'Équation 4.2 est obtenue pour de l'eau avec une masse volumique de 1000 kg/m^3 et une accélération gravitationnelle de 9.81 m/s^2, comme c'est le cas dans cette étude.

$$P_{hydr} = 2.725HQ \tag{4.2}$$

Il est également possible d'obtenir la puissance hydraulique en multipliant directement une hauteur manométrique en kPa par un débit en L/s. De plus, il suffit de diviser une puissance hydraulique en W par 746 afin de la convertir en horsepower (hp). À titre d'exemple, la Figure 4.2 présente la puissance hydraulique pour différentes combinaisons de débit et de hauteur manométrique typiques aux circulateurs, et ce, selon les systèmes international et impérial.

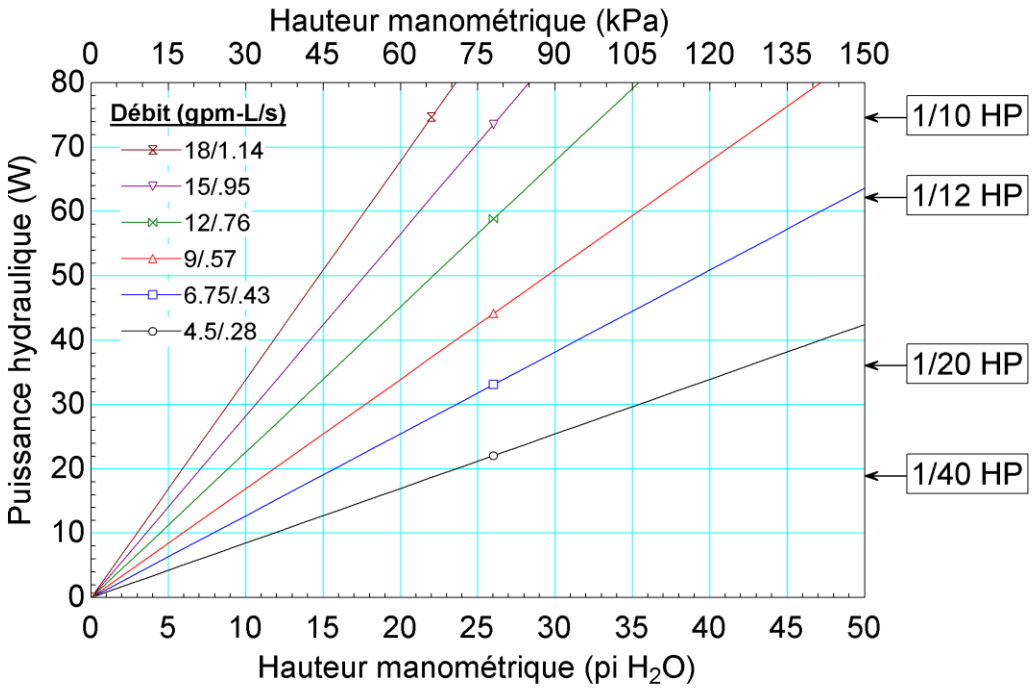

Figure 4.2 : Puissance hydraulique en fonction du débit et de la hauteur manométrique

Ensuite, la puissance électrique requise par chaque circulateur à son point de fonctionnement nominal est notée. Cette puissance est la puissance totale requise par la pompe, le moteur et le variateur de vitesse le cas échéant. Avec ces deux puissances, le rendement nominal du circulateur, η_{nom}, peut être calculé en utilisant l'Équation 4.3.

$$\eta_{nom} = \frac{P_{hydr}}{P_{élec}} \tag{4.3}$$

Il est à noter que, dans le cadre de cette étude, le rendement global au point nominal est également fourni par les manufacturiers en plus de la puissance électrique. Ce rendement, très semblable à celui obtenu avec l'Équation 4.3, est celui qui a été utilisé dans la présente étude. Le Tableau 4.2 présente un exemple de données obtenues pour trois circulateurs.

Ensuite, afin d'étudier la sensibilité du rendement des circulateurs en fonction du débit, le rendement a été obtenu à partir des utilitaires de sélection de pompes des manufacturiers pour des débits correspondants à 75% et 125% du débit nominal. Le rendement des circulateurs est ainsi obtenu pour trois débits.

Tableau 4.2: Exemple de données de circulateurs opérant au point de fonctionnement nominal

Débit volumique (m^3/h)	**Hauteur manométrique (m)**	**Puissance hydraulique (W)**	**Puissance électrique (W)**	**Rendement total (%)**
1.97	4.73	25.4	50.1	50.6
5.08	5.86	81.1	138.9	58.3
15.3	3.87	161.4	246.2	65.5

4.4 Résultats

4.4.1 Rendement nominal

La Figure 4.3 présente le rendement des circulateurs en fonction de leur puissance hydraulique (0-300 W). Cette figure a été reproduite d'un article écrit en anglais et présenté au Chapitre 6. Ce rendement est le rendement global du fil à l'eau (wire-to-water) et comprend le rendement de la pompe, du moteur et du variateur de fréquence si présent. Les circulateurs ont été séparés en trois catégories en fonction de leur efficacité. C'est ainsi que les catégories « Best Efficiency », « High Efficiency » et « Low Efficiency » ont été établies. Cette classification est basée sur la position des points sur le graphique, qui suivent trois tendances, ainsi que sur les gammes proposées par les manufacturiers. Par exemple, si tous les circulateurs de la gamme A du manufacturier B sauf un se retrouvent dans la catégorie « High Efficiency », ce dernier est également considéré dans cette classe pour respecter la gamme du manufacturier. Ces trois classes sont utilisées sur la Figure 4.3. Il apparaît donc que les circulateurs ont pour la plupart des rendements supérieurs à la valeur de 25% citée par Kavanaugh et Rafferty (2015).

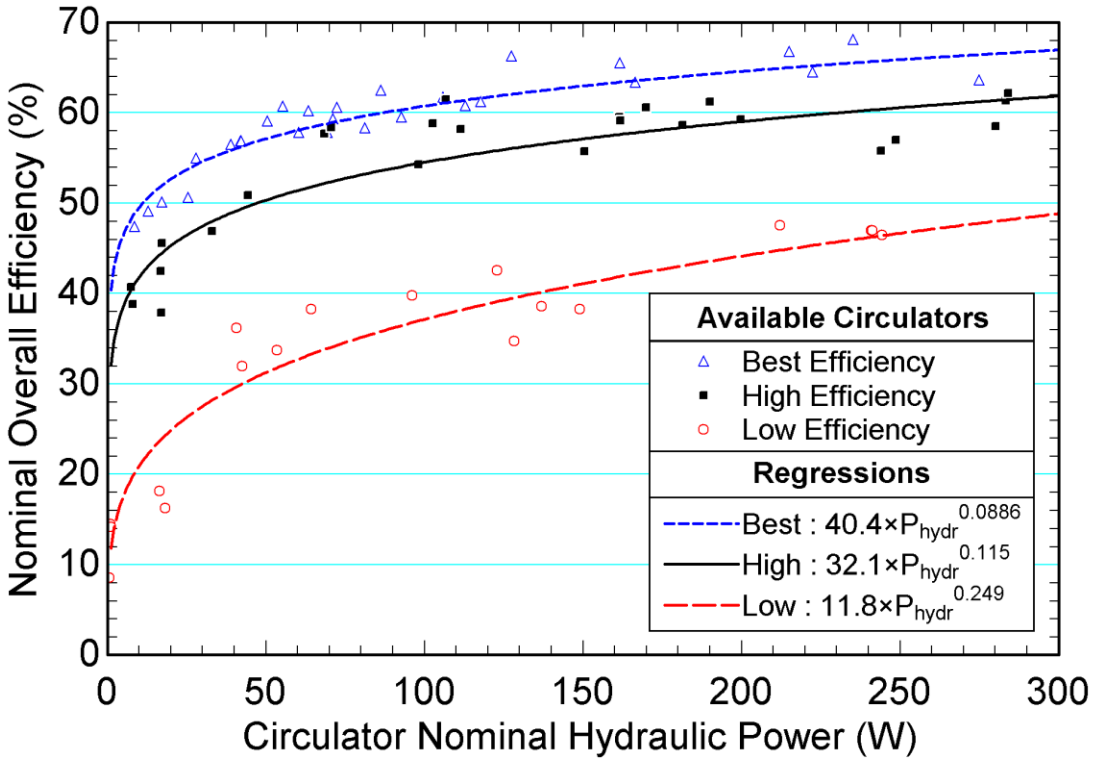

Figure 4.3 : Rendement nominal de circulateurs en fonction de leur puissance hydraulique

Pour chacune des trois catégories de circulateurs, une régression donnant le rendement (en %) en fonction de la puissance hydraulique a été ajoutée à la Figure 4.3. Ces régressions sont reproduites aux Équations 4.4, 4.5 et 4.6. Il est à noter que les trois corrélations possèdent un coefficient de régression R^2 de 0.89, 0.86 et 0.91, respectivement.

$$\eta_{best} = 0.404 {P_{hydr}}^{0.0886} \tag{4.4}$$

$$\eta_{high} = 0.321 {P_{hydr}}^{0.115} \tag{4.5}$$

$$\eta_{low} = 0.118 {P_{hydr}}^{0.249} \tag{4.6}$$

Il est intéressant de noter qu'aucun circulateur de la présente étude ne possède un rendement inférieur à la courbe du COSTIC (2003) présentée à la Figure 2.1. Cette dernière résume le rendement moyen des circulateurs au début des années 2000. Les circulateurs à haute efficacité actuels (High Efficiency) sont généralement plus performants que le rendement prédit par l'étude allemande de Ludwig et Roth (2008) servant de référence à la norme EuP (Figure 2.1). Cela

témoigne de la volonté des manufacturiers, principalement européens, de respecter et de surpasser cette norme.

4.4.2 Rendement à un autre débit

Tel que mentionné précédemment, le rendement des circulateurs a été évalué pour trois débits: débit nominal, débit nominal -25%, et débit nominal +25%. Chaque nouvelle puissance hydraulique équivalente a également été calculée. Ces données sont présentées sur les Figures 4.4 et 4.5. La Figure 4.4 présente les circulateurs « Best Efficiency » alors que la Figure 4.5 présente les circulateurs « Low Efficiency ». L'analyse des circulateurs « High Efficiency » engendre des résultats similaires à ceux des circulateurs « Best Efficiency » et n'est donc pas présentée. Pour chaque figure et pour chaque groupe de débit, une régression du rendement en fonction de la puissance est tracée. Que le débit soit 25% plus élevé ou 25% plus faible que le débit nominal, le rendement est toujours inférieur au rendement nominal. La régression « Best Efficiency » pour un débit 25% plus élevé a un coefficient $R^2 = 0.92$ alors que $R^2 = 0.86$ pour un débit 25% plus faible. Finalement, les valeurs correspondantes pour les circulateurs « Low Efficiency » sont $R^2 = 0.93$ et 0.91, respectivement. À titre d'exemple de l'utilisation de la Figure 4.4, un rendement de 59% est prédit pour une puissance hydraulique de 150 W et un circulateur fournissant un débit 25% plus faible que son débit nominal.

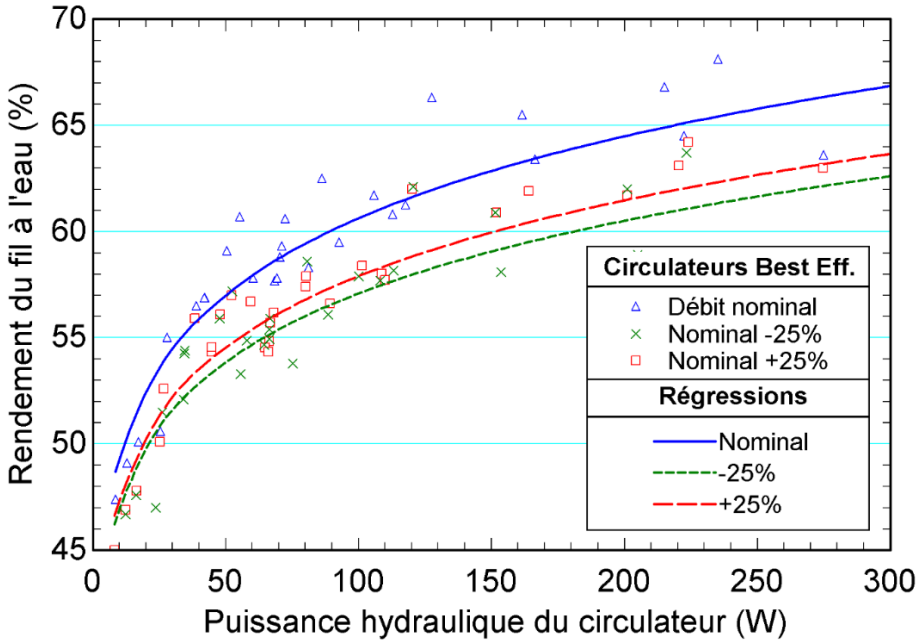

Figure 4.4 : Rendement des circulateurs Best Efficiency à leurs débits nominal, inférieur de 25% et supérieur de 25%

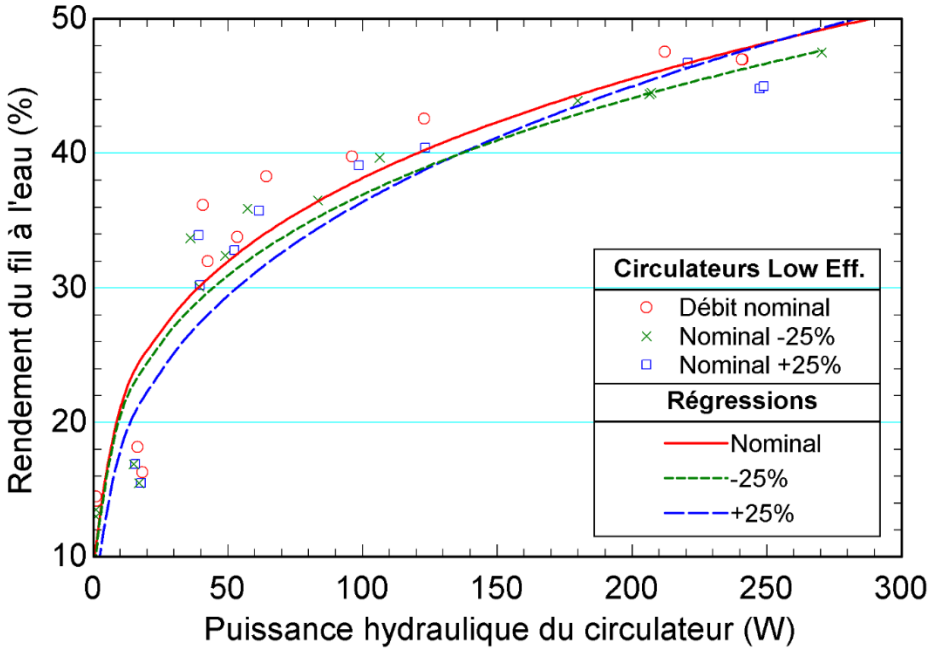

Figure 4.5 : Rendement des circulateurs Low Efficiency à leurs débits nominal, inférieur de 25% et supérieur de 25%

La Figure 4.6 présente la baisse de rendement relative au rendement nominal des circulateurs Low, High et Best Efficiency en fonction de leur puissance hydraulique nominale pour les cas où le débit est diminué ou augmenté de 25%. Si le circulateur fournit un débit 25% plus faible par rapport à son débit nominal, le rendement global diminue de 4 à 9%. Si le circulateur fournit un débit 25% plus élevé, le rendement global diminue de 1 à 8%.

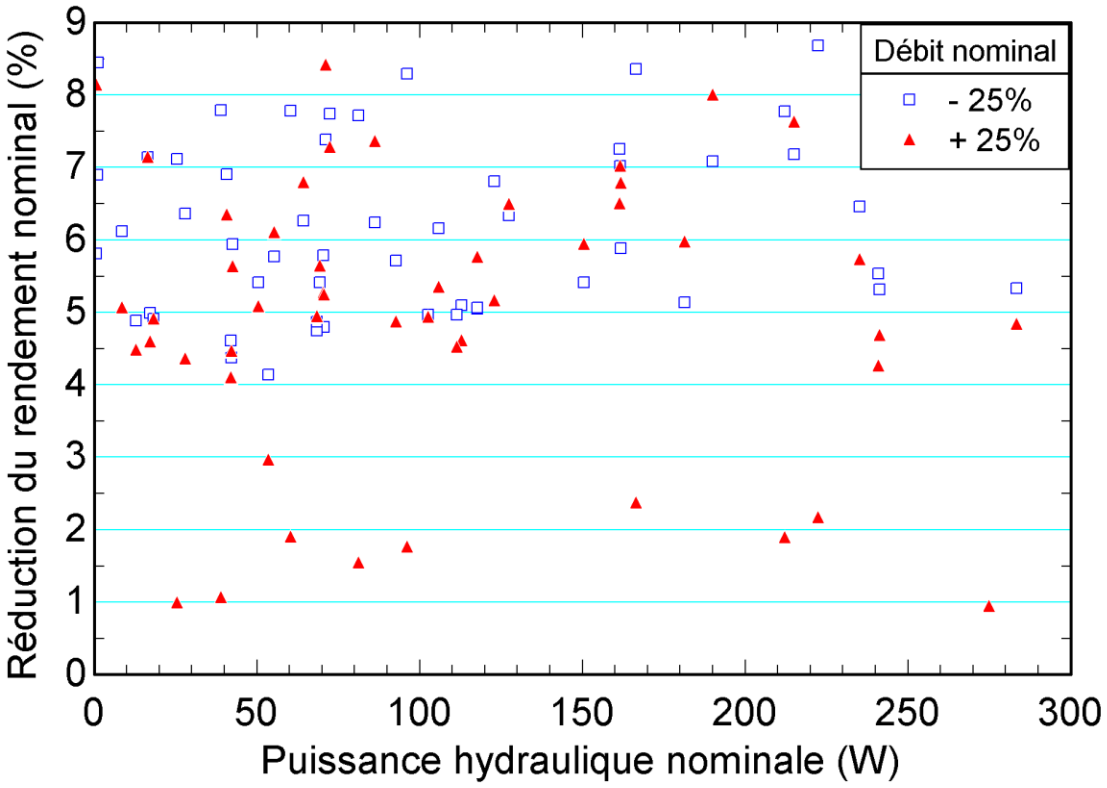

Figure 4.6 : Diminution du rendement des circulateurs Low, High et Best Efficiency par rapport à leur rendement nominal pour un débit 25% plus élevé ou plus faible que leur débit nominal

Cependant, aucune tendance ne se dégage et il n'est pas possible d'établir une corrélation claire qui prédirait la baisse du rendement selon la puissance hydraulique ou le débit. Les plages de pourcentages présentées plus haut permettent néanmoins de corriger approximativement le rendement d'un circulateur, qu'il soit obtenu avec les corrélations présentées aux Équations 4.4 à 4.6 ou directement à partir des données du manufacturier.

CHAPITRE 5 ARTICLE 1 : ACCOUNTING FOR BOREHOLE THERMAL CAPACITY WHEN DESIGNING VERTICAL GEOTHERMAL HEAT EXCHANGERS

Soumission :

Article de conférence accepté par l'ASHRAE dans le cadre de la 2016 ASHRAE Annual Conference, tenue du 25 au 29 juin 2016 à St-Louis, Missouri, États-Unis.

Auteurs :

- Laurent Gagné-Boisvert, Candidat M. Sc.A.
- Michel Bernier, Ph. D.

Présentation :

Laurent Gagné-Boisvert, 27 juin 2016, 2016 ASHRAE Annual Conference, St-Louis, MO, États-Unis

Référence :

Gagné-Boisvert, L., and M. Bernier. 2016. Accounting for Borehole Thermal Capacity when Designing Vertical Geothermal Heat Exchangers. *Presented at the 2016 ASHRAE Annual Conference*, St-Louis, MO, United States, June 25–29. Paper ST-16-C027.

5.1 Abstract

Steady-state heat transfer inside boreholes is usually assumed when sizing geothermal boreholes and a constant borehole thermal resistance is used to calculate the temperature difference from the fluid to the borehole wall. Thus, heat rejected into the fluid is assumed to be transferred immediately at the borehole wall. In reality, rejected heat will heat the fluid and the grout first before reaching the borehole wall and be transferred to the ground. These transient effects, caused by the fluid and grout thermal capacities, are beneficial as they reduce the peak ground loads and, consequently, the required borehole length. In the first part of this study, simulations are performed

on a residential ground-source heat pump system to quantify borehole transient effects. Then, correction factors for the current ASHRAE sizing equation are proposed to consider borehole thermal capacity. Results show that neglecting borehole transient effects leads to oversized boreholes and may overestimate heat pump energy consumption by about 5 %. A parametric study performed on several types of boreholes shows that the correction factor to the ASHRAE sizing equation varies from 0.69 to 1.24 for those particular cases. Correction factors below one are typically associated with oversized heat pumps which lead to intermittent heat pump operation and maximize the use of the borehole thermal capacity.

5.2 Introduction

The magnitude and duration of peak loads are important when sizing vertical geothermal boreholes. In the ASHRAE sizing equation for vertical geothermal boreholes, represented in a simplified form in Equation 5.1 (ASHRAE, 2015), the required length L is determined based on a sum of loads multiplied by equivalent thermal resistances divided by a temperature difference (mean fluid temperature in the borehole minus the undisturbed ground temperature). The second and third terms in this equation represent the contribution of the annual mean ground load, q_y, and peak monthly load, q_m, multiplied by their respective equivalent thermal resistance, R_{10y} and R_{1m}. The peak ground load, q_h, is present in the first and fourth terms in the numerator. In the first term, q_h multiplies R_b, an equivalent borehole thermal resistance from the fluid to the borehole wall. In the fourth term, q_h multiplies an equivalent ground thermal resistance, R_{6h}, which is typically based on a peak duration of 6 hours.

$$L = \frac{q_h R_b + q_y R_{10y} + q_m R_{1m} + q_h R_{6h}}{\frac{T_{inHP} + T_{outHP}}{2} - T_g} \tag{5.1}$$

For a residential system such as the one depicted in Figure 5.1, the peak ground load is determined based on the amount of heat rejected (or collected) by the heat pump for a given inlet fluid temperature, T_{inHP}. In ASHRAE's sizing equation, the peak ground load is assumed to be transferred immediately at the borehole wall. With reference to Figure 5.1, this means that q_b is equal to q_h. The temperature difference between the mean fluid temperature in the borehole and the borehole wall temperature is obtained using a steady-state borehole thermal resistance, R_b. In reality, when there is a change in the value of q_h, there is a time lag before q_b reaches q_h. During

that period, $q_b < q_h$ and R_b has not yet reached a steady-state value. Heat is stored in the borehole, due to the thermal capacity of the fluid and grout, before being released at the borehole wall. This transient period can last several hours depending on the characteristics of the borehole and cycling behavior of the system. The effects of the borehole thermal capacity are intimately linked to the operation of the heat pump. The heat pump will reject (or collect) heat as long as it operates. The period of operation will depend on the degree of oversizing of the heat pump. If the heat pump is undersized, it may run for more than the 6 hours suggested in Eq. 5.1. Conversely, an oversized heat pump will operate intermittently and will run for less than 6 consecutive hours.

In summary, borehole thermal capacity and heat pump sizing have an effect on the value of q_h and R_b in Equation 5.1. The objective of this paper is to quantify the combined effect of borehole thermal capacity and heat pump cycling on boreholes sizing. The paper is organized as follows. A literature review on the importance of borehole thermal capacity and some basic principles of borehole transient effects are presented first. Then, annual simulations of a residential ground-source heat pump (GSHP) system are performed with and without fluid and grout thermal capacities to determine the required length and heat pump energy consumption differences. Finally, simulations for various heat pump oversizing and several types of boreholes are performed. A borehole thermal capacity correction factor for the ASHRAE borehole sizing equation is then presented.

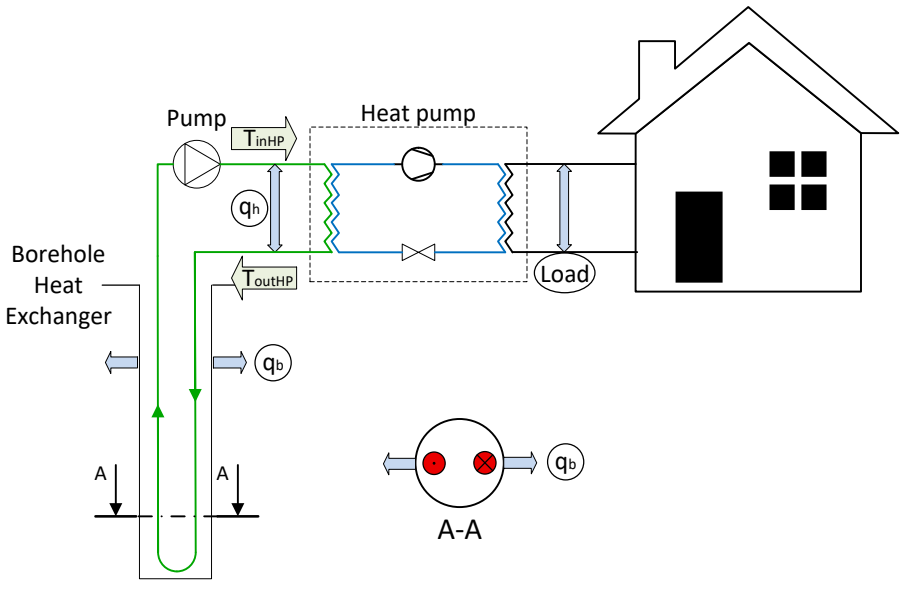

Figure 5.1 : Schematic representation of the simulation setup and heat transfer rates

5.3 Literature review

Hellström (1991) was perhaps the first author to discuss borehole thermal capacity. He explained that fluid thermal capacity plays an important role under a time t_b equivalent to $5\ r_b^2/\alpha$, where r_b is the borehole radius and α is the ground thermal diffusivity. This corresponds to about 2-3 hours for typical boreholes and longer for boreholes with small thermal diffusivities and large bore radius. During that time, a relatively large part of the thermal load entering the borehole is absorbed by the fluid instead of being instantly transferred to the ground.

Kavanaugh and Rafferty (1997), in their GSHP design guide, considered a constant equivalent bore thermal resistance R_b. They stated that the thermal mass of the grout, pipes and liquid are too small when compared to the adjacent ground to be considered. This formed the basis of the steady-state borehole heat transfer assumption used in the current ASHRAE sizing equation. The alternative sizing equation introduced in the 2015 handbook also assumes a steady-state borehole thermal resistance.

Young (2004) developed the borehole fluid thermal mass model (BFTM), a borehole model accounting for fluid and grout thermal mass. He compared the results of simulations using a classic steady-state model and his dynamic model. Relatively large differences in the outlet fluid temperature are obtained (1.3 °C/2.3 °F), especially with short peak load cases. He also concluded that yearly energy performance is correctly estimated by the use of a steady-state model. Xu and Spitler (2006) developed a one-dimensional borehole model accounting for fluid thermal mass. They noted that fluid thermal capacity has a tendency to damp outlet fluid temperature peaks. Their work used short time-step response factors, based on a model accounting for borehole thermal mass (Yavuzturk and Spitler, 1999).

Salim-Shirazi and Bernier (2013) also developed a one-dimensional transient ground heat exchanger model accounting for fluid and grout thermal capacities. They replaced the two-pipe geometry with an equivalent cylinder but kept the thermal mass of the fluid and grout intact. It has been used to perform short-time and annual simulations. They stated that neglecting borehole thermal capacity always leads to lower outlet fluid temperature in heating mode. The difference is more important as heat pump operates intermittently. Their results show that the predicted annual heat pump Coefficient of Performance (COP) is underestimated by an average of 4.5%.

Parisch et al. (2015) developed a pre-pipe model accounting for the fluid and grout thermal capacities. This pipe is located upstream of the borehole. It is coupled with a conventional steady-state borehole model to simulate its dynamic behavior. Residential simulations performed with the pre-pipe increased the seasonal performance factor of the GSHP system from 2.5 up to 3.5 and reduced the required length from 110 to 90 m (361 to 295 ft).

Ma et al. (2015) used their quasi-3D model, which is based on effective overall thermal resistances, to modify the resistance terms in the ASHRAE sizing equation. This model considers the grout heat capacity and evaluates ground heat transfer with the full-scale g-functions. This approach leads to slightly shorter boreholes, especially when the daily peak pulse has a short duration (1-3 hours). This method is also more accurate to size short boreholes.

Godefroy and Bernier (2014) developed a thermal resistance and capacity model (TRCM) and implemented it in the TRNSYS environment. This model considers the fluid and grout thermal capacities. It has been experimentally validated (Godefroy et al., 2016). Annual energy simulations showed that heat pump energy consumption can be overestimated by 3 % when thermal capacity is neglected. They also concluded that the grout thermal capacity has a minor effect and that the fluid thermal capacity is the dominant parameter. Finally, it should be noted that the most commonly used model for simulating bore fields, the so-called Duct ground Storage (DST) model (Hellström et al., 1996), assumes a steady-state condition in the borehole and uses a constant borehole thermal resistance.

5.4 Thermal capacity effects

The thermal capacity of a typical borehole with a 15 cm (6 in) diameter and a length of 150 m (492 ft) is in the order of 9 MJ/K (4.7 kBTU/°F). Thus, a power injection of 2.5 kW (8.5 kBTU/hr) during one hour will increase the average borehole temperature by 1 K (1.8 °F).

In this section, two simple cases are examined to quantify the difference between q_h and q_b when boreholes are subjected to varying conditions. The main characteristics of the borehole are given in Table 5.1.

Table 5.1 : Main characteristics of the borehole

Parameter	S.I. Value	S.I. Unit	I.P. Value	I.P. Unit
Depth	180	m	591	ft
Borehole diameter	0.15	m	6	in
Inside pipe radius	0.013	m	0.51	in
Outside pipe radius	0.016	m	0.63	in
Borehole thermal resistance	0.182	m.K/W	0.315	hr.ft.°F/BTU
Grout conductivity	0.83	W/m.K	0.48	BTU/hr.ft.°F
Grout thermal capacity	3000	$kJ/m^3.K$	44.7	$BTU/ft^3.°F$
Ground thermal conductivity	2.2	W/m.K	1.27	BTU/hr.ft.°F
Ground thermal diffusivity	0.096	m^2/day	0.94	ft^2/day
Fluid thermal capacity	3.87	kJ/kg.K	0.924	BTU/lbm.°F
Pipe conductivity	0.42	W/m.K	0.24	BTU/hr.ft.°F
Flowrate	0.56	L/s	9	gpm

Simulations are performed using TRNSYS and the TRCM model of Godefroy (2014). This model discretizes the borehole in a series of thermal resistances and capacitances much like in a finite difference approach but with a relatively coarse grid so as to make computational cost reasonable when performing annual simulations. This model has been verified with other borehole models that include thermal capacity and validated against experimental results (Godefroy, 2014 and Godefroy et al., 2016). Furthermore, simulations were also performed with the DST model (Hellström et al., 1996) for cases when thermal capacity is neglected. The results obtained with the DST model were in excellent agreement with the TRCM when the fluid and grout thermal capacities are artificially set to a very small value. A root-mean-square error (RMSE) of 0.083 K (0.15 °F) for the outlet fluid temperature and of 0.078 kW (0.27 kBTU/hr) for the heat transfer rate were obtained for the data presented in Figure 5.2.

In the first case, the borehole is subjected to three hourly heat collection rates, q_h, of 2, 4, and 8 kW (6.8, 13.6 and 27.3 kBTU/hr) followed by a 3-hour recovery phase where q_h = 0. This results in a total extraction of 14 kWh (48 kBTU) over a 6-hour period. Simulation results, performed with a 36 second time step (0.01 hr), are shown in Figure 5.2. The top curve shows that q_b is lower than q_h when thermal capacity is accounted for. For example, at t = 3 hours, $q_b \approx$ 4.4 kW (15 kBTU/hr) while q_h = 8 kW (27.3 kBTU/hr). Thus, for this condition, 4.4 kW (15 kBTU/hr) are taken from the ground and 3.6 kW (12.3 kBTU/hr) are extracted from stored energy in the borehole. During the first three hours, about 9 kWh (31 kBTU) have been retrieved from the borehole. For t > 3

hours, q_h = 0, but q_b is non zero (for example, at t = 6 hours, $q_b \approx$ 0.7 kW (2.4 kBTU/hr)). Heat is thus being transferred from the ground to thermally "regenerate" the borehole.

As shown on the bottom graph of Figure 5.2, the outlet fluid temperature decreases at a much slower rate with borehole thermal capacity. At t = 3 hours, $T_{inHP} \approx$ 4 °C (39 °F) when borehole thermal capacity is considered. The corresponding value without borehole thermal capacity is ≈ 1 °C (34 °F). These lower outlet fluid temperature predictions when borehole thermal capacity is neglected have an impact on the heat pump COP and on the required borehole length as it will now be shown.

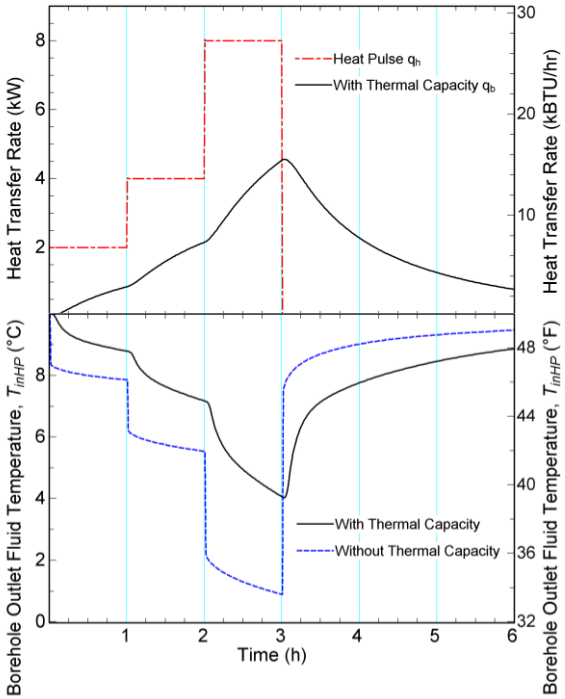

Figure 5.2 : Heat transfer rate (top) and borehole outlet fluid temperature (bottom) for 3 hourly heat extraction pulses and a 3-hour recovery period for borehole models with and without thermal capacity

To evaluate the required borehole length with and without borehole thermal capacity, dynamic simulations using TRNSYS v17 (Klein et al. 2010) are performed with a 6-minute time step, small enough to capture transient effects in the borehole. The system under study is the one presented in Figure 5.1 and consists of a 3-ton (10.5 kW) water-to-air ground-source heat pump providing space heating for a single-family house. The house is simulated in a heating dominated climate (Montreal, Canada). For the present case, the heat pump is oversized by 50 % giving an effect coverage of 150

%. The effect coverage is defined here as the heat pump capacity at peak load conditions divided by the building peak load. The house loss coefficient is set to have a peak load of 5.4 kW (kBTU/hr) and an annual heating energy requirement of 14 500 kWh. The energy performance and temperatures of the system are obtained by running 10 years + 1 month + 6 hours simulations (88350 hours) in accordance with the duration of the three ground heat pulses of the ASHRAE sizing equation (Eq. 5.1). Typical models found in TRNSYS for the house (Type 88), heat pump (Type 919) and thermostat (Type 108) are used. The main characteristics of the borehole are given in Table 5.1. The TRCM borehole model from Godefroy and Bernier (2014) is used to model the single U-tube borehole. The intent of these simulations is to find the required length which gives a minimum heat pump inlet temperature equal to 0 °C (32 °F).

Table 5.2 : Sizing with and without thermal capacity

Calculation method	**Thermal capacity**	**Minimum value of T_{inHP}**	**Required length**	**Annual heat pump energy consumption**	**Relative heat pump energy consumption**
		°C/°F	**m/ft**	**(kWh)**	**(-)**
Simulations	No	0 °C (32 °F)	156/512	5 853	1.0
Simulations	Yes	1.5 °C (34.7 °F)	156/512	5 460	0.93
Simulations	Yes	0 °C (32 °F)	131/430	5 586	0.95
Eq. 1 (ASHRAE)	No	0 °C (32 °F)	180/591	-	-

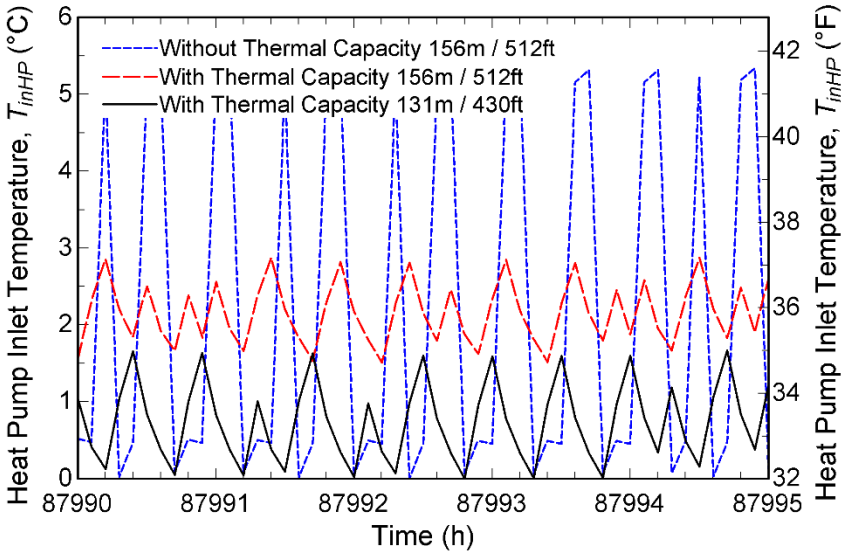

Figure 5.3 : Heat pump inlet temperature for models with and without thermal capacity

Results are summarized in Table 5.2 for four cases. The three first cases are also presented in Figure 5.3 where only the hours near the peak ground loads are shown, i.e. from t = 87990 to 87995 hours, with approximately two on-off heat pump cycles per hour. In the first simulation, borehole thermal capacity is neglected and a borehole length of 156 m (512 ft) is required to reach the minimum setpoint of 0 °C (32 °F) for the inlet temperature. With each heat pump cycle, the inlet fluid temperature oscillates over a ≈ 5.5 °C (10 °F) range. For the second case, the borehole length is kept at 156 m (512 ft) and simulations are run with borehole thermal capacity. Temperature oscillations are reduced down to about ≈ 1 °C (1.8 °F) and the borehole is clearly oversized as the minimum heat pump inlet temperature is ≈ 1.5 °C (≈ 34.7 °F). Finally, if the heat pump inlet temperature is allowed to reach a value of 0 °C (32 °F) then the required borehole length is 131 m (430 ft). This constitutes a length reduction of 16 % when compared to the first case. On the heat pump side, there is a 5 % difference in the energy consumption between the first and third cases. Thus, properly sizing a borehole by considering its thermal capacity can reduce the required length and the predicted energy consumption. As noted on the last line of Table 5.1, the ASHRAE sizing equation (Eq. 5.1) gives a length of 180 m (592 ft), which is longer than the dynamic sizing neglecting thermal capacity (156 m/512 ft). This is because the peak hourly load q_h lasts less than the 6 hours considered in the ASHRAE equation.

5.5 Corrections to the ASHRAE sizing equation

The actual sizing equation presented by ASHRAE (Eq. 5.1) does not consider the energy stored in the borehole (fluid and grout). Also, the sizing equation assumes that the peak load is constant for 6 consecutive hours. This case only happens if the heat pump is undersized and runs continuously at peak conditions. Most often, the heat pump will operate intermittently during the 6 hour period and borehole thermal capacity will be beneficial in that it will reduce the length requirement.

Several simulations with different operating conditions are performed to quantify the sizing error made when neglecting borehole thermal capacity and heat pump size. Much like results presented in Figure 5.3, simulations are performed over 10 years, 1 month and 6 hours, ending with the day with the peak conditions. In the simulations, the length is adjusted until T_{inHP} reaches 0 °C (32 °F). The required length according to the ASHRAE equation is also determined for each case. The hourly, monthly and annual ground pulses are obtained using the results of the dynamic simulations. The annual and monthly ground pulses are the average of the first ten years and of the

last month of operation, respectively. The hourly peak is determined as the highest heat pump extraction rate, occurring during the last month of operation.

Three main parameters are varied: i) Effect coverage (i.e. heat pump undersizing/oversizing); ii) Flowrate; iii) High/low ground and grout thermal conductivities and bore diameter. The effect coverage is varied from 50 % to 150 %. To modify the effect coverage, the peak load is changed by adapting the building heat loss coefficient. Thus, the same 3-ton heat pump unit is used in all simulations. For undersized heat pumps (effect coverage < 100 %), a two-stage auxiliary electrical system is added to the heat pump, each with a capacity equal to half the difference between peak load and heat pump capacity. Two flowrates are used, 0.28 and 0.56 L/s (4.5 and 9 gpm), representing flowrates of 1.5 and 3.0 gpm/ton. Finally, two types of boreholes are simulated. The first borehole, referred to as borehole B, is the one described in Table 5.1. It is considered to have low thermal conductivities for both the borehole and the ground. Borehole A has the same characteristics as the one presented in Table 5.1 except that it is located in a more conductive ground (3.5 W/m.K or 2 BTU/hr.ft.°F), it has a smaller borehole diameter of 0.1 m (4 in) and a grout conductivity of 2.1 W/m.K (1.2 BTU/hr.ft.°F) with a corresponding steady-state borehole thermal resistance, R_b, of 0.074 m.K/W (0.13 hr.ft.°F/BTU). Borehole B' is also examined with a 1.5 in diameter pipe (0.019 m inside pipe radius) and a R_b value of 0.22 m.K/W (0.39 hr.ft.°F/BTU). Finally, two B boreholes are evaluated in parallel and in series configurations for cases where it is cheaper to drill two shallow holes instead of a deeper one. For the parallel setup, the 4.5 and 9 gpm flowrates (0.28 and 0.56 L/s) are split equally in both boreholes.

Results are presented in Figure 5.4 in a form of a correction factor, F_{corr}, defined as the ratio between the length determined by dynamic simulations and the length calculated using the ASHRAE equation.

$$F_{corr} = \frac{L_{dynamic\ simulation}}{L_{ASHRAE}} \tag{5.2}$$

As shown on Figure 5.4, the correction factor varies from 0.69 to 1.24 for the four combinations studied here. In all cases, the value of F_{corr} decreases as the effect coverage increases. When the heat pump is 25-50 % oversized (i.e. effect coverage of 125-150 %), the ASHRAE equation overestimates the length. This is because the heat pump operates intermittently, even during the peak load period. Consequently, the hourly ground load, q_h, does not last 6 hours as is typically

the case in Eq. 5.1 and the thermal capacity effects are more pronounced. For an effect coverage of 50 to 100 %, the heat pump is operating continuously for 5 to 100 hours during peak load. This is illustrated in Figure 5.5 which shows the house load during the last month of the simulation for the 50 % effect coverage case. Considering that the 3-ton heat pump has an 8 kW (27.3 kBTU/hr) capacity at peak conditions, it is clear that the heat pump will work continuously for more than 6 hours. For example, the house load is above the heat pump capacity for more than 100 hours around t = 88000 h. For those cases, the duration of the hourly ground load in the ASHRAE equation is too short, which underestimates the required length. The equation also neglects thermal capacity effects, which overestimate required length. These effects influence the correction factor in opposite directions.

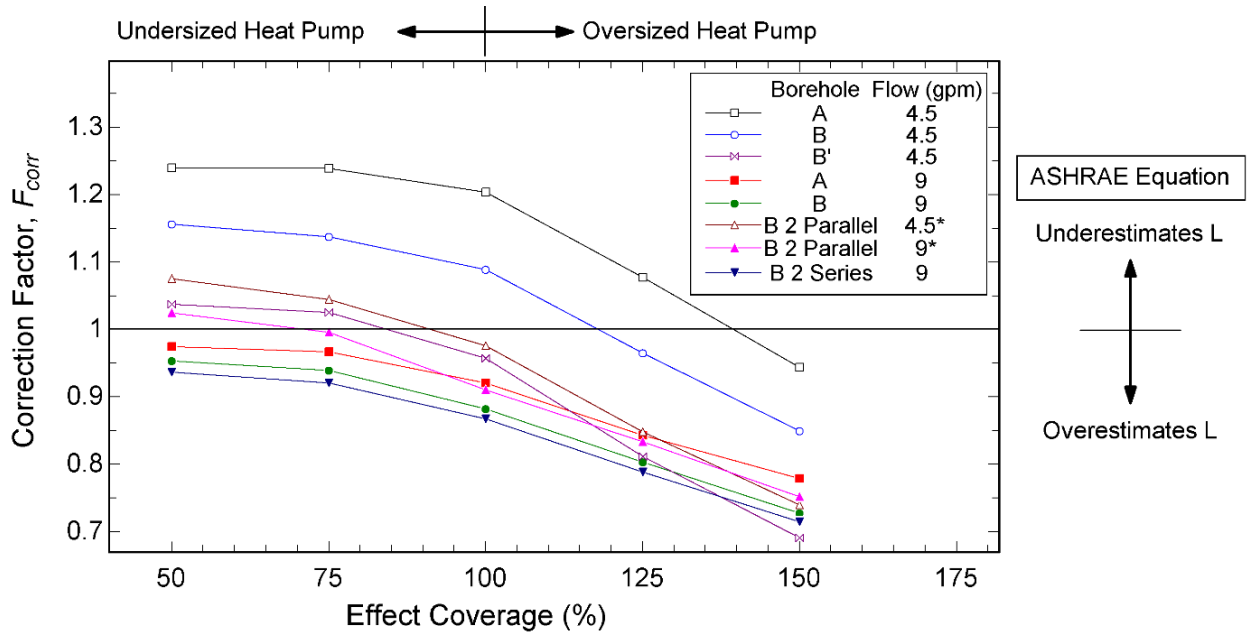

Figure 5.4 : Correction factor to modify the ASHRAE sizing equation for boreholes A (4 in. diameter, high conductivities), B (6 in. diameter, low conductivities) and B' (1.5 in. pipe). Note: 4.5 and 9 gpm stand for 0.28 and 0.56 L/s. For the two boreholes in parallel, * stands for the total flow in both boreholes

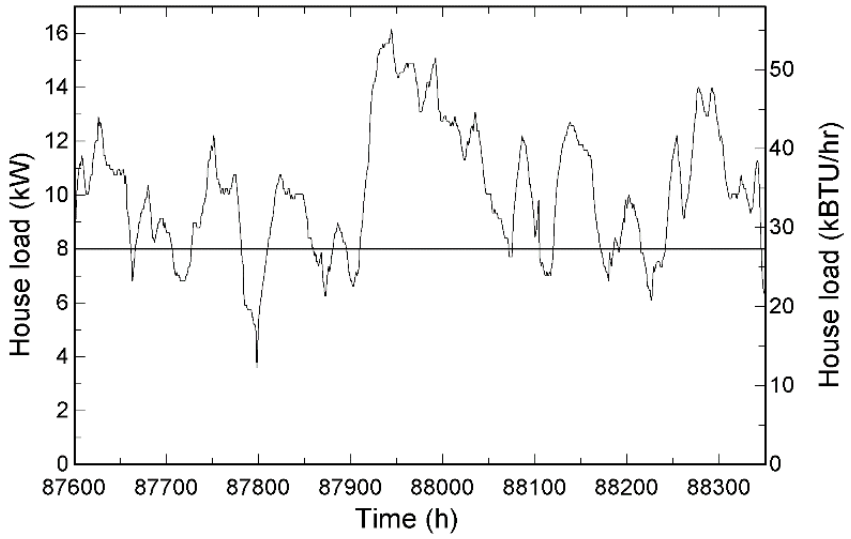

Figure 5.5 : House peak load for the 50 % effect coverage case during the last month after 10 years of simulation. The horizontal line is the heat pump capacity

The flowrate has also a significant impact on F_{corr}, which decreases as the flowrate increases. A larger flowrate (more gpm/ton) leads to a higher average fluid temperature in the borehole and a smaller temperature difference between the fluid and the ground, which, according to Eq. 5.1, leads to longer lengths. For the parallel configurations, two scenarios are observed. The 9 gpm (0.56 L/s) parallel case leads to higher correction factors because only 4.5 gpm (0.28 L/s) are flowing in each borehole. The 4.5 gpm case gives 2.25 gpm (0.14 L/s) in each borehole, leading to a laminar flow. A laminar flow reduces heat transfer and leads to thermal capacity effects lasting longer, reducing F_{corr} when compared to the one borehole 4.5 gpm case. Figure 5.4 then shows that placing two B boreholes in series has little impact on thermal capacity effects as F_{corr} is slightly smaller.

Finally, the borehole characteristics affect F_{corr} by introducing more or less thermal capacity effects. Borehole B has lower correction factors than borehole A because the effects relative to the borehole thermal capacity last longer. Those effects improve the borehole performances and have a tendency to reduce borehole length. Moreover, borehole B' has lower correction factors than borehole B. This is because its larger pipes store more fluid allowing more energy storage and longer thermal capacity effects. The lowest value of F_{corr} (0.69) is observed for B' and an effect coverage of 150%.

In summary, these results show that when sizing a residential borehole using the ASHRAE sizing equation, designers should be aware that borehole thermal capacity and heat pump oversizing affect

the required borehole length. Heat pump oversizing leads to intermittent heat pump operation and to lower required length because of thermal capacity effects. At the other end of the spectrum, heat pump undersizing leads to continuous heat pump operation which increases the duration of the peak load and increases the required length.

5.6 Conclusion

Borehole thermal capacity and heat pump cycling, which are not included in the ASHRAE borehole sizing equation, can change the required borehole length. Borehole transient effects, caused by the fluid and grout thermal capacities, are beneficial as they reduce the peak ground loads and, consequently, the required borehole length. Correction factors for the current ASHRAE sizing equation are proposed to consider borehole thermal capacity. Annual simulation results on a typical residential system show that neglecting borehole transient effects leads to oversized boreholes. Furthermore, heat pump energy consumption is overestimated by about 5 %. The correction factor can reach 0.69, a length reduction of 31 % compared to ASHRAE's equation. The largest reductions in the required length occur when heat pumps operate intermittently with an oversized heat pump. The ASHRAE equation can also underestimate the length, by up to 24 % in the present case (correction factor of 1.24), when an undersized heat pump and low thermal capacity boreholes are used. The results of this study indicate that dynamic simulations are required to properly size the borehole to account for borehole thermal capacity and heat pump cycling.

5.7 Acknowledgments

The authors would like to express their sincere gratitude to ASHRAE for the Grant-In-Aid awarded to the first author. Also, Hydro-Quebec and the Natural Sciences and Engineering Research Council of Canada provided scholarships to the first author. Their support is gratefully acknowledged. Finally, this work was performed with funds provided by NSERC's Smart Net-Zero Energy Buildings Strategic Research Network.

5.8 References

ASHRAE. 2015. *Geothermal energy, ASHRAE Handbook, HVAC applications.* Atlanta, GA: ASHRAE.

Godefroy, V., and M. Bernier. 2014. A simple model to account for thermal capacity in boreholes. *Proceedings of the 11th IEA Heat Pump Conference*, Montreal, Qc, Canada. Paper #P.4.8.

Godefroy, V., Lecomte, C., Bernier, M., Douglas, M., and M. Armstrong. 2016. Experimental Validation of a Thermal Resistance and Capacity Model for Geothermal Boreholes. *ASHRAE Winter Meeting*, Orlando, Fl. OR-16-C047.

Hellström, G. 1991. *Ground Heat Storage – Thermal Analyses of Duct Storage Systems - I. Theory.* Department of Mathematical Physics,University of Lund, Sweden.

Hellström, G., Mazzarella, L., and D. Pahud. 1996. *Duct ground storage model—TRNSYS version.* Department of Mathematical Physics, University of Lund, Sweden.

Kavanaugh, S., and K. Rafferty. 1997. *Ground-Source Heat Pumps: Design of geothermal systems for commercial and institutional buildings.* Atlanta, GA: ASHRAE

Klein, S. A. 2010. *TRNSYS, a transient simulation program.* Solar Energy Laboratory, University of Wisconsin-Madison, USA.

Ma, W., Li, M., Li, P., and A. Lai. 2015. New quasi-3D model for heat transfer in U-shaped ground heat exchangers: Effective overall thermal resistance. *Elsevier Energy.* doi: 10.1016/j.energy.2015.07.098

Pärisch, P., Mercker, O., Oberdorfer, P., Bertram, E., Tepe, R., and G. Rockendorf. 2015. Short-term experiments with borehole heat exchangers and model validation in TRNSYS. *Renewable Energy*, 74, 471-477.

Shirazi, A. S., and M. Bernier. 2013. Thermal capacity effects in borehole ground heat exchangers. *Energy and Buildings*, 67 352-364.

Yavuzturk, C., and J.D. Spitler. 1999. A Short Time Step Response Factor Model for Vertical Ground Loop Heat Exchangers. *ASHRAE Transactions*. 105(2): 475-485.

Young, T. 2004. *Development, Verification, and Design Analysis of the Borehole Fluid Thermal Mass model for Approximating Short Term Borehole Thermal Response*. (Masters of Science), Oklahoma State University.

CHAPITRE 6 ARTICLE 2 : A COMPARISON OF THE ENERGY USE FOR DIFFERENT HEAT TRANSFER FLUIDS IN GEOTHERMAL SYSTEMS

Soumission :

Article de conférence accepté par l'IGSHPA dans le cadre de la 2017 IGSHPA Conference and Expo, tenue du 14 au 16 mars 2017 à Denver, Colorado, États-Unis.

Auteurs :

- Laurent Gagné-Boisvert, Candidat M. Sc.A.
- Michel Bernier, Ph. D.

Référence :

Gagné-Boisvert, L., and M. Bernier. 2017. A comparison of the energy use for different heat transfer fluids in geothermal systems. Proceedings of the 2017 IGSHPA Conference and Expo, March 14-16 2017, Denver, USA, pp. 336-345.

6.1 Abstract

Geothermal systems that operate under 0 °C must use antifreeze mixtures instead of water to avoid operational problems. This paper examines the energy consumption of the circulating pump and heat pump for various heat transfer fluids used in a residential geothermal system. Propylene glycol, ethanol and methanol solutions at different concentrations are compared. Effects of fluid temperature and viscosity on head losses, borehole thermal resistance and heat pump operation are reviewed. Efficiency curves for currently available circulators are proposed. Annual energy simulations are then performed on a residential GCHP system. Energy consumption (pump and heat pump) is evaluated subhourly based on fluid temperature and properties prevailing during each time step. Results show, as expected, that higher mixture concentrations and higher flow rates lead to higher energy consumption. Methanol with a concentration of 15% and a 1.5 gpm/ton flow rate provides the best energy performances while ethanol at 30% with 3 gpm/ton is the worst choice, requiring 16% more energy and 525% more pumping power than for the methanol case. Laminar

flow in boreholes appears to be favorable when compared to turbulent flow which leads to relatively high pumping energy consumption. Shorter boreholes piped in parallel decrease energy consumption as well.

6.2 Introduction

A typical residential ground-coupled heat pump (GCHP) system is presented in Figure 6.1. When such a system operates under 0 °C, an antifreeze mixture must be used to avoid operational problems. Typically, designers select a solution with a freezing point approximately 3 °C (5 °F) lower than the lowest anticipated temperature (Dow, 2001). Antifreeze solutions affect the performance of the system in many ways. The greater viscosity of these fluids may lead to laminar flow in boreholes with a corresponding increase of the borehole thermal resistance. Pressure drops in the various parts of the system (Δp_{Pipe}, Δp_{Bore}, Δp_{HP} and Δp_{Valve} in Figure 6.1) as well as pumping power (W_{Pump}) are increased when a fluid other than water is used. Moreover, antifreeze mixtures affect heat transfer in the source-side heat exchanger of the heat pump, which decreases heat pump capacity (Q_{Cap}) and heat pump input power (W_{HP}) but to a lesser extent. The objective of this paper is to study the total energy consumption (pump and heat pump) for various heat transfer fluids typically used in GCHP systems.

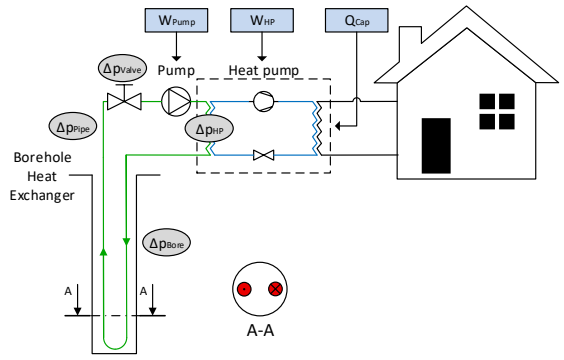

Figure 6.1 : Representation of a residential GCHP system

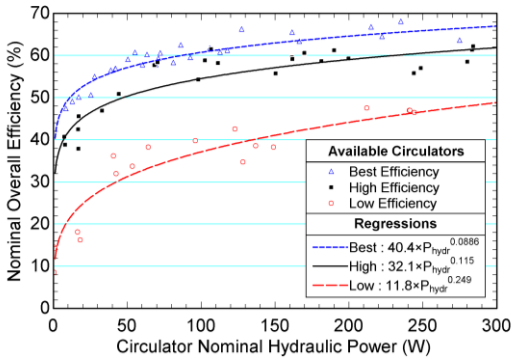

Figure 6.2 : Overall efficiency of available circulators

6.3 Literature review

Solutions of methanol, ethanol and propylene glycol are often used in GCHP systems. An ASHRAE sponsored study (Heinonen, 1997) concluded that propylene glycol was the best

compromise mainly because of its low environmental risk despite the fact that systems with propylene glycol use more energy as noted by Bernier et al. (2005). The toxicity of the inhibitors added to propylene glycol solutions must however be considered.

Pumping energy, which increases with the use of antifreeze, is sometimes considered negligible when compared to the overall energy consumption of a geothermal system. In reality, it can represent up to 45% of the total energy consumption, even in recent geothermal systems (Liu et al., 2015). Pumping energy is also influenced by the pumping strategy (Kavanaugh and McInerny, 2001). Kavanaugh and Kavanaugh (2012) suggested a maximum ground loop pump power of 10 hp/100 tons (2.1 kW_{elec}/100 $kW_{thermal}$).

A decrement factor (*DF*) evaluating heat pump convective heat transfer variations due to the use of antifreeze mixtures was developed by Spitler and Jin (2003). The *DF* corrects the fluid-side heat transfer coefficient initially calculated for water. In a follow-up study, Khan and Spitler (2004) stated that propylene glycol increases system energy consumption by 6 to 7% compared to ethanol or methanol. In a residential case study, with relatively balanced heating and cooling loads and low antifreeze concentrations, they concluded that typical antifreeze mixtures have similar life-cycle costs while water presents a higher life-cycle cost because a longer borehole is required.

Spitler and Ghelin (2015) challenged the standard industry recommendations to have turbulent flow in the borehole at all times and to maintain head losses in the range of 1 to 3 ft/100 ft of pipe (10 to 29 kPa/100 m). Their work confirmed Kavanaugh's warning (2011) that high fluid velocities may result in high pumping power with little thermal benefit and even less economic advantage over occasional laminar flow. They also confirmed Mescher's guideline expressed in an ASHRAE Webcast (ASHRAE, 2011) stating that a properly designed bore field should have a head loss (Δp_{Bore}) of less than 25 ft (75 kPa) with a maximum total system pressure drop of 50 ft (150 kPa).

6.4 Circulator efficiency

Circulators are low power pumps typically used to circulate fluid in residential, one-pipe and decentralized GCHP systems. Until recently, circulators had typical efficiency around 20 to 25% (Kavanaugh and Rafferty, 2015). However, the efficiency of circulators has nearly doubled in recent years (Bidstrup, 2012). Following the methodology used by the COSTIC (2003), an in-house analysis performed for the present study examined the efficiency of 86 commercially available

circulators from two manufacturers (Grundfos, 2016 and Salmson, 2016). In each case, the best efficiency point (BEP) was used to extract the nominal overall efficiency at a given nominal hydraulic power. The results of this analysis are shown in Figure 6.2, which shows the circulator wire-to-water efficiency as a function of the hydraulic power in the 0 to 300 W range. Circulators are categorized into three classes (Low, High and Best Efficiency) each with its own regression equation. In this work, circulators with the "High" efficiency are used.

6.5 Heat transfer and required hydraulic power

The thermophysical properties used in this work are obtained from the EES software (Klein et al., 2015). For concentration of 30% by weight (m/m), this tool gives the following freezing points: -13 ºC for propylene glycol, -20 ºC for ethanol, and -27 ºC for methanol. The viscosity of antifreeze mixtures is the property having the most notable effect on the energy consumption of geothermal systems. High fluid viscosities lead to low Reynolds numbers and laminar flows in the borehole which tend to decrease the heat transfer coefficients inside borehole pipes. Figure 6.3a (left) shows the steady-state convective thermal resistance, R_{conv}, and steady-state thermal resistance, R_b, of a typical borehole using propylene glycol (30% m/m) and different flow rates (characteristics are given in Table 6.1). R_b is the effective borehole thermal resistance between the fluid and the ground and is the sum of the grout, pipe and convective resistances (Eq. 6.1). The well-known relations from Hansen and Gnielinski/Petukhov are used to evaluate the convective heat transfer coefficient in borehole pipes for laminar and turbulent flows.

$$R_b = R_{grout} + R_{pipe} + R_{conv} \tag{6.1}$$

As shown in Figure 6.3a, R_{conv} increases significantly when the flow becomes laminar at a flow rate smaller than 0.32 L/s (for propylene glycol 30% m/m at 0 °C). In turn, this increases the borehole thermal resistance, R_b, from 0.12 mK/W to 0.20 mK/W. Thus, for a given ground load, the fluid temperature for the laminar case must be lower than for the turbulent case in order to increase the temperature difference between the fluid and the ground. However, as shown by the P_{hydr} curve on Figure 6.3a, the required hydraulic power for laminar flow is significantly less than for turbulent flow. The transition to laminar flow also depends on the fluid temperature and pipe diameter. This is shown in Figure 6.3b where the dip in each curve represents the transition to

laminar flow. The linear head loss is about three to four times higher for a 9 gpm flow rate in a 1.25” pipe than for a 4.5 gpm flow rate in a 1.25” pipe.

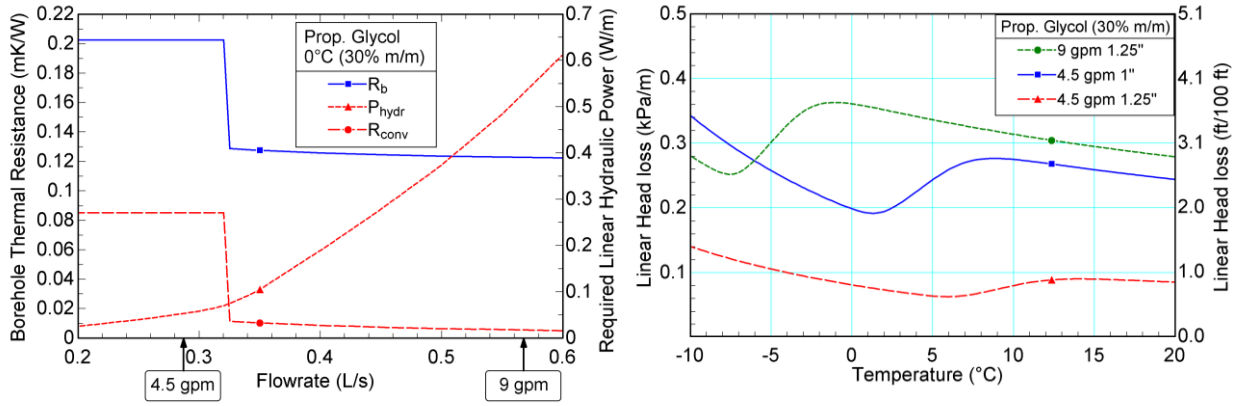

Figure 6.3 : a) Borehole thermal resistances and required hydraulic power (left) and b) head loss as a function of temperature (right)

Table 6.1 : Main characteristics of the borehole used in this study

Parameter	S.I. Value	S.I. Unit	I.P. Value	I.P. Unit
Depth	150	m	492	ft
Borehole diameter	0.15	m	6	in
Inside pipe radius	0.013	m	0.51	in
Outside pipe radius	0.016	m	0.63	in
Grout conductivity	1.5	W/m.K	0.87	BTU/hr.ft.°F
Grout thermal capacity	3000	kJ/m^3.K	44.7	BTU/ft^3.°F
Ground thermal conductivity	2.2	W/m.K	1.27	BTU/hr.ft.°F
Ground thermal diffusivity	0.096	m^2/day	0.94	ft^2/day
Pipe conductivity	0.42	W/m.K	0.24	BTU/hr.ft.°F
Flow rate	0.28/0.57	L/s	4.5/9	gpm
Borehole resistance R_b at 0 °C (PG30%)	0.202/0.123	m.K/W	0.350/0.213	hr.ft.°F/BTU

High fluid viscosities also increase pumping power due to increased pipe friction. Head losses (Δp_{Pipe}, Δp_{Bore}, Δp_{HP} and Δp_{Valve}) increase as viscosity affects the friction coefficient. With higher head losses, pumping power W_{Pump} is increased and a larger pump must be used. Increasing flow rate to maintain turbulent flow also increases pumping power. In this work, the Darcy-Weisbach equation is used for pipe head losses and the Churchill equation is used for the friction factor (Eq. 5.2) as it is suitable for laminar, transient and turbulent flows. A Power Parameter, *PP*, is also

proposed to combine flow rate and pipe diameter (Eq. 5.3) to allow simple pumping power predictions.

$$f = 8\left(\left(\frac{8}{Re}\right)^{12} + \left(\left(2.457\ln\left(\left(\frac{7}{Re}\right)^{0.9} + \frac{0.27\varepsilon}{D}\right)\right)^{16} + \left(\frac{37530}{Re}\right)^{16}\right)^{-1.5}\right)^{1/12} \quad (6.2)$$

$$PP = \frac{Flow^3}{D_{pipe}^5} \quad (with\ Flow\ in\ gpm\ and\ D_{pipe} in\ inches) \quad (6.3)$$

Figure 6.4a shows the required linear hydraulic power for PG30% at 0 °C as a function of *PP*. Dots represent detailed calculations while the straight line represents a linear regression through the data. The same exercise is performed for different antifreeze solutions with flow rates varying from 2 to 12 gpm and pipe diameters varying from 0.75 to 1.5". Linear regressions are then obtained for each fluid (Figure 6.4b). Each regression presents an absolute RMSE under 0.015 W/m and allows an adequate first estimate of pumping power. The well-known criteria of 3 ft/100 ft of pipe (29 kPa/100 m) for head loss is also overlayed for 4.5 and 9 gpm flow rates (Kavanaugh and Rafferty, 2015). Figure 6.4b also shows that for a specific flow rate and pipe diameter, pumping power is higher as fluid viscosity increases. Pumping PG30% at 0 °C requires approximately 45% more power than for water.

The use of Figure 6.4b is best illustrated with an example. A flow of 9 gpm of ethanol (30% m/m) at 0 °C through a 1 meter pipe with a diameter of 0.032 m (1.25") leads to a value of *PP* = 239 gpm^3/in^5 with a corresponding value of 0.18 W of hydraulic power (0.19 W/m is obtained with a detailed calculation). If the system consists of a 100 m borehole with 10 m of connecting pipes to the heat pump (thus a total pipe length of 220 m) then 39.6 W of hydraulic power is required. Pumping this fluid with a 50% efficient circulator would then require 79 W of electrical power, W_{Pump}.

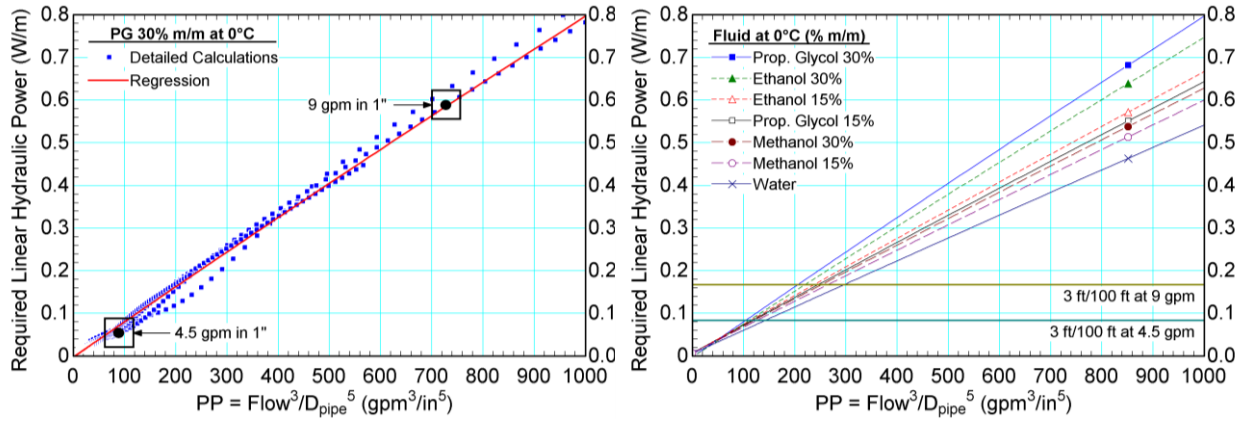

Figure 6.4 : a) Required hydraulic power at 0 °C calculated for PG30% (left) and b) predicted for different fluids (right)

Head losses through the source heat exchanger of the heat pump as well as in connecting hoses and valves are also important. Heat pump heat exchanger head loss is typically given by manufacturers and is function of flow rate and inlet fluid temperature. Equation 6.4, where Δp_{HP} is in kPa, *Flow* in L/s and T_{inHP} in °C, is a regression based on a heat pump performance map presenting head loss for several flow and temperature combinations (ClimateMaster, 2012). It is valid for flow ranging from 0.284 to 0.568 L/s (4.5 to 9 gpm) and for inlet temperatures ranging from -1.1 to 48.9 °C (30 to 120 °F). Valve and hose head losses, combined in one term, Δp_{Valve}, are calculated using flow coefficients used by Kavanaugh and Rafferty (2015): C_v equals 25 for the valve and 8 for hoses (based on flows in gpm and a 1 psi (6.9 kPa) pressure drop). For 4.5 and 9 gpm flow rates, pressure drops then vary from 0.2 to 0.9 kPa (0.07 to 0.3 ft) for the valve and from 2.2 to 8.7 kPa (0.7 to 2.9 ft) for connecting hoses.

$$\Delta p_{HP} = 88.0 \times Flow - 0.179 \times T_{inHP} - 13.3 \tag{6.4}$$

An antifreeze correction factor for these head losses, f_{WPD}, is proposed (Eq. 6.6). This factor, based on Blasius' equation (Eq. 6.5), corrects manufacturers' pressure drops, which are based on water. Blasius' equation is valid for low turbulent Reynolds number (White, 2009), which is the case in typical small diameter hoses and heat exchangers. The value of f_{WPD} (Eq. 6.6) is then the ratio of the pressure drop for the antifreeze solution over the one for water. This factor evaluated for different antifreezes and concentrations at 0 °C was verified against manufacturer's data (ClimateMaster, 2012). As shown in Table 6.2, the method proposed here (Eq. 6.5 and 6.6) is within 2% of the manufacturer's data for PG. Similar results were obtained for other fluids. Δp_{HP}

and Δp_{Valve} (valve and hoses), calculated for water, are then multiplied by this factor to obtain the actual antifreeze pressure drop, Δp_a.

$$\Delta p = 0.158 L \rho^{0.75} \mu^{0.25} D^{-1.25} V^{7/4} \tag{6.5}$$

$$f_{WPD} = \frac{\Delta p_a}{\Delta p_w} = \left(\frac{\rho_a}{\rho_w}\right)^{0.75} \left(\frac{\mu_a}{\mu_w}\right)^{0.25} \tag{6.6}$$

Table 6.2 : WPD, capacity and power correction factors for PG

Prop. Glycol (% m/m)	f_{WPD}		$f_{cap,heat}$		$f_{power,heat}$	
	Eq. 6.6	**Manufacturer**	**Eq. 6.9**	**Manufacturer**	**Eq. 6.9**	**Manufacturer**
5%	1.07	1.07	0.991	0.989	0.998	0.997
15%	1.20	1.21	0.972	0.968	0.993	0.990
25%	1.37	1.36	0.945	0.947	0.987	0.983

6.6 Heat pump capacity and power

The use of antifreeze mixtures also affects heat transfer in the source-side heat exchanger of the heat pump, which has a detrimental effect on heat pump performance. Heat pump heating capacity Q_{Cap} decreases because of reduced convection in the heat exchanger pipes. Viscosity, density, thermal capacity and conductivity variations reduce capacity, by up to 10% for a 30% ethanol solution (ClimateMaster, 2012). Power consumption W_{HP} is also affected and it can decrease by up to 3% as capacity decreases. However, heat pump energy consumption increases with the use of antifreeze as it must operate for longer periods to meet the load as capacity is reduced.

Capacity and power consumption can be adjusted by correction factors to account for those effects. A capacity correction factor derived from Nguyen's work is used here (2010). This factor, $f_{capacity}$, (Eq. 6.9) predicts heat pump capacity variation based on heat pump constants (C_1 and C_2) and Spitler and Jin's (2003) Decrement Factor (Eq. 6.7). As shown by Eq. 6.8, the two constants are used to evaluate the total heat pump source-side thermal resistance R_t. C_1 stands for the fluid convective resistance initially calculated for water. It is divided by *DF* to correct the fluid-side convective heat transfer coefficient. C_2 combines the pipe conductive, the refrigerant convective and the fouling thermal resistances, which are not affected by the choice of the antifreeze solution. C_1 and C_2 are back calculated using a pair of capacity correction factors from a manufacturer (ClimateMaster, 2012) with *DF* calculated for each fluid and each concentration. This leads to a two equations/two unknowns system that can be solved easily. C_1 and C_2 equal 1.0 and 16.35,

respectively, when calculated using propylene glycol. C_1 and C_2 differ slightly when calculated for ethanol and methanol. Fluid specific values of C_1 and C_2 are used to predict $f_{capacity}$ for the simulations performed in this paper.

$$DF = \frac{h_a}{h_w} = \left(\frac{\mu_a}{\mu_w}\right)^{-0.47} \left(\frac{\rho_a}{\rho_w}\right)^{0.8} \left(\frac{Cp_a}{Cp_w}\right)^{0.33} \left(\frac{k_a}{k_w}\right)^{0.67} \tag{6.7}$$

$$R_t = R_{conv,fluid} + R_{cond,pipe} + R_{conv,refrig} + R_{fouling} = R_{conv,fluid} + \Sigma R = \frac{C_1}{DF} + C_2 \tag{6.8}$$

$$f_{capacity} = \frac{R_{t,w}}{R_{t,a}} = \frac{C_1 + C_2}{\frac{C_1}{DF} + C_2} \tag{6.9}$$

It also appears that the use of this capacity correction factor proves to be accurate to correct the heat pump power consumption ($f_{capacity}$ is replaced by f_{power} in Eq. 6.9). The same *DF* is used but C_1 and C_2 are based on the manufacturer's power correction factors. They equal 1.0 and 75.68, respectively, when calculated using propylene glycol. As shown in Table 6.2, the predicted capacity and power correction factors are in good agreement with manufacturer's data. It should be noted, as inferred in Eq 6.7, that *DF* accounts for the variations of density, specific heat, thermal conductivity and viscosity.

Finally, there are operational benefits resulting from the use of antifreeze mixtures. Indeed, allowing colder fluid temperatures to the heat pumps (-3 °C instead of 0 °C for example) leads to shorter boreholes as the temperature difference between the borehole fluid and the ground is larger. However, this effect might be counterbalanced by increased pumping energy and reduced borehole and heat pump performances. It is thus important to evaluate the overall effects of using a specific antifreeze solution. This is done using annual simulations as shown in the next section.

6.7 Annual simulations

Annual simulations using TRNSYS v17 (Klein et al., 2010) are performed to compare the energy consumption of a GCHP system using different antifreeze mixtures (PG, EA and MA) and two flow rates (4.5 and 9 gpm or 1.5 and 3 gpm/ton). A 1-minute time step is used, which is small enough to capture borehole transient effects. The system under study is the one presented in Figure 6.1. It consists of a 3-ton (10.5 kW) water-to-air ground-coupled heat pump linked to a 150 m borehole. The GCHP system provides space heating for a single-family house with enough capacity

to avoid the need for an auxiliary heater. The building is simulated in a heating dominated climate (Montreal, Canada) with an annual heating requirement of about 20 000 kWh. Typical models found in TRNSYS for the building, thermostat, heat pump and pump are used. Heat pump performance is modeled based on a manufacturer's steady-state performance data (ClimateMaster, 2012). The TRCM borehole model from Godefroy and Bernier (2014) is used to model the single U-tube borehole. This experimentally validated model (Godefroy et al., 2016) accounts for fluid and grout thermal capacity, which indirectly affects heat pump performance (Gagné-Boisvert and Bernier, 2016). The main characteristics of the borehole are given in Table 6.1. The pump is a high efficiency wet rotor circulator. When operating, it is assumed that it provides a constant volumetric flow rate year-round. Pump efficiency is evaluated based on the "High" regression curve presented in Figure 6.2. Thermophysical properties, correction factors, head losses, and borehole thermal resistance are calculated at each time step.

6.7.1 Comparison results

Tables 6.3 and 6.4 present one-year simulation results while Figure 6.5 shows the pump power and heat pump inlet temperature evolution over the year. In these tables, pump fraction is the ratio of the pumping energy over the total energy consumption; seasonal performance factor (*SPF*) is the ratio of the annual heating requirement over the total energy consumption (Nordman and Zottl, 2011); $Head_{max}$ is the highest total head loss over the year while pump power is the highest required pump power. As illustrated in Figure 6.5, pumping power decreases by about 10-15% with higher fluid temperature occurring in summer. R_b also varies over the year as fluid temperature fluctuates, as shown by minimum and maximum values in Tables 6.3 and 6.4. These tables show the importance of considering the antifreeze properties and how they influence system operation.

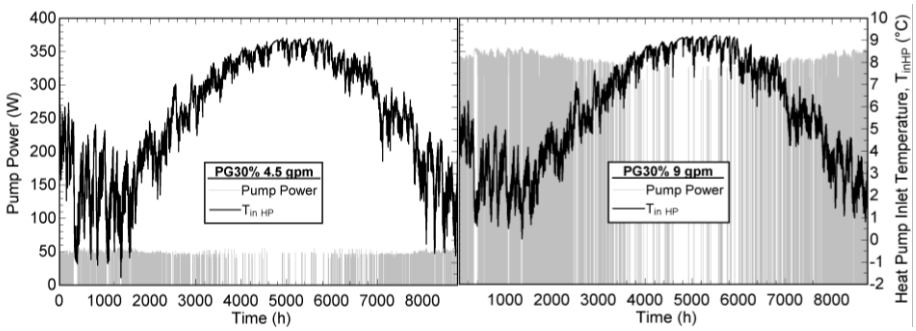

Figure 6.5 : Pump power and heat pump inlet temperature for PG30% at a) 4.5 (left) and b) 9 gpm (right) over one year

Table 6.3 : Simulation results for 4.5 gpm flow rate

Fluid (% m/m)	Total (kWh)	Pump (kWh)	Pump fraction (%)	SPF (-)	$Head_{max}$ (kPa/ft)	Pump power (W)	$R_{b\ min/max}$ (W/mK)	$T_{inHP,min}$ (°C/°F)
Prop. Glycol 15%	6 027	126	2.10%	3.36	93.8/31.4	56.9	0.122/0.123	0.4/33
Prop. Glycol 30%	6 286	125	2.00%	3.22	99.5/33.3	60.0	0.127/0.204	-1.7/29
Prop. Glycol 40%	6 545	187	2.86%	3.09	155.2/51.9	88.9	0.212/0.213	-1.4/29
Ethanol 15%	6 114	130	2.13%	3.31	92.5/30.9	56.2	0.123/0.125	0.5/33
Ethanol 30%	6 368	120	1.88%	3.18	90.5/30.3	55.1	0.127/0.209	-1.3/30
Methanol 15%	6 014	119	1.98%	3.36	87.3/29.2	53.4	0.122/0.123	0.5/33
Methanol 30%	6 113	127	2.07%	3.31	89.6/30.0	54.7	0.124/0.125	0.8/33
Water	5 878	102	1.74%	3.44	75.8/25.4	47.1	0.120/0.121	0.6/33

Table 6.4 : Simulation results for 9 gpm flow rate

Fluid (% m/m)	Total (kWh)	Pump (kWh)	Pump fraction (%)	SPF (-)	$Head_{max}$ (kPa/ft)	Pump power (W)	$R_{b\ min/max}$ (W/mK)	$T_{inHP,min}$ (°C/°F)
Prop. Glycol 15%	6 561	653	10.0%	3.08	302/101	296	0.120/0.121	-0.1/32
Prop. Glycol 30%	6 917	821	11.9%	2.93	374/125	358	0.121/0.123	0.1/32
Ethanol 15%	6 670	683	10.2%	3.03	313/105	305	0.120/0.121	0.1/32
Ethanol 30%	6 966	786	11.3%	2.91	347/116	334	0.121/0.123	0.4/33
Methanol 15%	6 519	616	9.4%	3.10	282/94.3	278	0.119/0.120	0.0/32
Methanol 30%	6 647	654	9.8%	3.04	292/97.7	287	0.120/0.121	0.3/33
Water	6 324	539	8.5%	3.20	250/83.6	250	0.119/0.119	0.0/32
PG 30% Parallel	6 101	265	4.3%	3.32	107.5/36.0	119	0.126/0.204	1.9/34
MA 15% Parallel	5 865	214	3.7%	3.45	86.5/28.9	97.8	0.122/0.123	2.2/36
Water Parallel	5 729	187	3.3%	3.53	76.7/25.7	88.0	0.120/0.121	2.3/36

Results show that higher concentrations and higher flow rates increase total energy consumption of the GCHP system. Using methanol with a concentration of 15% and 4.5 gpm gives the best energy performances with an energy consumption of 6014 kWh, a *SPF* of 3.36 and a maximum pump power of 53.4 W. It is worth mentioning that propylene glycol at 15% with 4.5 gpm is not recommended for that application considering its -5 °C freezing point. Ethanol 30% with 9 gpm requires 6966 kWh (+16%) and 334 W of pump power (+525%) with a *SPF* of 2.91 (-13%). This case gives the worst energy performance and a bigger and more expensive pump would be required.

For pumping, flow rates of 4.5 and 9 gpm lead to pump fractions of about 2% and 10%, respectively. Based on an average 8 kW peak heating load, a pumping grade of A on the Kavanaugh and Rafferty (2015) scale is achieved for all 4.5 gpm cases. A grade of F is obtained for 9 gpm cases. Higher flow rates and concentrations are responsible for bigger head losses, leading to higher

pumping power and energy consumption. It appears that systems with head losses under 100 kPa (4.5 gpm) lead to better overall energy performances than ~300 kPa (9 gpm) cases, which is in line with Mescher's statement presented earlier. Interestingly, for propylene glycol 30% and ethanol 30% with 4.5 gpm, pumping energy is lower than for cases with a 15% concentration, which is counterintuitive as these solutions are more viscous. This is because those two cases are in laminar flow around 90% of the operation time, which leads to lower head losses (Figure 6.3b). The PG40% at 4.5 gpm case always operates in laminar flow and presents higher head losses than the PG30% case. Its minimum heat pump inlet temperature is also slightly higher because more energy comes from the heat pump compressor and less from the ground.

It is important to note that these three 4.5 gpm laminar cases, with typical laminar R_b values and lower loop temperatures, yield lower energy consumption (-10%) than the same cases with the fully turbulent 9 gpm flow rate. This is mainly due to the higher pumping requirements. Based on that, a common GCHP system using propylene glycol at 30% would require less energy if working with 4.5 gpm versus 9 gpm, even if the borehole flow is almost always laminar. This confirms Kavanaugh's recommendation. Thus, designers must be aware that the heat transfer advantage of turbulent flows is small compared to the increased pumping energy consumption in GCHP systems. Figures 6.6a and 6.6b present a breakdown of peak head losses to help understand flow rate effects on results. Cases with 4.5 and 9 gpm using propylene glycol 30% are presented. As expected, the various head losses are about four times higher when the flow rate is doubled.

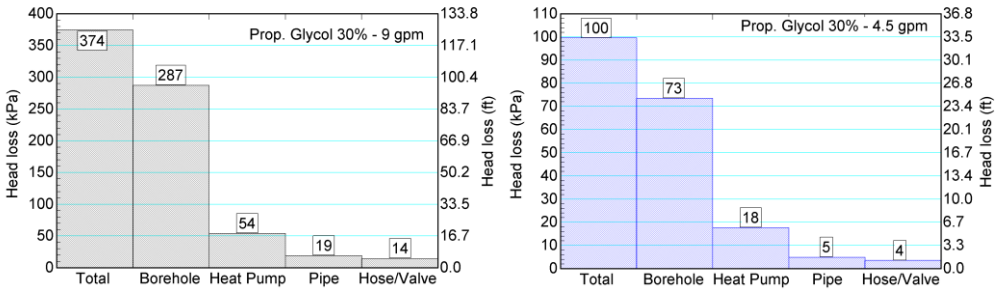

Figure 6.6 : Breakdown of peak head losses for PG30% at a) 4.5 gpm (left), b) 9 gpm (right) and c) in parallel (bottom)

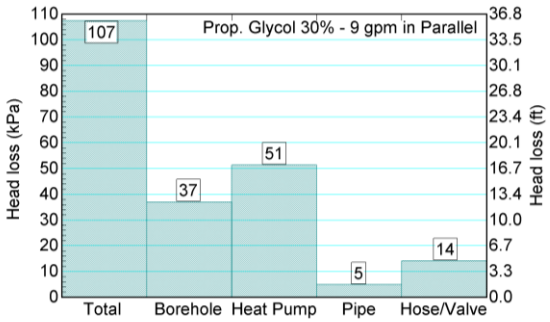

Figure 6.6 (suite) : Breakdown of peak head losses for PG30% at a) 4.5 gpm (left), b) 9 gpm (right) and c) in parallel (bottom)

The same simulations are performed without the correction factors ($f_{capacity}$, f_{power} and f_{WPD}) to assess their importance. In all cases, neglecting correction factors underestimates energy consumption. The extent of the underestimation is higher for higher antifreeze concentrations. Neglecting the capacity and power correction factors underestimates heat pump energy consumption by 2 to 6%, pump consumption by 3 to 9% and overall energy consumption by 2 to 7%. Neglecting the head loss correction factor (heat pump, hoses and valve) underestimates pump energy consumption by 3 to 8% and overall energy consumption by 0.1 to 0.7% as pumping represents 2 to 10% of the total. Neglecting both factors underestimates pump energy consumption by 6 to 15% and overall energy consumption by 2 to 7%. Table 6.5 presents these differences for propylene glycol 15 and 30% at 9 gpm.

Table 6.5 : Effects of correction factors on energy consumption (Propylene Glycol 9 gpm)

	Pump	**Without**			**Total**	**Without**		
Fluid % m/m	**(-)**	f_{cap}+f_{power}	f_{WPD}	f_{cap}+f_{power} +f_{WPD}	**(-)**	f_{cap}+ f_{power}	f_{WPD}	f_{cap}+f_{power} +f_{WPD}
PG15% (kWh)	653	635	633	615	6 561	6 430	6 541	6 410
Difference (%)		-2.8%	-3.2%	-5.9%		-2.0%	-0.3%	-2.3%
PG30% (kWh)	821	762	773	717	6 917	6 561	6 870	6 517
Difference (%)		-7.2%	-5.9%	-12.7%		-5.2%	-0.7%	-5.8%

As a final test, two 75 m boreholes are piped in parallel with a total flow rate of 9 gpm. Head losses are consequently modified (Figure 6.6c). As shown in Table 6.4, this leads to the lowest overall energy consumptions and highest *SPF*. Using MA15% requires 5865 kWh with a corresponding *SPF* of 3.45. Using shorter boreholes in parallel must then be considered as an effective design in terms of energy performance, even if laminar flow occurs in boreholes. Shorter parallel boreholes

also lead to higher values of $T_{inHP,min}$ which may decrease the required antifreeze concentration or boreholes length.

6.8 Conclusion

The main objective of this paper is to compare the energy consumption of a GCHP system using various antifreeze solutions. It reviews the effects of antifreeze on head losses, borehole thermal resistance and heat pump operation. It also proposes efficiency curves for currently available circulators; a graph estimating required hydraulic power for different flows and pipe diameters; and antifreeze correction factors to correct heat pump capacity, power and head loss. Annual energy simulations are then performed on a residential GCHP system. Results show, as expected, that higher concentrations and higher flow rates increase total energy consumption. Methanol with 15% concentration and a flow rate of 1.5 gpm/ton gives the lowest annual energy consumption. Ethanol at 30% and 3 gpm/ton is the worst choice, requiring 16% more energy and 525% more pumping power compared to the methanol case. Laminar flow in boreholes appears to be favorable when compared to turbulent flow, which lead to relatively high pumping energy consumption. Finally, placing shorter boreholes in parallel appears to decrease energy consumption and increase the seasonal performance factors.

6.9 Acknowledgments

The authors would like to express their sincere gratitude to ASHRAE, Hydro-Quebec and the Natural Sciences and Engineering Research Council of Canada (NSERC) who provided scholarships to the first author. This work was also performed with funds provided by NSERC's Smart Net-Zero Energy Buildings Strategic Research Network.

6.10 Nomenclature

C = Antifreeze concentration (%)

C_1, C_2 = Heat pump constants

C_v = Flow coefficient (gpm)

Cp = Thermal capacity (kJ/kg.K)

D = Pipe diameter (m)

ε = Pipe rugosity (m)

f = Friction factor (-)

h = Convection coefficient ($W/m^2.K$)

k = Thermal conductivity (W/m.K)

Δp = Pressure drop/Head (kPa)

PP = Power Parameter (gpm^3/in^5)

ρ = Density (kg/m^3)

Q = Capacity power (W)

Re = Reynolds number (-)

μ = Dynamic viscosity (kg/m.s)

SPF = Seasonal performance factor (-)

V = Fluid speed (m/s)

W = Power (W)

6.10.1 Subscripts

a = Antifreeze mixture

cap = Capacity

$conv$ = Convection

HP = Heat pump

min = Minimum

t = Total

w = Water

WPD = Water pressure drop

$\%\ m/m$ = Mass Concentration

6.11 References

ASHRAE. 2011. *Ground Source Heat Pump Systems: Putting the Earth to Work for You* (K. Mescher). ASHRAE Webcast Dvd.

Bernier, M., Ladang, O., Hulot, J. Effet du choix du fluide caloporteur sur l'énergie de pompage des systèmes de pompes à chaleur géothermiques, *VIIème Colloque Interuniversitaire Franco-Québécois sur la Thermique des Systèmes*, 23-25 mai 2005, Saint-Malo.

Bidstrup, N. 2012. EU Pump Regulations. *ASHRAE Journal* 54(5): 106-110.

ClimateMaster. 2012. *Tranquility 27 (TT) Series Performance Map*. USA: ClimateMaster.

COSTIC. 2003. *Circulators efficiency based on manufacturers catalogs* (Study 24.013). Angers, France: ADEME.

Dow. 2001. *Engineering and Operating Guide: DOWFROST Inhibited Propylene Glycol-based Heat Transfer Fluids*. USA: Dow Chemical Company.

Gagné-Boisvert, L., and M. Bernier. 2016. Accounting for Borehole Thermal Capacity when Designing Vertical Geothermal Heat Exchangers. Presented at the *2016 ASHRAE Annual Conference*, St-Louis, MO, June 25–29.

Gehlin, S.E.A., and J.D. Spitler. (2015). Effects of Ground Heat Exchanger Design Flow Velocities on System Performance of Ground Source Heat Pump Systems in Cold Climates. *ASHRAE Meeting.*

Godefroy, V., and M. Bernier. 2014. A simple model to account for thermal capacity in boreholes. *Proceedings of the 11th IEA Heat Pump Conference*, Montreal, Qc, Canada. Paper #P.4.8.

Godefroy, V., Lecomte, C., Bernier, M., Douglas, M., and M. Armstrong. 2016. Experimental Validation of a Thermal Resistance and Capacity Model for Geothermal Boreholes. *ASHRAE Winter Meeting*, Orlando, Fl. OR-16-C047.

Grundfos Canada. 2016. *Product Center*. http://product-selection.grundfos.com. Access on March 14-25th 2016.

Heinonen, E.W., M.W. Wildin, A.N. Beall, R.E. Tapscott. (1997). Assessment of antifreeze solutions for ground-source heat pump systems. *ASHRAE Transactions*, 103(2): 747-756.

Jin, H., and J.D. Spitler. 2003. Parameter estimations based model of water-to-water heat pumps with scroll compressors and water/glycol solutions. *Building Serv. Eng. Res. Technol*. 24(3): 203-219.

Kavanaugh, S.P., and S.A. McInerny. 2001. Energy Use of Pumping Options for Ground-Source Heat Pumps. *ASHRAE Transactions*. 107(1): 589-599.

Kavanaugh, S.P. 2011. Less Pumping Means Cooler Ground Loops. *ASHRAE Journal* 53(7): 26-35.

Kavanaugh, S.P., and J. Kavanaugh. 2012, Long-Term Commercial GSHP Performance Part 2: Ground Loops, Pumps, Ventilation Air and Controls. *ASHRAE Journal* 54(7): 26-34.

Kavanaugh, S.P., and K. Rafferty. 2015. *Ground-Source Heat Pumps: Design of geothermal systems for commercial and institutional buildings*. Atlanta, GA: ASHRAE.

Khan, M.H., and J.D. Spitler. 2004. Performance Analysis of a Residential Ground Source Heat Pump System with Antifreeze Solution. *Proceedings of SimBuild 2004*, Boulder, Colorado August 4-6.

Klein, S. A. et al. 2010. *TRNSYS, a transient simulation program*. Solar Energy Laboratory, University of Wisconsin-Madison, USA.

Klein, S. A. et al. 2015. *EES: Engineering Equation Solver*. Madison, WI: F-Chart Software.

Liu, X., M. Malhotra, P. Im, B. Habibzadeh. 2015. Case studies for GSHP demonstration projects in the US. *IEA Heat Pump Center*, Newsletter, Vol. 33, No. 3.

Nguyen, A. 2010. Personnal communication about antifreeze correction factors.

Nordman, R., and A. Zottl. 2011. SEPEMO-Build - a European project on seasonal performance factor and monitoring for heat pump systems in the building sector. *REHVA Journal* 48(4): 56-61.

Salmson. 2016. *Product Center*. http://selecson.salmson.fr. Access on March 14-25th 2016.

White, F.M. 2009. *Fluid Mechanics*. 7th edition. McGraw-Hill. p.366.

CHAPITRE 7 ARTICLE 3 : INTEGRATED MODEL FOR COMPARISON OF ONE- AND TWO-PIPE GCHP NETWORK CONFIGURATIONS

Soumission :

Article soumis le 20 février 2017 à la revue Science and Technology for the Built Environment.

Auteurs :

- Laurent Gagné-Boisvert, Candidat M. Sc.A.
- Michel Bernier, Ph. D.

7.1 Abstract

Several network configurations are possible when designing the interior portion of centralized ground-coupled heat pump (GCHP) systems. In this study, three different configurations are examined: Two-pipe networks with either a direct-return or a reverse-return and one-pipe systems. One-pipe networks typically require less piping than two-pipe systems. However, heat pump energy consumption might be higher because the inlet temperature to the heat pumps tends to increase (in cooling) or decrease (in heating) along the network. In this work, a versatile integrated modelling tool is developed in the TRNSYS environment to study the energy consumption (pumps and heat pumps) of each type of network. A control method for one-pipe systems, based on the bore field return temperature, is also proposed. The tool is first compared to detailed individual models in annual simulations where it is shown to give good results. The results obtained with four different case studies indicate that the total annual energy consumption of one-pipe networks is up to 5% higher than two-pipe networks even though the pumping portion of the annual energy consumption is up to 36% lower for one-pipe networks. No significant differences are observed in the required borehole depth.

7.2 Introduction

There are several possible piping configurations when designing the indoor portion of centralized ground-coupled heat pump (GCHP) systems. Three of these configurations are studied in this paper. They are presented schematically in Figure 7.1. In the reverse-return two-pipe network (Figure 7.1a), heat pumps are piped in parallel and have the same inlet fluid temperature. One of the main advantage of these systems is that they are somewhat easier to balance, since each parallel circuit has more or less the same pressure drop. However, a supplementary return pipe might be required if the heat pumps are positioned in-line as indicated in Figure 7.1a. It is possible to avoid the supplementary pipe if the heat pumps are positioned such that the circuit forms a loop. Finally, variable flow pumping can be used to reduce pumping energy consumption.

In direct-return two-pipe networks (Figure 7.1b), heat pumps are also piped in parallel but the flow out of the first heat pump is the first to be returned to the main pump, thereby eliminating the need for a supplementary return pipe. Each circuit has a different pressure drop and balancing valves are typically required to maintain the desired flow rate in each heat pump. Variable flow pumping can also be used to reduce energy consumption.

In one-pipe networks, each heat pump draws and rejects fluid from and to the same primary pipe (Figure 7.1c). The main flow rate, controlled to maintain a favorable bore field return temperature, is constant along the primary pipe while individual circulator pumps are typically activated in tandem with their corresponding heat pump. Heat pumps are operated in series each with a different inlet temperature as the primary pipe fluid temperature is influenced by the operation of the previous units. If all heat pumps are operating in cooling (or heating), heat pumps located towards the end of the loop will receive a less favourable inlet temperature leading to higher heat pump energy consumption. However, one-pipe systems are known to be simpler to design and operate with reduced piping costs.

This paper proposes a tool to perform annual simulations of one- or two-pipe networks to evaluate the annual operating energy costs related to pumping and heat pumps. The tool integrates into a single TRNSYS Type: heat pump modelling, pressure drop calculations through pipes and valves, as well as pump and circulator calculations. The paper is subdivided into several sections. First, the features and operation of the three networks are reviewed. Then, the modelling methodologies used in the tool are presented. This is followed by a comparison between results obtained using the

integrated tool and a detailed simulation involving individual models. Finally, four case studies are presented and analysed in the application section.

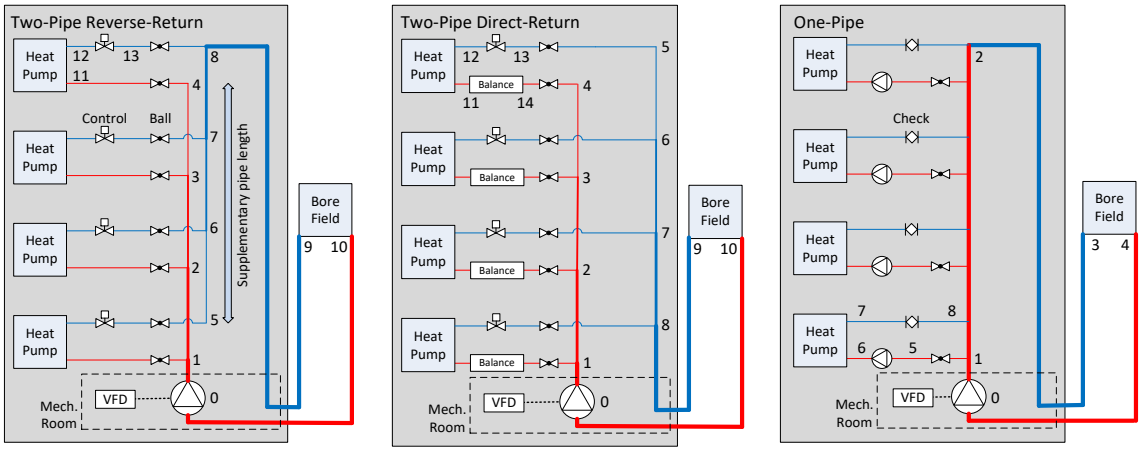

Figure 7.1 : a) Reverse-return Two-pipe (left), b) Direct-return Two-pipe (center) and c) One-pipe (right) GCHP networks with connection diagram

7.3 Literature review

Several piping strategies are possible for centralized GCHP systems, including one-pipe systems (Boldt and Keen, 2015). Stethem (1994) re-examined hydronic one-pipe systems, which were common around 1950 (Stethem, 1995). He points out the advantages associated with reduced piping needs and a decrease in the energy consumption which result from the use of fewer valves and the decoupling of the primary and secondary loops. Application to GCHP systems was not specifically addressed. However, he stated that one-pipe networks are efficient in high-rise buildings and schools using heat pumps.

Kavanaugh and McInerny (2001) showed that the selection of a pumping strategy influences pumping energy consumption. Kavanaugh et al. (2003) found that decentralized systems relying on on/off circulators require less energy for low to moderate occupancy buildings (less than 60 hours/week), centralized systems with a variable-speed pump being a close second. Their study, based on simple bin calculations, also concluded that these centralized systems are the most efficient for high occupancy buildings (over 60 hours/week).

Bernier et al. (2005) presented a methodology to compare the energy consumption and *LCC* of centralized and decentralized GCHP pumping systems. They stated that pumping costs over 20

years are lower for centralized systems while overall costs are lower for decentralized systems due to expensive piping required in centralized systems. However, this study did not account for the total required borehole length which is typically longer for decentralized systems that cannot take advantage of load diversity.

Cunniff and Zerba (2006) stated that one-pipe systems use small circulators to replace the expensive and energy-consuming control valves and balancing valves. They concluded that circulators deliver the fluid to where it is needed, instead of forcing it where it is not needed resulting in reduced piping and installation costs as well as energy savings. One-pipe networks coupled to fan coil units have been shown to be energy efficient and cost effective in a residential tower retro-fit (Cunniff, 2011).

Mescher (2009) stated that GCHP one-pipe systems are less expensive and more energy efficient than two-pipe systems and that their design, installation and balancing are simpler. A two-pipe network requires additional pipes, fittings, piping size reductions and insulation compared to a one-pipe system. He shows that a one-pipe system equipped with two parallel constant speed pumps has lower pumping and total energy consumption than a two-pipe system with a single variable-speed pump. He also specified that the selection of a one-pipe system in actual building retrofits led to piping installation cost savings of \$0.50 to \$1.50/ft^2 (\$5.38 to \$16.15/m^2). He mentioned that one-pipe systems can be almost as energy efficient as decentralized unitary loops with the added benefit that one-pipe networks can potentially lead to shorter boreholes because of load diversity.

Kavanaugh (2011) performed a GCHP systems survey and found that one-pipe systems presented the highest Energy Star ratings along with decentralized unitary loops. He specified that five 1950s schools that were retrofitted with one-pipe GCHP systems obtained an average Energy Star rating of 96. He also proposed to add a third smaller parallel main pump providing flow up to a 25% part-load operation in one-pipe systems to reduce energy consumption. However, using a variable-speed main pump in one-pipe systems has not been assessed.

Until recently, circulators had typical wire-to-water efficiencies around 20 to 25% (Kavanaugh and Rafferty, 2015). These relatively low efficiencies made their use less attractive in one-pipe systems. However, circulator efficiency nearly doubled in recent years (Bidstrup, 2012). Gagné-Boisvert and Bernier (2017) looked at commercially available circulators and proposed three sets of curves

for low, high and best efficiencies (Figure 7.2). As shown on this figure, circulator efficiency has improved substantially.

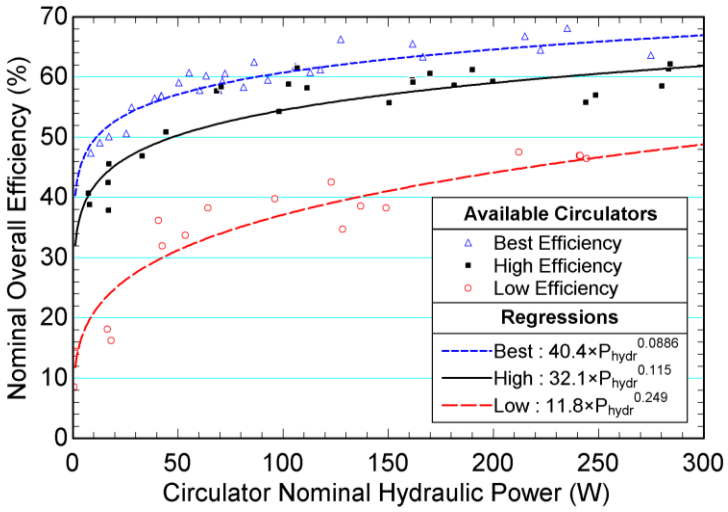

Figure 7.2 : Overall wire-to-water efficiencies of commercially available circulators (Gagné-Boisvert and Bernier, 2017)

In summary, the literature survey indicates that there are advantages in using one-pipe systems. However, there are no systematic studies that compared one-pipe networks to conventional direct-return and reverse-return networks. It is the objective of this study to develop a modelling tool that can perform annual simulations to assess the performance of these three systems.

7.4 Network features and operation

Piping lengths and diameters are different for each network. In a reverse-return system, the supply pipe section out of the bore field (segment 10-1 in Figure 7.1a) has the largest diameter as it must handle the full flow. The supply pipe flow rate then decreases along the network (from 1 to 4) and so does the diameter. The supply pipe section for the last heat pump (3-4) has the smallest diameter. The flows in the return pipe are symmetrical to the flows in the supply pipe as they increase from 5 to 8. Hence, the return pipe after the last heat pump (8-9) has the largest diameter because it handles the full flow.

In a direct-return system (Figure 7.1b), the return pipe flow rate decreases along the network in phase with the supply pipe (from 8 to 5). Then, the first pipe section has the largest supply and return pipe diameters (10-1 and 8-9).

Finally, in a one-pipe system, the primary pipe has typically the same diameter from beginning to end removing the need for reduction fittings. One of the main advantage of a one-pipe system is that its interior primary pipe is up to 50% shorter than with a reverse-return two-pipe system. Kavanaugh (2011) and Mescher (2009) also stated that simpler systems, such as one-pipe systems, tend to be more energy efficient over time. The average diameter is typically larger than for two-pipe systems. However, overall piping costs are generally lower for one-pipe systems. Finally, one-pipe systems require a circulator for each heat pump (5-6) which is not the case for two-pipe networks.

The design and operation of a two-pipe network is relatively more complex with motorized isolation valves, strainers, inverters and differential pressure controls (Mescher, 2009). Additional pipes, fittings, piping size reductions and pipe insulation are also required compared to a one-pipe system. Balancing valves (flow control) must also be added in direct-return systems (Duda, 2015) while they are generally not required in reverse-return systems (Taylor and Stein, 2002).

Table 7.1 presents a summary of the basic components required in each network as presented by Mescher (2009) and Taylor and Stein (2002). Hose kits are assumed to be installed on each heat pump. They are positioned between connections 11 and 12 for two-pipe systems (Figures 7.1a and b) and between connections 6 and 7 for one-pipe systems (Figure 7.1c). An on/off control valve is required (as shown between 12-13 in Figures 7.1a and b) at each heat pump in two-pipe networks to stop the flow when the heat pump is not operating. Direct-return systems need a balancing valve for each unit to allow the right flow to be supplied in each different hydraulic path (14-11 in Figure 7.1b). It is also common practice to install ball valves to isolate each heat pump branch from the primary pipe. However, as presented in Figure 7.1c, one-pipe networks require only one ball valve (1-5) since a check valve is added (7-8) (Mescher, 2009).

All these fittings induce pressure drops that need to be properly accounted to determine pumping energy consumption. The concept of flow coefficients (C_v) is used here to evaluate valve and hose pressure drops (Kavanaugh and Rafferty, 2015). The last column in Table 7.1 shows C_v values used in the present work. These values are typical for a 3-ton heat pump unit, which is a frequently used capacity (Kavanaugh and Gray, 2016). For example, C_v values are equal to 25 for the two-way control valve and 8 for the hoses (based on flows in gpm and a 1 psi (6.9 kPa) pressure drop). Using the definition of C_v ($=flow/\sqrt{\Delta p}$) where the flow is in gpm and the Δp is in psi, the pressure

drop is equal, respectively, to 0.13 and 1.3 psi (0.9 and 8.7 kPa) for the control valve and the connecting hoses for a 9 gpm flow rate (3 gpm/ton). A 3-ton capacity heat pump is used as the reference capacity in the proposed modelling tool; C_v are scaled for other capacities as explained later.

Table 7.1 : One- and two-pipe network components

Equipment	Components per heat pump			C_v
	One-pipe**	Two-pipe reverse-return***	Two-pipe direct-return**/***	Selected for 3-ton HP
Hose kit	1	1	1	8*
On/off control valve		1	1	25*
Shut-off ball valve	1	2	2	23.5*
Balancing valve			1	5.2**
Check valve	1			21*
Circulator	1			
*Kavanaugh and Rafferty (2015), **Mescher (2009), ***Taylor and Stein (2002)				

In all cases considered in this paper, the main pump is equipped with a variable frequency drive (VFD). The resulting variable-speed pump can then modulate the flow rate to reduce pumping power. Modulation is based here on differential pressure for two-pipe networks and on bore field return temperature for one-pipe networks, respectively. VFD can usually decrease the main pump flow rate up to a minimum percentage of the nominal flow. The main pump also shuts down if no heat pumps are in operation.

For two-pipe networks, the main flow is a function of the number of heat pumps in operation, as shown in Figure 7.3a. The main flow decreases linearly as a function of the required flow to the heat pumps up to a certain minimum (30% in this case) after which the main flow rate remains constant. The VFD regulates the main pump speed based on the signal generated by a differential pressure switch measuring the pressure difference between the inlet and outlet of the farthest heat pump branch. This would be between points 4 and 8 in Figure 7.1a. The differential pressure switch set point is generally set to the pressure drop in a heat pump branch at nominal flow. Each heat pump is equipped with a motorized two-way control valve which closes when the heat pump is off. When a heat pump is turned off, more flow will be supplied to other units, increasing momentarily the differential pressure in each operating heat pump branch. In turn, this induces a reduction of the VFD speed to supply each heat pump with its required flow. This common two-pipe control

strategy requires a similar pressure drop in each parallel branch, which is achieved by adding balancing valves in direct-return networks. The balancing valve, which is frequently an automatic flow limiting valve (Mescher, 2009), allows a specific flow to a heat pump. If too much flow is supplied to a balancing valve after another unit shut-off, its pressure drop increases to limit the flow, increasing the differential pressure and reducing the VFD speed. Balancing valves are useful devices but present higher pressure drop compared to other valves, even when fully opened. More details on hydronic balancing and balancing valves are given by Taylor and Stein (2002).

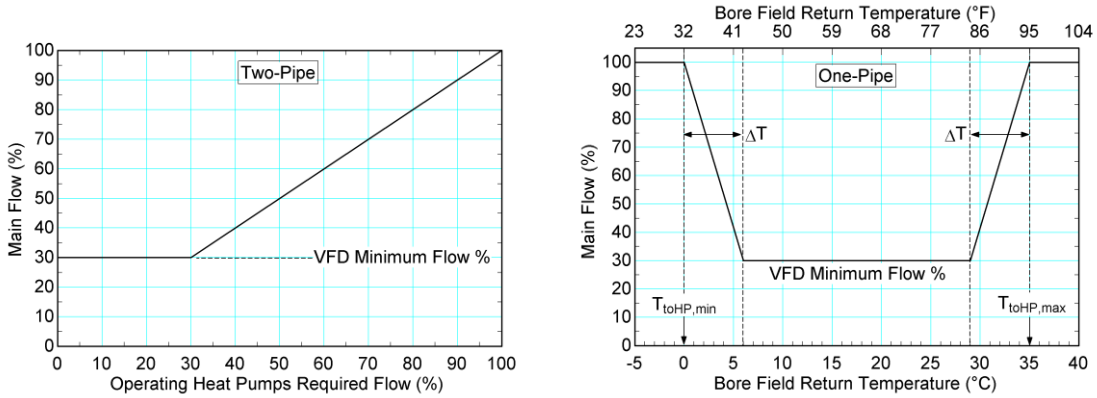

Figure 7.3 : Typical fraction of the main flow as a function a) of the number of operating heat pumps for two-pipe network (left) and b) of the bore field return temperature for one-pipe network (right)

In two-pipe networks, if the operating heat pumps require a smaller total flow rate than the lower limit of the VFD, heat pump branch differential pressure will increase. The supplementary flow is then bypassed as presented by Taylor and Stein (2002) and recombined with the flow exiting all the heat pumps.

In a one-pipe system, the main flow does not directly supply the heat pumps. It is not a function of the number of operating units like for two-pipe systems. It is typically controlled to maintain a favorable bore field return temperature. However, no guidelines could be found in the literature regarding the range of acceptable bore field return temperatures. A control method is therefore proposed in this paper and is illustrated in Figure 7.3b. This figure presents the required flow rate for the expected temperature span where $T_{toHP,min}$, $T_{toHP,max}$ and ΔT are operational variables. The main flow control method proposed here is a function of the fluid temperature exiting the main pump and entering the first heat pump, T_{toHP}. If T_{toHP} reaches the high ($T_{toHP,max}$) or low ($T_{toHP,min}$)

operating temperature limits (e.g. 0 °C or 35 °C as shown in Figure 7.3b), the VFD must provide 100% of the maximum flow. If T_{toHP} is between $T_{toHP,min}+\Delta T$ and $T_{toHP,max}$ $-\Delta T$, the VFD is set to supply its minimum flow to reduce pumping power. The flow varies linearly between minimum and maximum values, as shown in Figure 7.3b. With this control scheme, the value of ΔT has to be correctly specified to reduce energy consumption. A high ΔT increases the main pump energy consumption as higher flow rates are required on average. On the other hand, heat pump energy consumption is reduced as higher flow rates lead to more favorable bore field return temperature and less temperature changes between heat pumps. Based on the four test cases which will be presented later, the total energy consumption is minimized when ΔT = 6 °C.

7.5 Integrated modelling tool

It is possible to model and simulate piping networks of GCHP systems in simulation software tools such as TRNSYS. However, it becomes impractical and time consuming when there is a large number of heat pumps, valves, pipes to link together. Furthermore, for comparative studies, different assemblies need to be constructed for the one-pipe, reverse-return two-pipe and direct-return two-pipe networks.

In order to make these comparisons simpler and faster, a general integrated modelling tool has been developed to compare the energy performances of a GCHP system with one- or two-pipe interior networks. The tool is developed in the TRNSYS v17 environment (Klein et al., 2010) in the form of a single TYPE. It needs to be linked to a main circulating pump model and a bore field model.

The parameters, inputs and outputs of the TYPE are presented in Figure 7.4. They are also described in more details in Table 7.7 in Appendix A. The user can modify several parameters including the type of network, the pipe linear head loss, heat pump COPs, and valve pressure drops. Heat pump positions (X,Y), nominal heat pump capacity (tons) and required flow rate (gpm/ton) are also user-selected. Building loads associated with each heat pump (Load (i) in Figure 7.4) are inputs to the TYPE. Typically, these loads are given on an hourly basis but other time steps can be used. The assumptions, the methodology and some intermediate results obtained with this tool will now be presented.

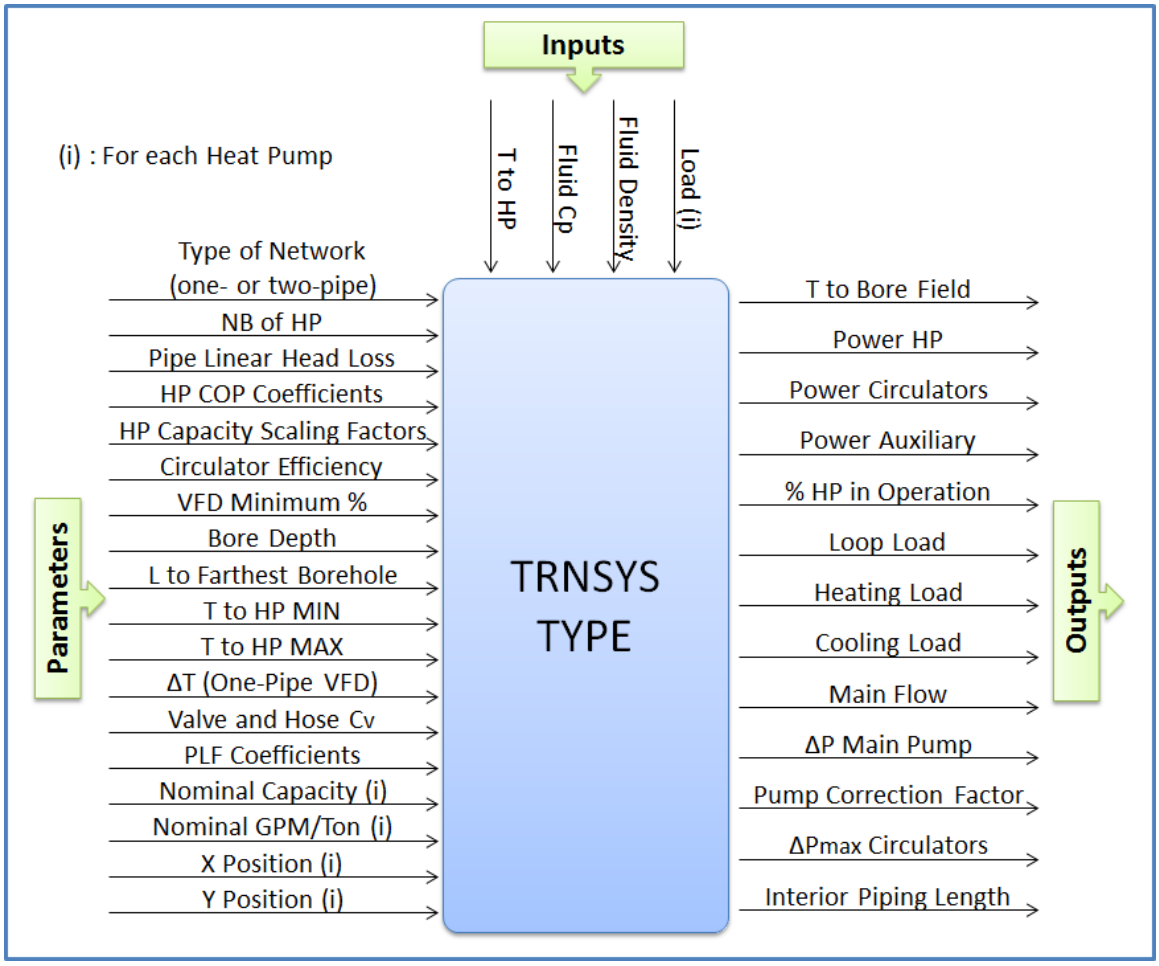

Figure 7.4 : Schematic diagram of the integrated modelling tool

7.5.1 Assumptions

The calculations performed by the tool are based on the following assumptions.

- The cooling (heating) energy supplied by each heat pump equals the cooling (heating) load at every time step. In heating, each heat pump has an auxiliary heating source in case the heating load is larger than the heat pump capacity during a given time step.
- Heat pumps are single-stage and cycle (on/off) if the load is lower than the capacity.
- Heat pumps are installed close to the main pipe and the pressure drop in the pipe sections between a heat pump and the main pipe are assumed to be negligible when compared to valve pressure drops.

- Each parallel heat pump segment, comprising valves and hose kit, has the same pressure drop.
- The main pipe follows the shortest path between each consecutive heat pump.
- Pipes and U-tubes in boreholes are designed so that the nominal linear pressure drop is the same everywhere in the network. A default value of 2 ft wc/100 ft is assumed.
- The reference heat pump has a 3-ton (10.6 kW) nominal capacity.
- All heat pumps have the same normalized performance and capacity curves as the reference heat pump. These values depend only on the entering fluid temperature (Hackel et al., 2008).

7.5.2 Methodology

7.5.2.1 Main flow control

The maximum main flow rate, $\dot{m}_{tot}$, is the sum of the nominal flow rate of every heat pump, $\dot{m}_i$ (Eq. 7.1). It is then multiplied by the VFD fraction, f, which varies between the minimum fraction (f_{min}) and 100%, to obtain the main flow rate, $\dot{m}$, during a given time step (Eq. 7.2).

In one-pipe systems, the scenario proposed in Figure 7.3b is used to determine the VFD fraction for one-pipe systems, f_{1pipe}, based on the input value of T_{toHP} prevailing during a given time step.

The VFD fraction for two-pipe systems, f_{2pipe}, is a function of the number of heat pumps in operation during a time step and of their specific nominal flow rate (Eq. 7.3). The heat pump nominal flow rate is defined as the heat pump nominal capacity (in tons) multiplied by its specific flow rate per ton. If the VFD fraction is inferior to the minimum flow fraction, then f_{2pipe} is set to f_{min}. As indicated earlier, the superfluous flow is then bypassed and recombined with the fluid exiting all the heat pumps (Taylor and Stein, 2002).

$$\dot{m}_{tot} = \sum \dot{m}_i \tag{7.1}$$

$$\dot{m} = f \times \dot{m}_{tot} \tag{7.2}$$

$$f_{2pipe} = MAX\left[f_{min}, \frac{\sum_i^{Operating\ HP} \dot{m}_i}{\dot{m}_{tot}}\right] \tag{7.3}$$

7.5.2.2 Heat pump locations and piping lengths

The selection of one of the three networks influences the interior piping length, which affects the pressure drop. The tool must then account for heat pump location to evaluate the various pipe lengths and uses the following procedure to do so. As shown in Figure 7.5, each numbered heat pump is located with (X,Y) coordinates which are sets as parameters in the TRNSYS TYPE (Figure 7.4). By convention, the mechanical room and main circulating pump are located at (0,0). Then, the shortest length between each element (heat pump or mechanical room) is calculated.

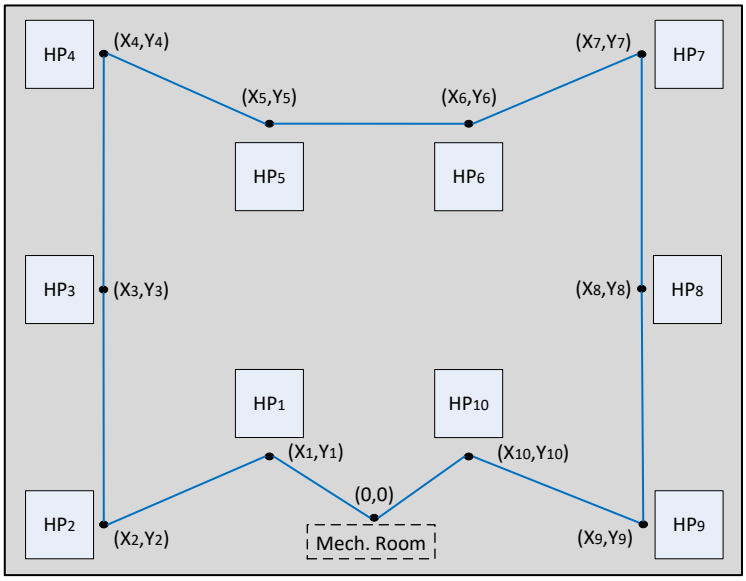

Figure 7.5 : Example of heat pump locations in a building

The length used to calculate the worst hydraulic path, which determines the overall piping pressure drop, is then evaluated. It includes the length of the supply and return pipes between the mechanical room and the last heat pump, the length of the supply and return pipes to the farthest borehole, and the length of the upward and downward legs in a borehole.

7.5.2.3 Head losses

The main pump head, H, is a function of the supplied flow rate and installed accessories with their associated pressure drops (Table 7.1). It is specific to the chosen configuration and varies over time. The tool calculates the main pump head at every time step which is then outputted along with the main flow rate to an external pump model to evaluate pumping energy consumption.

In two-pipe systems, each operating parallel branch presents the same pressure drop. The main pump head is then the sum of the pressure drop in a heat pump branch (heat pump and associated valves) in its supply and return pipe segments, and in the main pipe and borehole. In a reverse-return network like the one presented in Figure 7.1a, the main pump nominal head when all heat pumps are in operation, $H_{2pipe,rev}$, is calculated according to Equation 7.4.

$$H_{2pipe,rev} = \Delta p_{1-2} + \Delta p_{2-3} + \Delta p_{3-4} + \Delta p_{4-8} + \Delta p_{8-9} + \Delta p_{9-10} + \Delta p_{10-1} \quad (7.4)$$

where Δp_{8-9} and Δp_{10-1} are related to the main pipe segments with the largest diameter and total flow. They also include the pipe length from the mechanical room to the farthest borehole. Δp_{9-10} is the sum of the pressure drop through the upward and downward legs of a U-tube borehole. Δp_{1-2}, Δp_{2-3}, and Δp_{3-4} are related to the last heat pump supply pipe. The nominal pressure drop in each of these segments is equal to its length multiplied by the nominal linear head loss which is based on the maximum design flow and provided as a parameter to the TRNSYS TYPE. Δp_{4-8}, calculated by Equation 7.5, is the pressure drop in a heat pump branch.

$$\Delta p_{4-8} = \Delta p_{4-11} + \Delta p_{11-HP} + \Delta p_{HP} + \Delta p_{HP-12} + \Delta p_{12-13} + \Delta p_{13-8} \quad (7.5)$$

Δp_{4-11} and Δp_{13-8} are equal and represent the pressure drop in both ball valves while Δp_{12-13} is the two-way control valve pressure drop. The sum of $\Delta p_{11-\mathrm{HP}}$ and $\Delta p_{\mathrm{HP}-12}$ represents the hose kit pressure drop. Valve and hose pressure drops are calculated using flow coefficients and Equation 7.6, where $\Delta p_{\mathrm{Valve}}$ is in kPa and $\dot{m}_i$ is in L/s. Components and their specific C_v are selected for a 3-ton heat pump operating with the standard 3 gpm/ton. These values are set as parameters in the TRNSYS model. If a specific heat pump has a different nominal capacity, CAP_{nom}, it requires a different flow rate and different valves are selected. This is done using a capacity ratio, CR (Eq. 7.7), which is simply the unit capacity versus the reference capacity. For example, a 5-ton heat pump using 3 gpm/ton has a CR of 1.67 and requires 67% more flow than the reference case. Valves with C_v that are 67% higher are required to maintain the same pressure drop. The values of C_v are then corrected by CR to obtain an adapted C_v, $C_{v,corr}$ (Eq. 7.8).

$$\Delta p_{Valve} = 6.9 \times \left(\frac{\dot{m}_i}{C_{v,corr}}\right)^2 \quad (7.6)$$

$$CR = \frac{CAP_{nom}}{3}, in\ tons \quad (7.7)$$

$$C_{v,corr} = C_v \times CR \quad (7.8)$$

Δp_{HP} is the heat pump heat exchanger pressure drop and is a function of the flow rate and inlet fluid temperature. Equation 7.9, where Δp_{HP} is in kPa, $\dot{m}_i$ in L/s and T_{inHP} in °C, is a regression based on a 3-ton heat pump performance map presenting pressure drops for several flow rate and temperature combinations (ClimateMaster, 2012). It is valid for flow rates ranging from 0.284 to 0.568 L/s (4.5 to 9 gpm) and for inlet temperature ranging from -1.1 to 48.9 °C (30 to 120 °F). The flow is divided by CR (Eq. 7.7) to allow the use of Eq. 7.9 with different heat pump capacities. A larger heat pump would have a heat exchanger sized accordingly to maintain a similar pressure drop than with a 3-ton unit but with a higher flow. This flow correction procedure was verified with other heat pump capacities from the same manufacturer (ClimateMaster, 2012).

$$\Delta p_{HP} = 88.0 \times \left(\frac{\dot{m}_i}{CR_i}\right) - 0.179 \times T_{inHP} - 13.3 \tag{7.9}$$

When the main flow is reduced from the nominal operating condition, the main pump head varies along the system curve (head vs flow rate). With a constant differential pressure maintained at each heat pump, the pressure drop across heat pumps does not change. Consequently, as explained by Bernier and Lemire (1999), the system curve does not tend towards the origin of the head vs flow rate graph but rather towards the differential pressure switch setting. Thus, if only a small fraction of the heat pumps are in operation, the friction head in the main pipes is negligible because of the lower flow rate and the pump must deliver a head equivalent to the differential pressure switch setting. The system then behaves like an open system with a static head.

The pressure drop in every pipe segment, Δp_s, varies with flow rate according to the assumption presented earlier. Thus, as shown in Eq. 7.10, the nominal pressure drop of each pipe segment (H_{linear}) is multiplied by the square of the fraction of the nominal flow in that segment, $\dot{m}_s/\dot{m}_{nom}$, and by its length, L, to obtain Δp_s. Similarly, the pressure drop in boreholes and in segments containing the main flow is the product of the nominal pressure drop and the square of the flow fraction.

$$\Delta p_s = L \times H_{linear}(\dot{m}_s/\dot{m}_{nom})^2 \tag{7.10}$$

The flow rate varies between heat pumps in the supply and return main pipes. If any heat pump is not in operation, the flow in some of these segments will be lower while being nominal in others. This irregular flow distribution in the supply and return pipes is considered in the tool as the flow in each segment is compared to its nominal flow at each time step.

For example, and with reference to Figure 7.1a, if only the first and third heat pumps are in operation during a time step, the main flow will be 50% of the nominal flow (assuming that all heat pumps require the same flow rate). The main pump head, $H_{2pipe,rev'}$, is then given by Eq. 7.11 representing the hydraulic path to the farthest operating heat pump. The heat pump branch pressure drop, Δp_{3-7}, which includes the third heat pump, is equal to Eq. 7.5 while pipe segments are different. The flow rate in segments 8-9, 9-10 and 10-1 is 50% of the nominal flow rate, leading to a pressure drop equal to 25% of the nominal pressure drop in these segments. Moreover, Δp_{7-8} is equal to 44% of this segment nominal pressure drop as it handles the return flow of two heat pumps instead of three.

$$H_{2pipe,rev'} = \Delta p_{1-2} + \Delta p_{2-3} + \Delta p_{3-7} + \Delta p_{7-8} + \Delta p_{8-9} + \Delta p_{9-10} + \Delta p_{10-1} \tag{7.11}$$

The main pump head in a direct-return system is evaluated the same way except for the balancing valve pressure drop which is added to the heat pump branch head loss. Different pipe segments are also considered as the hydraulic path is different.

Finally, in one-pipe systems, there are two different head losses to consider. The primary loop head (main pipe and boreholes) is handled by the main pump while the heat pump branch head (heat pump and valves) is handled by each circulator. Based on Figure 7.1c, the main pump nominal head is calculated using Eq. 7.12. The nominal main pump head, H_{1pipe}, then equals the total hydraulic path length multiplied by the nominal linear head loss. With a reduced main flow, this head is multiplied by the square of the main flow fraction as described earlier in Eq. 7.10.

$$H_{1pipe} = \Delta p_{1-2} + \Delta p_{2-3} + \Delta p_{3-4} + \Delta p_{4-1} \tag{7.12}$$

The heat pump branch pressure drops are calculated with an equation similar to Eq. 7.5 but with different valves (see Table 7.1). The heat pump branch pressure drop is independent from the main flow. This pressure drop is calculated for every operating heat pump branch so that individual circulator pumping power, W_{Circ_i}, can be obtained (Eq. 7.13). Circulator efficiencies, η_i, are based on regressions presented in Figure 7.2. The user can select which class (Low, High or Best Efficiency) to use.

$$W_{Circ_i} = \frac{\dot{m}_i \times \Delta p_i}{\eta_i} \tag{7.13}$$

7.5.2.4 Heat Pump COP and Capacity

The fluid inlet temperature influences heat pump *COP* and capacity. In two-pipe systems, it is assumed that all units have the same inlet fluid temperature during a given time step. Consequently, based on the assumption mentioned above, they also have the same normalized capacity and *COP*. However, in a one-pipe system, normalized capacity and *COP* vary since the fluid temperature changes as the operation of a specific unit influences the following ones. The tool models each heat pump individually to simulate this phenomenon. Thus, the *COP* and the capacity are calculated for each heat pump at each time step with the corresponding inlet fluid temperature. The heat pump energy consumption and loop heat rejection, W_{HP_i} and Q_{Loop_i}, are then obtained with Equations 7.14 and 7.15.

$$W_{HP_i} = \frac{|Load_i|}{COP_i \times PLF_i} \tag{7.14}$$

$$Q_{Loop_i} = W_{HP_i} - Load_i + (1 - \eta_i) W_{Circ_i} \tag{7.15}$$

As shown in Eq. 7.15, circulator heat losses to the fluid are added to the one-pipe loop loads. An electrical auxiliary heater is turned on if a heat pump heating capacity is lower than the load. The auxiliary power is then the difference between the load and the capacity. Inversely, if the capacity is higher than the cooling or heating load, the heat pump cycles to meet the load and a Part-Load Factor (PLF in Eq. 7.14) is used as explained in the following section.

In the proposed tool, heat pump *COP* and capacity variations are considered independent of the nominal capacity (Hackel et al., 2008). Furthermore, heating and cooling *COPs* and capacities are considered to vary linearly with the inlet temperature, T_{inHP_i}, as proposed by Bernier et al. (2007) and Hackel et al. (2008). Thus, as shown in Eq. 7.16, two parameters are needed in heating and two in cooling to set heating and cooling *COP* equations. For the capacity, each heat pump nominal capacity, CAP_{nom}, is set as a parameter in the TRNSYS TYPE. The scaling factor approach (Hackel et al., 2008) is then used to correct this capacity depending on the inlet temperature (Eq. 7.17). Heating and cooling Capacity Scaling Factors, CSF, are set using four parameters. In the following simulations, values from a manufacturer's performance map (ClimateMaster, 2012) are used (see Table 7.2). For example, using data of Table 7.2, $CSF_{heating}$ equals 0.75 at 0 °C (32 °F), which means that the heat pump heating capacity is equal to 75% of its nominal value.

$$\begin{aligned} COP_{heating_i} &= a + b \times T_{inHP_i} \\ COP_{cooling_i} &= c + d \times T_{inHP_i} \end{aligned} \tag{7.16}$$

$$\begin{aligned} CSF_{heating_i} &= e + f \times T_{inHP_i} \\ CSF_{cooling_i} &= g + h \times T_{inHP_i} \\ CAP &= CSF \times CAP_{nom} \end{aligned} \tag{7.17}$$

7.5.2.5 Part-load operation

Heat pumps and circulators cycle during a given time step to meet each zone load and to avoid overheating or cooling. The $PLR - PLF$ approach is used here to account for this phenomenon. The PLR (Eq. 7.18) represents the fraction of a time step during which a single-stage heat pump must operate to fill a specific load. A 50% PLR means that a 10 kW heat pump must run half of the time to fill a 5 kW load during a given time step. The Part-Load Factor (PLF) approach developed by Henderson et al. (2000) is used to correct the *COPs* to account for cycling losses as indicated in Eq. 7.14. As shown in Equation 7.20, the PLF is a function of the PLR and of the Energy Input Ratio (EIR). This last value is obtained using a 3rd order polynomial as a function of the PLR (Eq. 7.19). The calculation of the EIR requires four coefficients which are presented by Henderson for various unit efficiencies. These four coefficients are set as parameters in the tool. The "Good efficiency unit with off-cycle power" constants reported by Henderson et al. (2000) and shown in Eq. 7.19 are used in the following case studies.

$$PLR_i = \frac{Load_i}{CAP_i} \tag{7.18}$$

$$\begin{aligned} EIR &= a_0 + a_1 \times PLR + a_2 \times PLR^2 + a_3 \times PLR^3 \\ with\ a_0 &= 0.009881, a_1 = 1.080, a_2 = -0.1053\ and\ a_3 = 0.01514 \end{aligned} \tag{7.19}$$

$$PLF_i = \frac{PLR_i}{EIR_i} \tag{7.20}$$

Pump power is also corrected to account for heat pump cycling as flow rate may vary over a time step. For one-pipe systems, the circulator power is multiplied by the PLR as a circulator cycles with its heat pump. If a heat pump is on during half of a time step, its circulator will also operate during half of the time resulting in half of the energy consumption during that time step. The one-

pipe main pump flow rate is not related to the number of heat pumps in operation so it is not correlated with the PLR.

For two-pipe systems, the main pump flow rate is a function of the number of heat pumps in operation during a time step. However, each heat pump may cycle randomly during this time step. As an attempt to account for these flow variations during time steps, the following method has been used. First, the main pump power is calculated based on the total required flow during each time step. Then, a main pump correction factor, F_{pump}, is calculated (Eq. 7.21) to correct the required main pump power. F_{pump} constitutes the average of all the operating heat pump PLR weighted with their corresponding flow rate.

$$F_{pump} = \frac{\sum_{i}^{Operating\ HP} PLR_i \times \dot{m}_i}{\dot{m}} \tag{7.21}$$

7.5.2.6 Outlet fluid temperature

Heat pump outlet fluid temperature must be calculated for two reasons: to calculate the overall outlet temperature returning to the bore field and to evaluate the temperature variation along a one-pipe loop. In all cases, the outlet temperature of each heat pump is calculated with an energy balance based on the energy injected or rejected by the heat pump in the return pipe.

7.5.2.7 Outputs

Among the most useful outputs of the tool are the energy consumption of all heat pumps and circulators. The required main flow rate and the primary loop pressure drop are supplied to the pump model to calculate pumping power (corrected using F_{pump}). The variable-speed pump efficiency is based on the approach developed by Bernier and Lemire (1999).

The following example demonstrates the usefulness of the tool to compare one- and two-pipe networks. A four heat pump system as presented in Figure 7.1 is used in this example. The results of a 10-hour simulation (3-minute time step) are shown in Figure 7.6 with a sequence of operation involving 4, 3, 2, 1, 2, 3, 4 heat pumps (each with a nominal 3-ton capacity but providing 7 kW of heating when in operation). Heat pumps require a flow rate of 9 gpm and are 20 m apart from each other. Finally, a 2 ft/100 ft nominal pressure drop is set as a parameter.

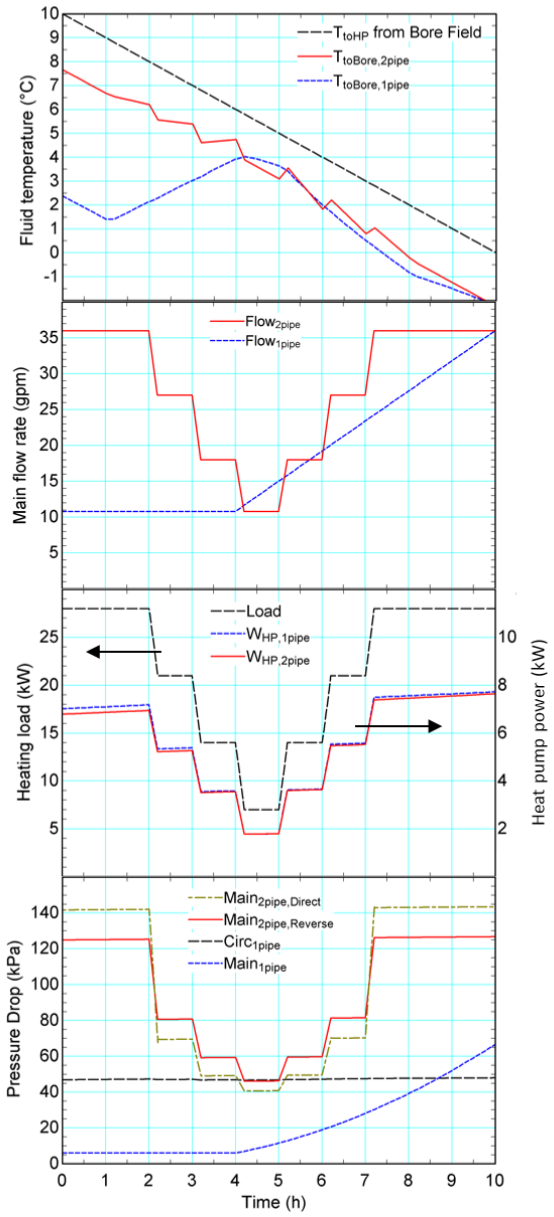

Figure 7.6 : a) Temperature (top), b) flow (center-top), c) power (center-bottom) and d) pressure drop (bottom) obtained with the simulation tool

Figure 7.6a first shows the resulting outlet temperature. Heat pump power, flow rates and pressure drops are also presented to show the behavior of the different networks. The value of T_{toHP} is arbitrarily set to vary from 10 to 0 °C in this example. Various flow rates are then required for both one- and two-pipe networks (Figure 7.6b).

As shown in Figure 7.6c, total heat pump input power varies as heat pumps cycle to meet the load. For both cases, heat pump input power increases slightly at each time step even if the load is

constant during a given hour. This is due to the fact that T_{toHP} drops with a corresponding drop in the value of the *COP*. The one-pipe case requires slightly more heat pump power as the fluid temperature supplying heat pumps decreases after each unit. However, the heat pump power is equal for both one-pipe and two-pipe systems between the fourth and fifth hours as only one heat pump is in operation. The outlet temperature variation (Figure 7.6a) can be explained by the combination of the main flow rate and the number of heat pumps in operation. The two-pipe outlet temperature difference (relative to T_{toHP}) is relatively constant as the flow rate is aligned with the number of operating heat pumps. In contrast, the one-pipe temperature difference is higher at the beginning as four heat pumps are in operation with a low main flow rate and it then stabilizes as the flow rate increases.

Finally, Figure 7.6d presents various pressure drops which are all a function of the main flow except for the circulator pressure drops (which have a negligible increase due to the inlet temperature drop). It shows that the main pump of two-pipe systems experiences a higher pressure drop than the one-pipe system. It also shows that the direct-return pressure drop is higher than the reverse-return at full flow, which is mostly due to the presence of balancing valves. However, when flow decreases, the direct-return presents a lower pressure drop. This is due to a reduction of the worst hydraulic path length as the farthest heat pumps are turned off first in that case.

7.6 Comparison with a detailed simulation

A detailed TRNSYS simulation of a GCHP system is performed to compare its results with the proposed modelling tool to ensure that the tool was correctly implemented. The system consists of four heat pumps (Figure 7.1) simulated individually with the required piping, valves and connections being considered separately in TRNSYS using equation TYPES. As shown in Figure 7.7, each heat pump is coupled to a single-zone building using a thermostat to control its operation. Circulators are also simulated and the control of the system is modified depending on whether a one- or two-pipe network is simulated.

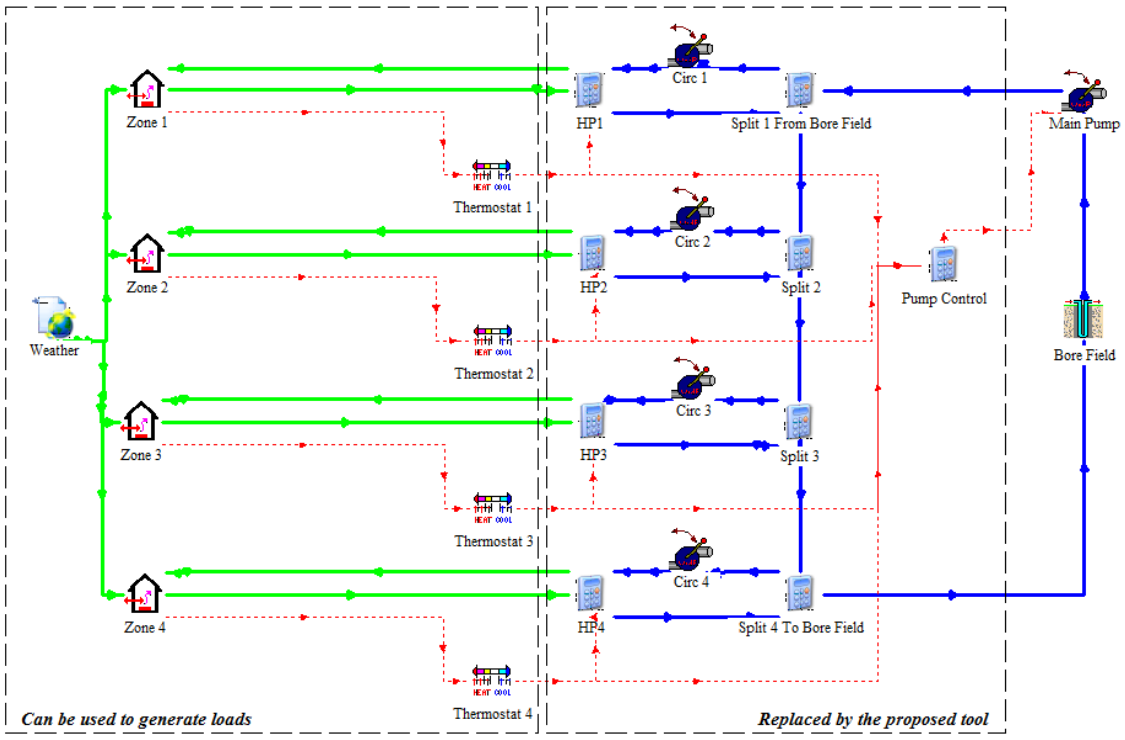

Figure 7.7 : Detailed modelling of a 4 heat pump GCHP system used to compare the proposed tool

Typical models found in TRNSYS are used for thermostats, circulators and buildings while heat pumps are modeled with the model of Ndiaye and Bernier (2012). This experimentally validated transient heat pump model accounts for cycling effects on heat pump power using start and stop time constants. Several preliminary simulations were performed with this model to obtain the corresponding *PLF* coefficients to use in the proposed tool to compare heat pumps with the same performances. The obtained coefficients, shown in Figure 7.8, are similar to the "Good efficiency unit without off-cycle power" presented by Henderson et al. (2000). The bore field model of Godefroy and Bernier (2012) has been used, as explained later.

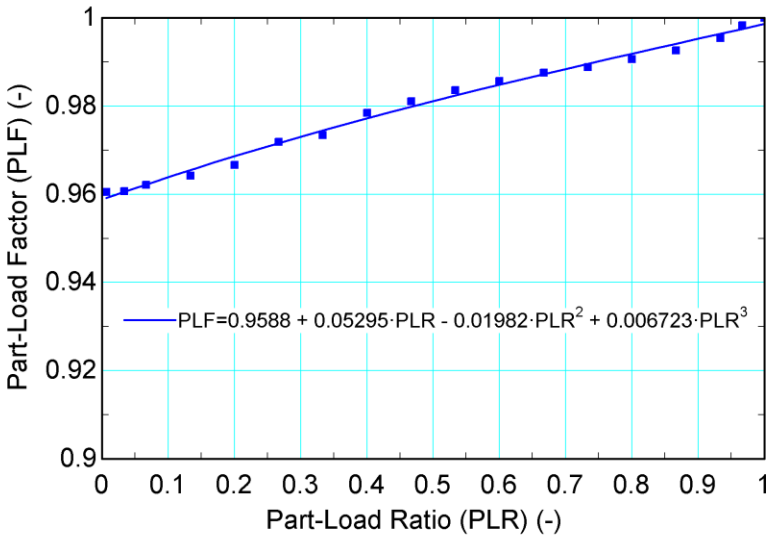

Figure 7.8 : PLF versus PLR obtained by simulating Ndiaye and Bernier's heat pump model (2012)

The operation of this detailed approach is simulated with a 3-minute time step over 30 hours during the heating season. A one-pipe and a reverse-return two-pipe configurations are simulated. The instantaneous heat pump power and bore field inlet and outlet temperatures are presented in Figures 7.10 (one-pipe) and 7.11 (two-pipe) with the *Inst* curves. Several oscillations are observed for both configurations, as heat pumps cycle to meet their zone load. Hourly moving averages are however added (*Avg* curves) to help in the interpretation of results.

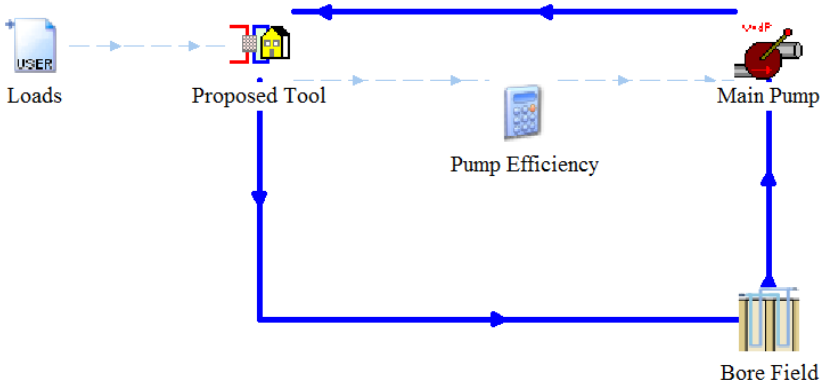

Figure 7.9 : GCHP system modelling using the proposed tool

The same one- and two-pipe cases are also simulated with the proposed tool, but with a 1-hour time step. Figure 7.9 shows the resulting TRNSYS assembly using the tool. The same system parameters

are used and heat pump performance coefficients required by the tool are based on a heat pump performance map (ClimateMaster, 2012) also used in the detailed modelling. The four zone loads are obtained from the detailed simulations by averaging required heating load over an hour (Figure 7.10a). The total heating load is 482 kWh during the 30-hour period. A text file containing these loads is then supplied to the tool leading to simulation results presented in Figures 7.10 and 7.11. As it can be observed, the same general tendencies observed with the detailed simulation (hourly averages) are predicted by the tool. One can note that the outlet temperature (inlet to the bore field) is lower in the one-pipe network as the flow rate is generally lower in the proposed tool. In terms of energy consumption, the tool predicts a total heat pump energy consumption of 134 kWh for the one-pipe and of 127 kWh for the two-pipe systems. The detailed simulations predict corresponding energy consumption of 136 and 128 kWh, representing less than a 1.5% difference. From this comparison, it can be concluded that the proposed tool is in very good agreement with detailed simulations. Both simulations require similar computational time if the same time step is used.

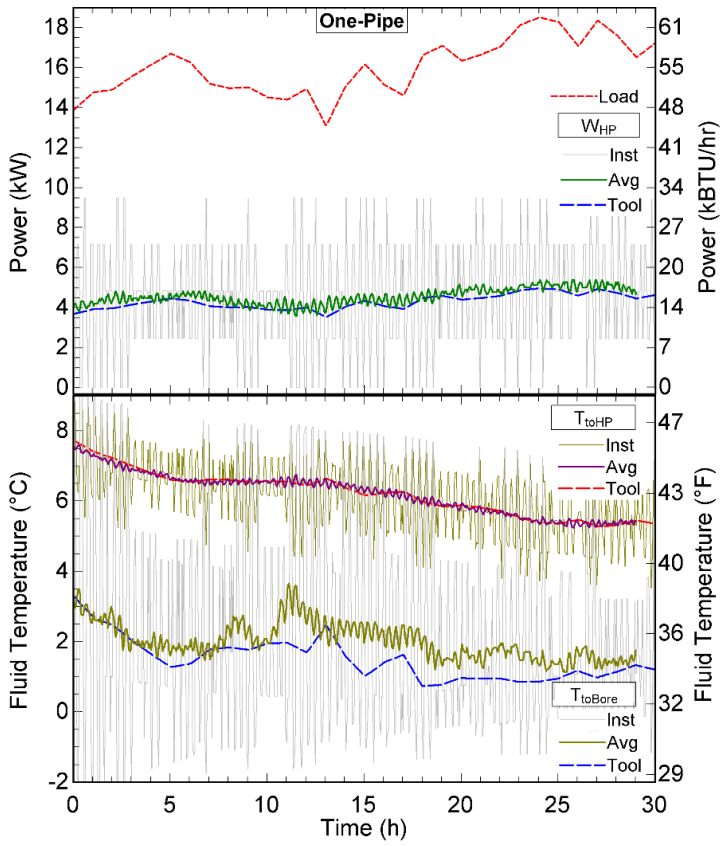

Figure 7.10 : Simulated a) power (top) and b) temperature (bottom) using the tool and a detailed modelling (One-pipe)

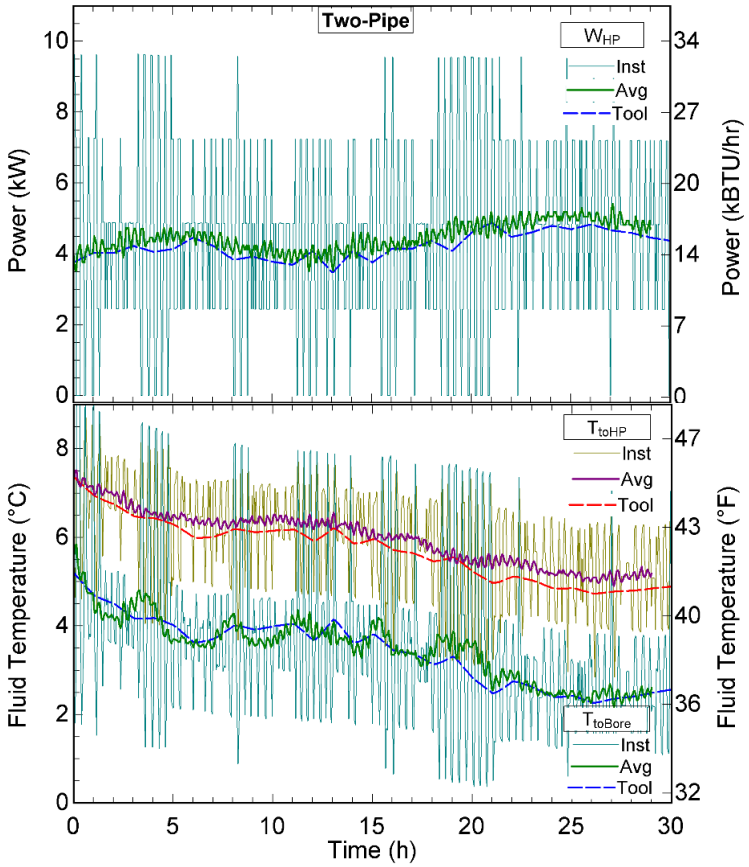

Figure 7.11 : Simulated a) power (top) and b) temperature (bottom) using the tool and a detailed modelling (Two-pipe)

The proposed tool was also used to find the best ΔT value for flow control in one-pipe systems (see Figure 7.3b). Several test cases were evaluated all giving similar results. As shown in Figure 7.12 for one of these cases (corresponding to Case 1 in the following section), increasing the ΔT increases the main pump energy consumption as higher flows are more often required. However, it also reduces heat pump energy consumption as higher flows lead to more favorable bore field return temperature and less temperature changes between heat pumps. The minimum total energy consumption for all studied cases, including the one shown in Figure 7.12, is obtained for a ΔT between 5.5 and 6.5 °C. Therefore, it is recommended to use a ΔT of 6 °C (11 °F) when using one-pipe systems.

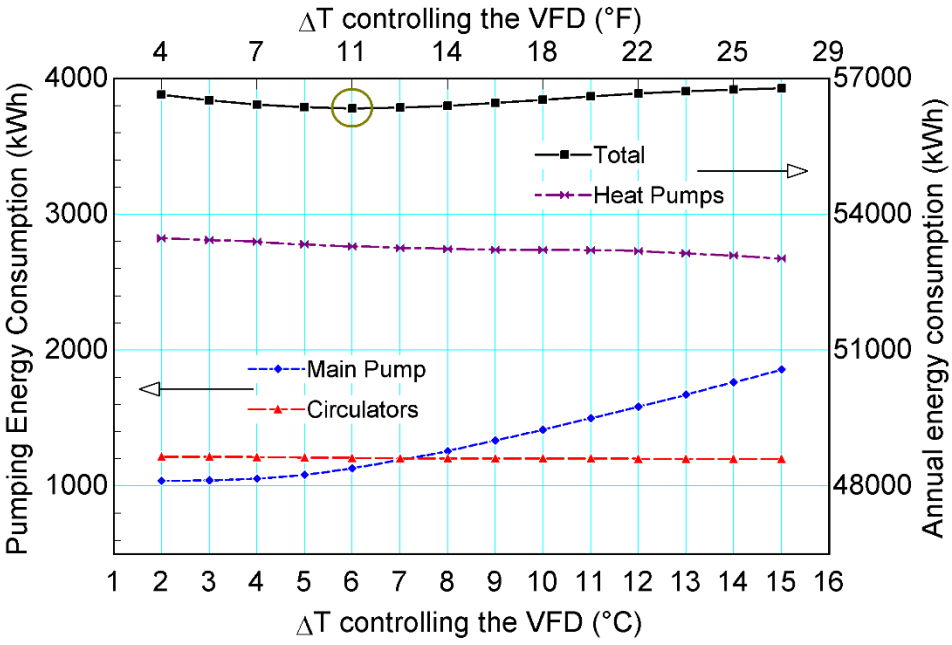

Figure 7.12 : ΔT optimization for the proposed one-pipe VFD control

7.7 Case studies

This section demonstrates how the proposed TRNSYS tool can be used to compare one- or two-pipe networks when designing a GCHP system. Four different cases are studied, addressing two building geometries and two load profiles with ten 3-ton heat pumps in each case. The first building, representing a 60×60 m (197×197 ft) square office building with a loop of four core and six perimeter heat pumps, is portrayed in Figure 7.5. The second building is a 10×90 m (33×295 ft) longitudinal building represented by Figure 7.13. The two load profiles are given in Figures 7.14a and 7.14b, showing total heating and cooling loads over a year (cooling and heating can occur simultaneously). The first one is a mixed load profile with an annual heating load of 101 800 kWh and an annual cooling load of 110 100 kWh. The second load profile is a cooling-only load profile with an annual cooling requirement of 214 300 kWh. Each system is coupled to a bore field composed of 10 boreholes. In all cases, borehole depth is selected such that the lowest or highest bore field return temperatures over the year reach 0 °C (32 °F) or 35 °C (95 °F), which are the heat pump operating limits used in these cases.

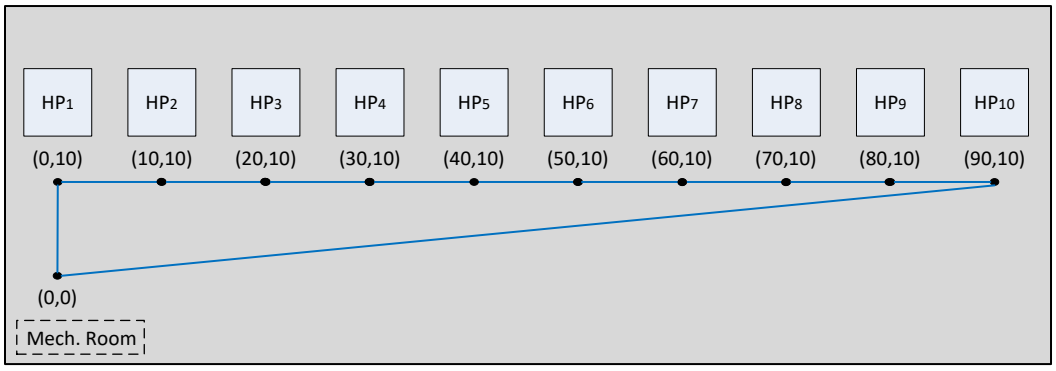

Figure 7.13 : Second building heat pump position (Longitudinal)

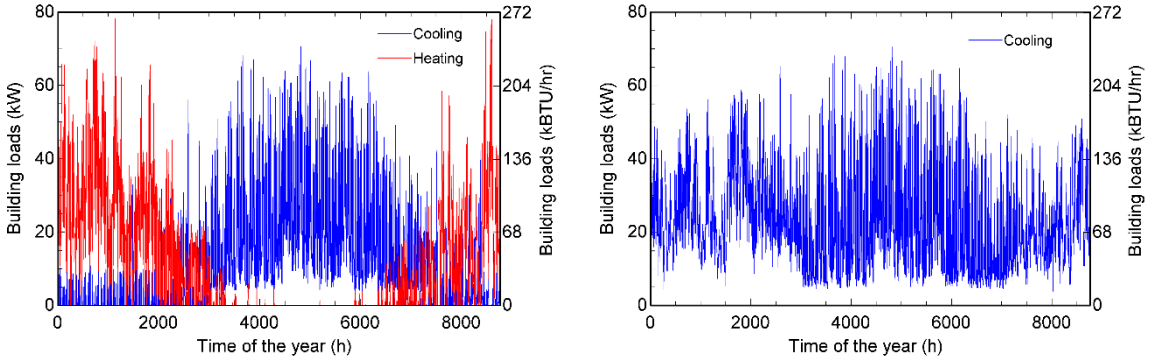

Figure 7.14 : a) Mixed (left) and b) cooling-only (right) building load profiles over a year

Loads are supplied to the tool which is coupled to a main pump and to a borehole model (Figure 7.9). The main parameters used are presented in Table 7.2. The so-called TRCM bore field model from Godefroy and Bernier (2014) is used to model the bore field. The model relies on g-functions to evaluate the thermal response of the ground (Cimmino and Bernier, 2014). The values of g-functions are obtained using the preprocessor developed by Cimmino and Bernier (2013). The borehole thermal resistance is also calculated at each time step, which is important as the main flow rate varies over time, often reaching laminar flow and influencing the borehole thermal resistance. Finally, this experimentally validated model (Godefroy et al., 2016) accounts for fluid and grout thermal capacity, which affects heat pump performance (Gagné-Boisvert and Bernier, 2016).

Table 7.2 : System parameters used for the four case studies

Category	Parameter	Value
Bore field	Ground conductivity	2.2 W/m-K (1.27 BTU/hr.ft.°F)
	Ground diffusivity	0.1 m^2/day (0.98 ft^2/day)
	Grout conductivity	1.5 W/m-K (0.87 BTU/hr.ft.°F)
	Pipe diameter (in-out)	0.027-0.033 m (1 in)
	Fluid (Mixed/Cool)	Prop. Glycol 20% / Water
	Initial ground temperature (Mixed/Cool)	10 °C / 20 °C (50 °F / 68 °F)
Other equipment	Main pump efficiency	Bernier and Lemire (1999)
	VFD Minimum %	30%
	Circulators efficiency	"High" regression
	Heat pump inlet temperature limits	0-35 °C (32-95 °F)
	Heat pump COP	Heat: 3.7+0.054T / Cool: 7.1-0.13T
	Heat pump capacity scaling factor	Heat: 0.75+0.018T / Cool: 1.16-0.0072T
	Nominal flow rate / Capacity	3 gpm/ton (0.054 L/s.kW)
	Mech. room to farthest bore	30 m (98 ft)
	Linear head loss	2 ft/100 ft (0.2 kPa/m)

The four building/loads combinations are then simulated with the three piping configurations and with a one hour time step (smaller steps lead to similar results). Resulting annual energy performances are presented in Tables 7.3 to 7.6 for each case. In these tables, *Pumping fraction* is the ratio of the total pumping energy consumption over the total energy consumption and the seasonal performance factor (*SPF*) is the ratio of the annual heating and cooling requirements over the total energy consumption (adapted from a definition of Nordman and Zottl, 2011).

Table 7.3 : Case 1 (Square/Mixed) - Simulation results for the 3 configurations

Case 1 (Square/Mixed)	**One-pipe**	**Two-pipe reverse-return**	**Two-pipe direct-return**
Total energy (kWh)	56 339	54 861	55 912
Heat pumps energy (kWh)	53 287	51 804	51 828
Main pump energy (kWh)	1 130	2 502	3 536
Circulators energy (kWh)	1 206	(-)	(-)
Pumping fraction (%)	4.1	4.6	6.3
SPF (-)	3.76	3.86	3.79
Main pump max Δp (kPa/ft)	112/37	160/54	226/76
Circulators max Δp (kPa/ft)	48/16	(-)	(-)
Interior piping (m/ft)	258/846	487/1598	487/1598
Bore depth (m/ft)	126/413	127/417	127/417

Table 7.4 : Case 2 (Square/Cooling) - Simulation results for the 3 configurations

Case 2 (Square/Cooling)	**One-pipe**	**Two-pipe reverse-return**	**Two-pipe direct-return**
Total energy (kWh)	73 583	69 778	70 915
Heat pumps energy (kWh)	71 115	67 100	67 209
Main pump energy (kWh)	1 344	2 678	3 706
Circulators energy (kWh)	1 124	(-)	(-)
Pumping fraction (%)	3.4	3.8	5.2
SPF (-)	2.91	3.07	3.02
Main pump max Δp (kPa/ft)	131/44	175/59	241/81
Circulators max Δp (kPa/ft)	44/15	(-)	(-)
Interior piping (m/ft)	258/846	487/1598	487/1598
Bore depth (m/ft)	176/577	174/571	174/571

Table 7.5 : Case 3 (Longitudinal/Mixed) - Simulation results for the 3 configurations

Case 3 (Longitudinal /Mixed)	**One-pipe**	**Two-pipe reverse-return**	**Two-pipe direct-return**
Total energy (kWh)	56 230	54 598	54 986
Heat pumps energy (kWh)	53 285	51 739	51 747
Main pump energy (kWh)	1 023	2 313	2 696
Circulators energy (kWh)	1 206	(-)	(-)
Pumping fraction (%)	4.0	4.2	4.9
SPF (-)	3.77	3.88	3.85
Main pump max Δp (kPa/ft)	99/33	148/50	170/57
Circulators max Δp (kPa/ft)	48/16	(-)	(-)
Interior piping (m/ft)	191/627	281/922	200/656
Bore depth (m/ft)	126/413	128/420	128/420

Table 7.6 : Case 4 (Longitudinal/Cooling) - Simulation results for the 3 configurations

Case 4 (Longitudinal /Cooling)	One-pipe	Two-pipe reverse-return	Two-pipe direct-return
Total energy (kWh)	73 432	69 724	70 156
Heat pumps energy (kWh)	71 104	67 236	67 283
Main pump energy (kWh)	1 204	2 488	2 874
Circulators energy (kWh)	1 124	(-)	(-)
Pumping fraction (%)	3.2	3.6	4.1
SPF (-)	2.92	3.07	3.05
Main pump max Δp (kPa/ft)	118/39	161/54	184/62
Circulators max Δp (kPa/ft)	44/15	(-)	(-)
Interior piping (m/ft)	191/627	281/922	200/656
Bore depth (m/ft)	176/577	173/568	173/568

7.7.1 Result analysis

First, results show that one-pipe systems have a total energy consumption about 3 to 5% higher than reverse-return systems and 1 to 5% higher than direct-return systems. One-pipe networks require less pumping energy compared to two-pipe systems as showed by the *Pumping fraction* but heat pumps use more energy due to the inlet temperature variations. *Pumping fraction* is 6 to 36% lower than with two-pipe systems while *SPF* is up to 5% lower. These one-pipe systems are then less efficient in these cases. The one-pipe main flow rate is generally lower than in two-pipe systems, decreasing pumping requirements but also main pump efficiency which reduces pumping energy savings over two-pipe systems. It is also interesting to note that the sum of the head losses for the one-pipe main pump and circulator is approximately equal to the reverse-return main pump head loss. This is due to similar hydraulic path lengths and valve pressure drops. Direct-return systems require more pumping energy than reverse return systems, leading to a slightly higher total energy consumption.

The cooling-only cases present a higher energy consumption difference between configurations. One-pipe network heat pumps experience an increasing inlet temperature along the loop as all units are in cooling. Consequently, this increases heat pump and total energy consumption of one-pipe networks.

Simulations using the proposed tool also show that choosing between a one- or two-pipe network has only a small influence on the required bore field length. Heat pump *COP* and pumping are influenced by the configuration, but not enough to significantly modify ground loads. For a mixed load profile, one-pipe configurations lead to a 1 or 2 m depth reduction. This is due to the temperature drop along the primary pipe which reduces heating *COP* and consequently the ground loads. However, for the cooling-only cases, deeper boreholes are required for one-pipe as *COP* decreases along the loop leading to more compressor power which is ultimately rejected into the ground.

The main objective is to develop a versatile simulation tool in which users can set several parameters. The studied cases were simulated to show how the proposed tool can be used. One should know that chosen parameters influence the results and that those conclusions are not valid for every system. The influence of some parameters is, however, not major. For example, reducing the control valve C_v to 3.5 increases pumping energy by 20% but total annual consumption by less than 1%.

The previous case studies were performed with frequently used flow rates (3 gpm/ton) and pipe head loss (2 ft/100 ft). Two parametric studies are performed with other nominal flow rates and pipe head losses. The results are presented in Figures 7.15 and 7.16 based on Case 1 (Square building/Mixed loads). The total annual energy consumption is shown on the left scale while relative values (compared to the reference one-pipe system) are shown on the right axis. Figure 7.15 presents the effect of different nominal pipe head losses for the three networks.

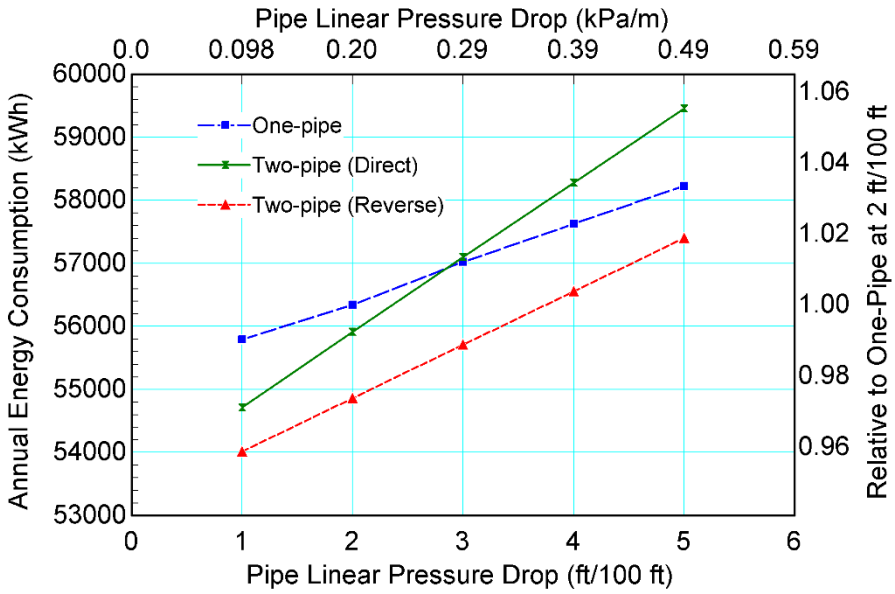

Figure 7.15 : Annual energy consumption influenced by pipe pressure drop (Case 1)

It is shown that two-pipe networks are more influenced by this parameter as the curves are steeper, which is mostly due to longer interior pipes. It is the main pump energy consumption which increases as heat pumps and circulators have similar energy consumption. It is also interesting to note that the one-pipe network uses less energy than the direct-return case for pressure drops higher than 3 ft/100 ft. This illustrates that the increase in pumping energy of two-pipe networks can exceed the increase in heat pump energy consumption of one-pipe networks.

Figure 7.16 presents the effect of different nominal heat pump flow rates for the three configurations. For two-pipe systems, heat pump energy consumption is similar while pumping energy increases with higher flows, leading to a total energy consumption increase with an increase in the nominal flow rate. For one-pipe systems, total energy consumption decreases when the nominal flow rate increases from 1.5 to 2.25 gpm/ton and then increases when using 3 gpm/ton. As the flow is increased from 1.5 to 2.25 gpm/ton, pumping energy increases but heat pump energy consumption decreases even more as the loop temperature is less influenced by the operation of preceding heat pumps. However, as the flow is increased from 2.25 to 3.0 gpm/ton, the pumping energy increase is greater than the drop in heat pump energy consumption.

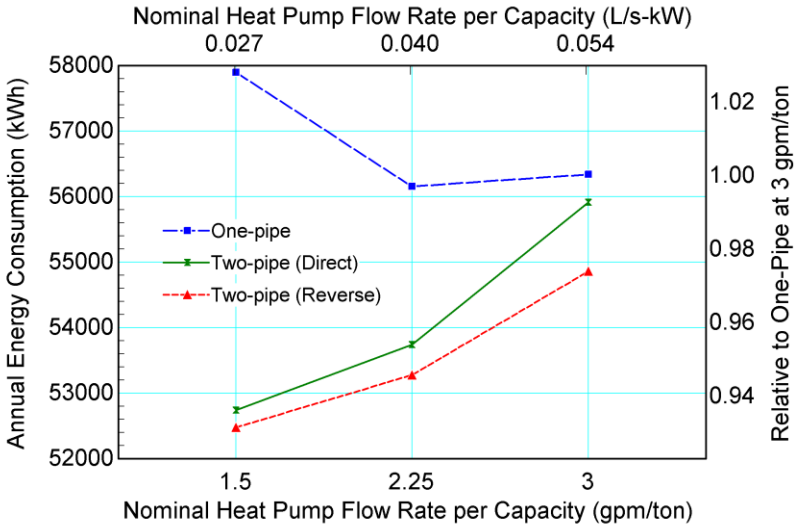

Figure 7.16 : Annual energy consumption influenced by nominal flow rate (Case 1)

7.8 Conclusion

Several piping configurations are available for designers of centralized GCHP systems. Two-pipe networks are common and can rely on a reverse or direct-return piping arrangement. However, they require more piping and pumping energy than a one-pipe network. One-pipe systems, which are less frequent, are simpler to design but require more heat pump energy. Choosing one of these solutions affects first costs, but also heat pump and pump energy consumption. This paper proposes a simulation tool to compare the energy consumption (pump and heat pump) of these configurations. A flow control method for one-pipe systems, based on the bore field return temperature, is also proposed. Four case studies are finally presented to show the usefulness of the tool. Based on these cases, one-pipe networks appear to require up to 5% more energy annually mainly due to increased heat pump energy consumption. Pumping energy is however lower in one-pipe networks. Results also show that the piping configuration has a relatively small influence on the size of the bore field.

7.9 Acknowledgments

The authors would like to express their sincere gratitude to ASHRAE, Hydro-Quebec and the Natural Sciences and Engineering Research Council of Canada (NSERC) who provided scholarships to the first author. This work was also performed with funds provided by NSERC's Smart Net-Zero Energy Buildings Strategic Research Network.

7.10 Appendix A – Tool parameter, input and output description

Table 7.7 describes the parameters, inputs and outputs used in the proposed tool and presented in Figure 7.4.

Table 7.7 : Tool parameter, input and output description

Parameters	
Type of Network	Piping configuration among one-pipe, two-pipe reverse-return and two-pipe direct-return.
NB of HP	Number of heat pumps to be simulated.
Pipe Linear Head Loss	Nominal linear pressure drop in main pipes and bores, based on the maximum designed flow in each pipe segment.
HP COP Coefficients	4 coefficients for the constant and variable terms of the heating and cooling COP linear regressions, which are function of the unit inlet temperature.
HP Capacity Scaling Factors	4 coefficients for the heating and cooling capacity scaling factor linear regressions, which are function of the unit inlet temperature.
Circulator Efficiency	Choice between 3 efficiency classes based on manufacturers data. Each class has a regression predicting efficiency as a function of the hydraulic power.
VFD Minimum %	Minimum fraction reached by the VFD. Represents the lowest achievable maximum flow fraction.
Bore Depth	Depth of the deepest and farthest borehole from the mechanical room. Used to evaluate the worst hydraulic path.
L to Farthest Borehole	Distance between the mechanical room (0,0) and the farthest borehole. Used to calculate the pressure drop in this segment.
T to HP Min	Heat pump inlet temperature minimum operating limit. Used to set the one-pipe main flow rate.
T to HP Max	Heat pump inlet temperature maximum operating limit. Used to set the one-pipe main flow rate.
ΔT (One Pipe VFD)	Temperature difference used to set the one-pipe main flow rate and over which the flow varies linearly.
Valve and hose C_v	5 valves/hose flow coefficients selected for a 3-ton heat pump using 3 gpm/ton. Used to evaluate pressure drop in each component.
PLF Coefficients	4 coefficients used to calculate the part-load factor based on heat pumps Part-Load Ratio. Set the first one (a_0) to 1 to neglect PLF effects.

Table 7.7 (suite) : Tool parameter, input and output description

Nominal Capacity (i)	Nominal capacity of heat pump (i) in tons. Used to determine heat pump nominal flow by multiplying the gpm/ton. This capacity is corrected depending on unit inlet temperature to evaluate the part-load operation.
Nominal GPM/Ton (i)	Nominal flow rate of heat pump (i) in gpm/ton. This flow, typically 1.5 or 3 gpm/ton, influences pressure drop in valves, heat pumps and pipes.
X Position (i)	X axis position of heat pump (i).
Y Position (i)	Y axis position of heat pump (i).
Inputs	
T to HP	Fluid temperature exiting the main pump (after the bore field) and entering in the first heat pump of the building (all heat pumps in two-pipe networks).
Fluid Cp	Fluid thermal capacity. As an input, it can vary over time or be fixed.
Fluid Density	Fluid density. As an input, it can vary over time or be fixed.
Load (i)	Heat pump load to be met during a time step. The selected convention states that a heating load is positive while cooling loads are negative.
Outputs	
T to Bore Field	Fluid temperature exiting all the heat pumps and entering in the bore field. It is calculated differently for one- and two-pipe systems.
Power HP	Sum of heat pump power consumption accounting for varying COP, capacity and PLR.
Power Circulators	Sum of circulator pump power.
Power Auxiliary	Sum of all electrical auxiliary power (heating).
% HP in Operation	Fraction of heat pumps having a load $\neq 0$.
Loop Load	Sum of power exchanged with main loop by each heat pump (ground load).
Heating Load	Sum of the zone loads in heating.
Cooling Load	Sum of the zone loads in cooling.
Main Flow	Flow that the main pump must provide. It is a function of the heat pumps in operation (two-pipe) or bore field return temperature (one-pipe). The maximum main flow is the sum of each heat pump nominal flow rate.
Δp Main Pump	Overall pressure drop provided to the main pump. Only pipes and boreholes are considered for one-pipe systems.
Pump Correction Factor	Overall Part-Load Ratio of all operating heat pumps. Used to correct main pump power for flow variations over a time step.
Δp_{max} Circulators	Maximum pressure drop experienced by circulators (one-pipe).
Interior Piping Length	Interior length of the main pipes to buy and install.

7.11 Nomenclature

Δp = Pressure drop (kPa)

ΔT = Temperature difference (°C)

η = Efficiency (%)

Avg = Average

CAP = Heat pump capacity (tons or kW)

COP = Coefficient of performance (-)

CR = Capacity ratio (-)

CSF = Capacity scaling factor (-)

C_v = Flow coefficient (gpm or L/s)

D = Pipe diameter (m or in)

EIR = Energy input ratio (-)

f = VFD flow fraction (-)

F_{pump} = Main pump correction factor (-)

H = Pump head (kPa)

Inst = Instantaneous

L = Pipe length (m)

LCC = Life-cycle cost ($)

$\dot{m}$ = Main flow rate (L/s)

$\dot{m}_i$ = Heat pump branch flow rate (L/s)

$\dot{m}_{tot}$ = Maximum main flow rate (L/s)

Mech. = Mechanical

*PL*F = Part-load factor (-)

PLR = Part-load ratio (-)

Q_{Loop} = Loop heat injection/rejection (kW)

SPF = Seasonal performance factor (-)

T = Temperature (°C)

TRCM = Thermal resistance and capacity model

VFD = Variable frequency drive

W = Power (kW)

X = Position relative to the X axis (m)

Y = Position relative to the Y axis (m)

7.11.1 Subscripts

1pipe = One-pipe network

2pipe = Two-pipe network

1...14 = Index relative to Figure 7.1

Circ = Circulator

corr = Corrected

HP = Heat pump

i = Specific to a heat pump

linear = Relative to a specific pipe length

min = Minimum

max = Maximum

nom = Nominal

rev = Reverse-return

s = Segment

toHP = Heat pump primary loop entrance/after main pump

7.12 References

Bernier, M., and N. Lemire. 1999. Non-Dimensional Pumping Power Curves for Water Loop Heat Pump Systems. *ASHRAE Transactions*. 105(2): 1226-1232.

Bernier, M., A. Sfeir, T. Million, A. Joly. 2005. A methodology to evaluate pumping enegy consumption in GCHP systems. *ASHRAE Transactions*. 111(1): 714-729.

Bernier, M., M. Kummert, S. Bertagnolio. 2007. Development and application of test cases for comparing vertical ground heat exchangers models. *Building Simulation Conference* (BS 2007).

Bidstrup, N. 2012. EU Pump Regulations. *ASHRAE Journal* 54(5): 106-110.

Boldt, J., and J. Keen. 2015. Hydronics 101. *ASHRAE Journal* 57(5).

Cimmino, M., and M. Bernier. 2013. Preprocessor for the generation of g-functions used in the simulation of geothermal systems. *13th Conference of International Building Performance Simulation Association (IBPSA)*, p. 2675-2682.

Cimmino, M., and M. Bernier. 2014. A semi-analytical method to generate g-functions for geothermal bore fields. *International Journal of Heat and Mass Transfer*, 70, p. 641-650.

ClimateMaster. 2012. *Tranquility 27 (TT) Series Performance Map*. USA: ClimateMaster.

Cunniff, G., and B. Zerba. 2006. Single-Pipe Systems for Commercial Applications. *HPAC Engineering* (October 2006), 42-46.

Cunniff, G. 2011. Less is more: single-pipe hydronic system solves high-rise troubles. *PM Engineer* (September 2011), 18-22. 139

Duda, S.W. 2015. Reverse-Return Reexamined. *ASHRAE Journal* 57(8): 40-44.

Gagné-Boisvert, L., and M. Bernier. 2016. Accounting for Borehole Thermal Capacity when Designing Vertical Geothermal Heat Exchangers. Presented at the *2016 ASHRAE Annual Conference*, St-Louis, MO, June 25–29.

Gagné-Boisvert, L., and M. Bernier. 2017. A comparison of the energy use for different heat transfer fluids in geothermal systems. Presented at the *2017 IGSHPA Conference*, Denver, CO, March 14–16.

Godefroy, V., and M. Bernier. 2014. A simple model to account for thermal capacity in boreholes. *Proceedings of the 11th IEA Heat Pump Conference*, Montreal, Qc, Canada. Paper #P.4.8.

Godefroy, V., C. Lecomte, M. Bernier, M. Douglas, M. Armstrong. 2016. Experimental Validation of a Thermal Resistance and Capacity Model for Geothermal Boreholes. *ASHRAE Winter Meeting*, Orlando, Fl. OR-16-C047.

Hackel, S., S. Klein., G. Nellis, J. Thornton. 2008. *Development of Design Guidelines for Hybrid Ground-Coupled Heat Pump Systems, ASHRAE 1384-RP*. Atlanta, GA: ASHRAE.

Henderson, H., D. Parker, Y. Huang. 2000. Improving DOE-2's RESYS routine: User Defined Functions to Provide More Accurate Part Load Energy Use and Humidity Predictions. *Proceedings of 2000 Summer Study on Energy Efficiency in Buildings*, American Council for an Energy-Efficient Economy. Washington, DC., August 2000.

Kavanaugh, S.P., and S.A. McInerny. 2001. Energy Use of Pumping Options for Ground-Source Heat Pumps. *ASHRAE Transactions*. 107(1): 589-599.

Kavanaugh, S.P., S. Lambert, D. Messer. 2003. *Development of guidelines for the selection and design of the pumping/piping subsystem for ground-coupled heat pump systems, ASHRAE 1217-RP*. Atlanta, GA: ASHRAE.

Kavanaugh, S.P. 2011. Less Pumping Means Cooler Ground Loops. *ASHRAE Journal* 53(7): 26-35.

Kavanaugh, S.P., and K. Rafferty. 2015. *Ground-Source Heat Pumps: Design of geothermal systems for commercial and institutional buildings.* Atlanta, GA: ASHRAE.

Kavanaugh, S.P., and C. Gray. 2016. A simple approach to affordable GSHPs. *ASHRAE Journal* 58(4): 14-24.

Klein, S. A. et al. 2010. *TRNSYS, a transient simulation program.* Solar Energy Laboratory, University of Wisconsin-Madison, USA.

Mescher, K. 2009. One-Pipe Geothermal Design: Simplified GCHP System. *ASHRAE Journal* 51(10): 24-40.

Ndiaye, D., and M. Bernier. 2012. Transient model of a geothermal heat pump in cycling conditions – Part B: Experimental validation and results. *International Journal of Refrigeration* 35(8):2124–2137.

Nordman, R., and A. Zottl. 2011. SEPEMO-Build - a European project on seasonal performance factor and monitoring for heat pump systems in the building sector. *REHVA Journal* 48(4): 56-61.

Stethem, W.C. 1994. Single-pipe hydronic systems – Design and load-matched pumping. *ASHRAE Transactions*. 100(1): 1507-1515.

Stethem, W.C. 1995. Single-pipe hydronic systems – Historical development. *ASHRAE Transactions.* 101(1): 1251-1259.

Taylor, S., and J. Stein. 2002. Balancing variable flow hydronic systems. *ASHRAE Journal* 44(10).

CHAPITRE 8 DISCUSSION GÉNÉRALE

Ce mémoire aborde plusieurs avenues permettant d'améliorer la conception de systèmes géothermiques. Les résultats obtenus ont ainsi été présentés dans les chapitres précédents. Ce chapitre vise maintenant à discuter des avancées réalisées et à dresser un sommaire des contributions de ce mémoire à l'avancement des connaissances.

8.1 Amélioration du rendement des circulateurs

Le premier objectif de ce mémoire consiste à rendre compte des avancées concernant les circulateurs. Une des conclusions est que les circulateurs ne doivent plus simplement être considérés comme des pompes inefficaces, une croyance souvent répétée par l'industrie. Grâce à des normes et aux efforts des manufacturiers, le rendement de nombreux appareils a augmenté.

Les trois corrélations développées (Éq. 4.4 à 4.6) permettront aux concepteurs d'estimer le rendement nominal du fil à l'eau d'un circulateur d'une certaine gamme (basse, haute ou meilleure efficacité). Ces corrélations constituent en quelque sorte une mise à jour de celle du COSTIC (2003).

L'étude présentée dans ce mémoire va cependant un peu plus loin en examinant la sensibilité du rendement d'un circulateur fonctionnant au-delà de son débit nominal mais pour une vitesse de rotation constante. Il apparaît qu'un débit 25% supérieur au débit nominal réduit le rendement de 1 à 8% alors qu'un débit inférieur de 25% réduit le rendement de 4 à 9%. Ces résultats permettront donc aux simulations d'être plus précises quant à la consommation énergétique reliée au pompage d'un système géothermique.

8.2 Influence de la capacité thermique sur le dimensionnement

L'article 1 mène tout d'abord à des conclusions similaires aux travaux trouvés dans la littérature. Il confirme notamment que le fait de considérer la capacité thermique d'un puits lors de sa simulation :

- Adoucit les pics de température du fluide sortant du puits;
- Réduit la consommation énergétique des pompes à chaleur;
- Réduit la longueur de puits requise.

Cette étude examine ensuite l'erreur découlant de l'utilisation de l'équation de dimensionnement de l'ASHRAE. Cette dernière est comparée à un dimensionnement basé sur des simulations annuelles tout en considérant la capacité thermique des puits. La Figure 5.4 permet de mettre en évidence l'influence des effets transitoires, mais aussi du temps de fonctionnement en continu de la pompe à chaleur durant la charge de pointe du bâtiment, caractérisé par « l'effect coverage ». L'équation de l'ASHRAE ne tient pas compte de ces deux phénomènes, ce qui engendre une surestimation ou une sous-estimation de la longueur de puits requise. Les concepteurs doivent donc être conscients de l'incertitude engendrée par l'utilisation de cette équation.

8.3 Dégradation des performances en fonction du fluide caloporteur

Le recours à certaines solutions d'antigel peut être pris en considération à l'aide de facteurs de correction présentés par les manufacturiers de pompes à chaleur. Cependant, la provenance de ces facteurs est souvent inconnue et il est difficile de les adapter pour d'autres conditions de fonctionnement (concentration d'antigel, débit, température, etc.). Cette étude a donc présenté une méthodologie pour corriger la capacité et la puissance requise d'une pompe à chaleur en fonction de l'antigel utilisé. Les résultats issus de cette méthodologie ont été validés en les comparant à des résultats provenant de manufacturiers. Les concepteurs pourront ainsi mesurer plus précisément les conséquences engendrées par l'utilisation d'un certain antigel. À l'instar d'autres travaux sur le sujet, l'article 2 a confirmé que le méthanol est l'antigel le moins pénalisant au niveau énergétique. Pour appuyer ses conclusions, l'étude a explicité l'influence des solutions d'antigel sur les différentes composantes d'un système, ce qui a poussé plus loin la compréhension des phénomènes engendrés.

Finalement, les résultats obtenus appuient la conclusion de Kavanaugh (2011) et de Spitler et Ghelin (2015) à savoir qu'il est préférable de permettre un écoulement laminaire occasionnel dans les puits géothermiques que de dépenser beaucoup d'énergie de pompage pour assurer un débit turbulent en tout temps.

8.4 Nouvel outil de simulation de réseaux de distribution

Plusieurs études décrivent les avantages d'un réseau de distribution à un tuyau par rapport aux réseaux classiques à deux tuyaux. Cependant, aucune ne les compare en se basant sur des simulations énergétiques annuelles, ce qui est essentiel afin d'évaluer l'influence de la variation de

la température du fluide caloporteur le long d'un réseau à un tuyau. L'article 3 présente une méthodologie servant à simuler ces réseaux. Cette étude a ainsi permis de mettre en évidence l'importance de la prise en compte de la stratégie de distribution du fluide vers les pompes à chaleur. Elle a aussi démontré que les réseaux à un tuyau peuvent consommer globalement plus d'énergie, tout en requérant moins de tuyauterie. L'outil présenté dans cette étude, implémenté dans un nouveau TYPE TRNSYS, permettra aux concepteurs de comparer la consommation énergétique et la puissance requise pour des réseaux à un et deux tuyaux. Avec ces données, il sera ensuite aisé de comparer ces options sur la base d'une analyse du coût du cycle de vie et de choisir le réseau à privilégier pour une certaine application. Il est à noter que l'étude n'a pas présenté de comparaison entre les réseaux sur une base économique car cette dernière dépend largement des paramètres financiers propres à chaque projet.

CHAPITRE 9 CONCLUSION ET RECOMMANDATIONS

Ce mémoire étudie diverses avenues dans le but d'améliorer la conception des systèmes de pompes à chaleur géothermiques. Ces derniers sont très efficaces mais coûteux à installer. Il importe donc de les dimensionner selon leur comportement réel et de prédire précisément leur consommation énergétique. Dans ce sens, cet ouvrage aborde les circulateurs, la capacité thermique des puits, les antigels et les réseaux de distribution. Les divers résultats obtenus permettront aux concepteurs de simuler et de dimensionner avec plus de précision les composantes d'un système géothermique.

Premièrement, une analyse du rendement de circulateurs disponibles sur le marché a permis de noter que ces derniers sont jusqu'à deux fois plus efficaces que par le passé. L'étude propose des corrélations permettant de prédire leur rendement en fonction de la puissance hydraulique à fournir. Elle permettra ainsi aux concepteurs de prédire le rendement d'un circulateur dans le cadre d'une application précise. À la lumière de ces résultats, plusieurs organismes, dont l'ASHRAE et le COSTIC, devraient mettre à jour leurs informations relatives au rendement des circulateurs afin de donner l'heure juste aux concepteurs. Il serait également intéressant de valider les corrélations proposées, issues de données de manufacturiers, avec des données expérimentales et de valider ces résultats avec des solutions d'antigel plus visqueuses.

Ensuite, il apparaît que l'inclusion de la capacité thermique du fluide et du coulis a un impact notable sur la simulation des puits géothermiques. Elle engendre des effets transitoires bénéfiques qui réduisent les charges de pointe au sol et, conséquemment, la longueur de puits requise. En effet, un dimensionnement basé sur des simulations utilisant un modèle de puits de type Thermal Resistance and Capacitance (TRC) indique que les longueurs de puits requises peuvent être sous-estimées jusqu'à 31% ou surestimées jusqu'à 24% par rapport à l'équation de dimensionnement de l'ASHRAE, qui néglige la capacité thermique des puits et le cyclage des pompes à chaleur. Ce mémoire conclut donc que l'équation de l'ASHRAE n'est pas assez précise pour déterminer la longueur de puits requise. Il est plutôt recommandé d'effectuer des simulations itératives avec un modèle de puits qui considère minimalement la capacité thermique du fluide, et idéalement aussi celle du coulis. Des travaux futurs pourraient tenter de modifier l'équation de l'ASHRAE afin qu'elle tienne compte de la capacité thermique des puits et du rapport entre la capacité de la pompe à chaleur et la charge de pointe du bâtiment. De plus, considérant que cette étude aborde seulement

des systèmes résidentiels, il serait pertinent de la poursuivre en étudiant les mêmes phénomènes dans des champs de puits alimentant de plus gros bâtiments.

Troisièmement, ce mémoire démontre que les antigels utilisés dans les puits affectent les performances d'un système géothermique. La puissance de pompage, l'échange thermique dans les puits, la transition laminaire-turbulent et la capacité d'une thermopompe sont fonction du type et de la concentration d'antigel utilisé. Des simulations utilisant différents types d'antigel ont démontré que le méthanol est l'antigel le moins pénalisant au niveau énergétique et qu'un faible débit de 0.027 L/s-kW (1.5 usgpm/tonne) est à favoriser par rapport au débit de 0.054 L/s-kW (3 usgpm/tonne), qui est souvent utilisé. Il apparaît que les avantages de la réduction de la puissance de pompage engendrée par de plus faibles débits surpassent les désavantages reliés à la baisse du transfert de chaleur liée à un écoulement laminaire occasionnel dans les puits. Ce mémoire recommande donc de poursuivre l'étude des conséquences d'un écoulement laminaire dans les puits. Il serait pertinent de confirmer qu'un écoulement laminaire occasionnel est à favoriser par rapport à un pompage excessif visant à assurer un écoulement turbulent à tout moment. Ces confirmations devraient se baser sur d'autres modèles et sur d'autres situations, mais aussi possiblement sur des tests expérimentaux.

Finalement, ce mémoire propose un nouvel outil de simulation servant à évaluer la consommation énergétique des systèmes géothermiques à un ou deux tuyaux. Les réseaux de distribution à un tuyau sont attrayants puisqu'ils nécessitent moins de tuyaux et sont généralement plus faciles à installer. Des études de cas utilisant cet outil ont démontré qu'un réseau à un tuyau nécessite jusqu'à 36% moins d'énergie de pompage qu'un réseau à deux tuyaux. Cependant, il consomme globalement jusqu'à 5% plus d'énergie à cause des températures d'entrée défavorables aux pompes à chaleur. Il serait maintenant intéressant de simuler le fonctionnement de réseaux à un et deux tuyaux existants afin de valider la précision de l'outil. L'outil pourrait ensuite servir à déterminer des tendances générales guidant les concepteurs à savoir dans quels cas opter pour un réseau à un tuyau.

BIBLIOGRAPHIE

AIE. 2013. *Transition to Sustainable Buildings - Strategies and Opportunities to 2050.* Agence Internationale de l'Énergie. Paris, France.

ASHRAE. 2011. *Ground Source Heat Pump Systems: Putting the Earth to Work for You* (K. Mescher). ASHRAE Webcast Dvd.

ASHRAE. 2015. *Geothermal energy, ASHRAE Handbook, HVAC applications*. Atlanta, GA: ASHRAE.

Bauer, D., W. Heidemann, H. Müller-Steinhagen, H.-J. Diersch. (2010). Thermal resistance and capacity models for borehole heat exchangers. *International Journal of Energy Research*, 35(4), 312-320.

Bernier, M., and N. Lemire. 1999. Non-Dimensional Pumping Power Curves for Water Loop Heat Pump Systems. *ASHRAE Transactions*. 105(2): 1226-1232.

Bernier, M., A. Sfeir, T. Million, A. Joly. 2005. A methodology to evaluate pumping enegy consumption in GCHP systems. *ASHRAE Transactions*. 111(1): 714-729.

Bernier, M., Ladang, O., Hulot, J. Effet du choix du fluide caloporteur sur l'énergie de pompage des systèmes de pompes à chaleur géothermiques, *VIIème Colloque Interuniversitaire Franco-Québécois sur la Thermique des Systèmes*, 23-25 mai 2005, Saint-Malo.

Bernier, M., M. Kummert, S. Bertagnolio. 2007. Development and application of test cases for comparing vertical ground heat exchangers models. *Building Simulation Conference* (BS 2007).

Bidstrup, N. 2012. EU Pump Regulations. *ASHRAE Journal 54(5): 106-110.*

Bidstrup, N. 2013. Circulators: The stony route to EU regulation 641/2009 (622/2012). Δ*p Global (ErP Special, Yearbook 2013): 22-29.*

Bidstrup, N. 2016. Communication personnelle à propos de la norme EuroPump.

Boldt, J., and J. Keen. 2015. Hydronics 101. *ASHRAE Journal* 57(5).

Brischoux, P. 2016. *Stockage thermique saisonnier par puits géothermiques pour bâtiments résidentiels équipés de panneaux photovoltaïques-thermiques.* Mémoire de maîtrise. École Polytechnique de Montréal, Montréal, Québec, Canada.

Cimmino, M., and M. Bernier. 2013. Preprocessor for the generation of g-functions used in the simulation of geothermal systems. *13th Conference of International Building Performance Simulation Association (IBPSA)*, p. 2675-2682.

Cimmino, M., and M. Bernier. 2014. A semi-analytical method to generate g-functions for geothermal bore fields. *International Journal of Heat and Mass Transfer*, 70, p. 641-650.

ClimateMaster. 2012. *Tranquility 27 (TT) Series Performance Map*. USA: ClimateMaster.

Commission Européenne. 2009. Commission Regulation No 641/2009 with regard to ecodesign requirements for glandless standalone circulators and glandless circulators integrated in products. *Official Journal of the European Union*. Bruxelles, Belgique.

COSTIC. 2003. *Circulators efficiency based on manufacturers catalogs (Study 24.013).* Angers, France: ADEME.

COSTIC. 2010. *Circulateurs pour les circuits de chauffage.* Angers, France: ADEME.

Cunniff, G., and B. Zerba. 2006. Single-Pipe Systems for Commercial Applications. *HPAC Engineering* (October 2006), 42-46.

Cunniff, G. 2011. Less is more: single-pipe hydronic system solves high-rise troubles. *PM Engineer* (September 2011), 18-22. 139

DOE. 2016. *Appliance and Equipment Standards Rulemakings and Notices - Circulator Pumps.* Washington, USA. U.S Department of Energy. Tiré de https://www1.eere.energy.gov/buildings/appliance_standards/standards.aspx?productid=66

Dow. 2001. *Engineering and Operating Guide: DOWFROST Inhibited Propylene Glycol-based Heat Transfer Fluids*. USA: Dow Chemical Company.

Duda, S.W. 2015. Reverse-Return Reexamined. *ASHRAE Journal* 57(8): 40-44.

EuroPump. 2011. *Energy Efficiency of Circulators*. EuroPump. Bruxelles, Belgique.

Gagné-Boisvert, L., and M. Bernier. 2016. Accounting for Borehole Thermal Capacity when Designing Vertical Geothermal Heat Exchangers. Presented at the *2016 ASHRAE Annual Conference*, St-Louis, MO, June 25–29.

Gagné-Boisvert, L., and M. Bernier. 2017. A comparison of the energy use for different heat transfer fluids in geothermal systems. Presented at the *2017 IGSHPA Conference*, Denver, CO, March 14–16.

Gehlin, S.E.A., and J.D. Spitler. (2015). Effects of Ground Heat Exchanger Design Flow Velocities on System Performance of Ground Source Heat Pump Systems in Cold Climates. *ASHRAE Meeting.*

Godefroy, V., and M. Bernier. 2014. A simple model to account for thermal capacity in boreholes. *Proceedings of the 11th IEA Heat Pump Conference*, Montreal, Qc, Canada. Paper #P.4.8.

Godefroy, V., Lecomte, C., Bernier, M., Douglas, M., and M. Armstrong. 2016. Experimental Validation of a Thermal Resistance and Capacity Model for Geothermal Boreholes. *ASHRAE Winter Meeting*, Orlando, Fl. OR-16-C047.

Grundfos Canada. 2016. Product Center. http://product-selection.grundfos.com. Access on March 14-25th 2016.

Hackel, S., S. Klein., G. Nellis, J. Thornton. 2008. *Development of Design Guidelines for Hybrid Ground-Coupled Heat Pump Systems, ASHRAE 1384-RP*. Atlanta, GA: ASHRAE.

Heinonen, E.W., M.W. Wildin, A.N. Beall, R.E. Tapscott. (1997). Assessment of antifreeze solutions for ground-source heat pump systems. *ASHRAE Transactions*, 103(2): 747-756.

Hellström, G. 1991. *Ground Heat Storage – Thermal Analyses of Duct Storage Systems - I. Theory*. Department of Mathematical Physics,University of Lund, Sweden.

Hellström, G., Mazzarella, L., and D. Pahud. 1996. *Duct ground storage model—TRNSYS version.* Department of Mathematical Physics, University of Lund, Sweden.

Henderson, H., D. Parker, Y. Huang. 2000. Improving DOE-2's RESYS routine: User Defined Functions to Provide More Accurate Part Load Energy Use and Humidity Predictions. *Proceedings of 2000 Summer Study on Energy Efficiency in Buildings*, American Council for an Energy-Efficient Economy. Washington, DC., August 2000.

Jin, H., and J.D. Spitler. 2003. Parameter estimations based model of water-to-water heat pumps with scroll compressors and water/glycol solutions. *Building Serv. Eng. Res. Technol*. 24(3): 203-219.

Kavanaugh, S.P., and S.A. McInerny. 2001. Energy Use of Pumping Options for Ground-Source Heat Pumps. *ASHRAE Transactions*. 107(1): 589-599.

Kavanaugh, S.P., S. Lambert, D. Messer. 2003. *Development of guidelines for the selection and design of the pumping/piping subsystem for ground-coupled heat pump systems, ASHRAE 1217-RP Report.* Atlanta, GA: ASHRAE.

Kavanaugh, S.P. 2011. Less Pumping Means Cooler Ground Loops. *ASHRAE Journal* 53(7): 26-35.

Kavanaugh, S.P., and J. Kavanaugh. 2012, Long-Term Commercial GSHP Performance Part 2: Ground Loops, Pumps, Ventilation Air and Controls. *ASHRAE Journal* 54(7): 26-34.

Kavanaugh, S., and K. Rafferty. 1997. *Ground-Source Heat Pumps: Design of geothermal systems for commercial and institutional buildings.* Atlanta, GA: ASHRAE

Kavanaugh, S., and K. Rafferty. 2015. *Ground-Source Heat Pumps: Design of geothermal systems for commercial and institutional buildings*. Atlanta, GA: ASHRAE.

Kavanaugh, S.P., and C. Gray. 2016. A simple approach to affordable GSHPs. *ASHRAE Journal* 58(4): 14-24.

Khan, M.H., and J.D. Spitler. 2004. Performance Analysis of a Residential Ground Source Heat Pump System with Antifreeze Solution. *Proceedings of SimBuild 2004*, Boulder, Colorado August 4-6.

Klein, S. A. et al. 2010. *TRNSYS, a transient simulation program*. Solar Energy Laboratory, University of Wisconsin-Madison, USA.

Klein, S. A. et al. 2015. *EES: Engineering Equation Solver*. Madison, WI: F-Chart Software.

Liu, X., M. Malhotra, P. Im, B. Habibzadeh. 2015. Case studies for GSHP demonstration projects in the US. *IEA Heat Pump Center, Newsletter, Vol. 33, No. 3.*

Ludwig, G., and Roth, M. 2008. *Results of Circulator Labelling Revision.* Université Technique de Darmstadt. Allemagne.

Ma, W., Li, M., Li, P., and A. Lai. 2015. New quasi-3D model for heat transfer in U-shaped ground heat exchangers: Effective overall thermal resistance. *Elsevier Energy*. doi: 10.1016/j.energy.2015.07.098

Mescher, K. 2009. One-Pipe Geothermal Design: Simplified GCHP System. *ASHRAE Journal* 51(10): 24-40.

Ndiaye, D., and M. Bernier. 2012. Transient model of a geothermal heat pump in cycling conditions – Part B: Experimental validation and results. *International Journal of Refrigeration* 35(8):2124–2137.

Nguyen, A. 2010. Personnal communication about antifreeze correction factors.

Nordman, R., and A. Zottl. 2011. SEPEMO-Build - a European project on seasonal performance factor and monitoring for heat pump systems in the building sector. *REHVA Journal* 48(4): 56-61.

NRCan-OEE. 2013. *Energy Efficiency Trends in Canada, 1990 to 2010.* Ottawa, ON, CAN. Natural Resources Canada, Office for Energy Efficiency.

Pärisch, P., Mercker, O., Oberdorfer, P., Bertram, E., Tepe, R., and G. Rockendorf. 2015. Short-term experiments with borehole heat exchangers and model validation in TRNSYS. *Renewable Energy*, 74, 471-477.

Salmson. 2016. Product Center. http://selecson.salmson.fr. Access on March 14-25th 2016.

Shirazi, A. S., and M. Bernier. 2013. Thermal capacity effects in borehole ground heat exchangers. *Energy and Buildings:* 67 352-364.

Stethem, W.C. 1994. Single-pipe hydronic systems – Design and load-matched pumping. *ASHRAE Transactions*. 100(1): 1507-1515.

Stethem, W.C. 1995. Single-pipe hydronic systems – Historical development. *ASHRAE Transactions.* 101(1): 1251-1259.

Taylor, S., and J. Stein. 2002. Balancing variable flow hydronic systems. *ASHRAE Journal* 44(10).

White, F.M. 2009. *Fluid Mechanics*. 7th edition. McGraw-Hill. p.366.

Xu, X., and J.D. Spitler. 2006. Modeling of Vertical Ground Loop Heat Exchangers with Variable Convective Resistance and Thermal Mass of the Fluid. *Proceedings of the 10th International Conference on Thermal Energy Storage*. Ecostock 2006, NJ.

Yavuzturk, C., and J.D. Spitler. 1999. A Short Time Step Response Factor Model for Vertical Ground Loop Heat Exchangers. *ASHRAE Transactions*. 105(2): 475-485.

Young, T. 2004. *Development, Verification, and Design Analysis of the Borehole Fluid Thermal Mass model for Approximating Short Term Borehole Thermal Response.* (Masters of Science), Oklahoma State University.